AD-A124 523 WIND TUNNEL INVESTIGATION OF CARGO EXTRACTION PARACHUTES IN THE WAKE OF A..(U) DAVID W TAYLOR NAVAL SHIP RESEARCH AND DEVELOPMENT CENTER BET.. G G HUSON

UNCLASSIFIED AUG 82 DTNSRDC/ASED-82/09 MIPR-79-102 F/G 1/3 NL

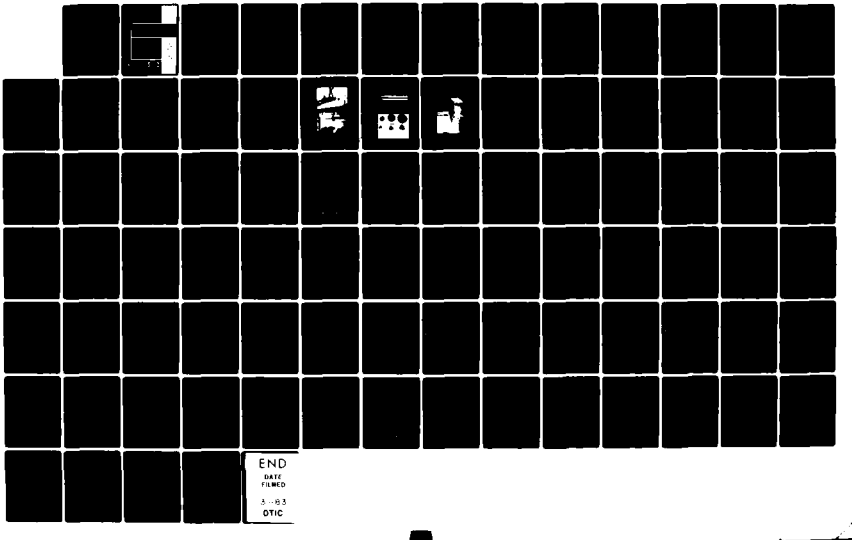

END

DATE FILMED

3-83

DTIC

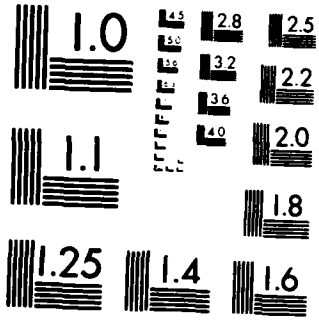

MICROCOPY RESOLUTION TEST CHART
NATIONAL BUREAU OF STANDARDS-1963-A

AD A124523

DTIC FILE COPY

WIND TUNNEL INVESTIGATION OF CARGO EXTRACTION PARACHUTES IN THE WAKE OF A LOCKHEED C-141B STARLIFTER AIRCRAFT

by

Gregory G. Huson

APPROVED FOR PUBLIC RELEASE:
DISTRIBUTION UNLIMITED

AVIATION AND SURFACE EFFECTS DEPARTMENT

DTNSRDC/ASED-82/09

August 1982

DAVID
W.
TAYLOR
NAVAL
SHIP
RESEARCH
AND
DEVELOPMENT
CENTER

BETHESDA
MARYLAND
20084

DTIC
ELECTE
FEB 17 1983
S D

83 02 016 062 A

UNCLASSIFIED

SECURITY CLASSIFICATION OF THIS PAGE (When Data Entered)

REPORT DOCUMENTATION PAGE	READ INSTRUCTIONS BEFORE COMPLETING FORM
1. REPORT NUMBER: DTNSRDC/ASED-82/09	2. GOVT ACCESSION NO.: AD-A124523
3. RECIPIENT'S CATALOG NUMBER:	
4. TITLE (and Subtitle): Wind Tunnel Investigation of Cargo Extraction Parachutes in the Wake of a Lockheed C-141B Starlifter Aircraft	5. TYPE OF REPORT & PERIOD COVERED: Final Report July-September 1981
	6. PERFORMING ORG. REPORT NUMBER:
7. AUTHOR(s): Gregory G. Huson	8. CONTRACT OR GRANT NUMBER(s): MIPR 79-102; MIPR 79-404
9. PERFORMING ORGANIZATION NAME AND ADDRESS: David Taylor Naval Ship R&D Center, Aviation and Surface Effects Department, Bethesda, Maryland 20084	10. PROGRAM ELEMENT, PROJECT, TASK AREA & WORK UNIT NUMBERS: Work Unit 1660-282
11. CONTROLLING OFFICE NAME AND ADDRESS: U.S. Army Natick R&D Laboratories, DRDNA - UAS, Natick, Massachusetts 01760	12. REPORT DATE: August 1982
	13. NUMBER OF PAGES: 91
14. MONITORING AGENCY NAME & ADDRESS (if different from Controlling Office)	15. SECURITY CLASS. (of this report): UNCLASSIFIED
	15a. DECLASSIFICATION/DOWNGRADING SCHEDULE

16. DISTRIBUTION STATEMENT (of this Report)

APPROVED FOR PUBLIC RELEASE: DISTRIBUTION UNLIMITED

17. DISTRIBUTION STATEMENT (of the abstract entered in Block 20, if different from Report)

18. SUPPLEMENTARY NOTES

19. KEY WORDS (Continue on reverse side if necessary and identify by block number)

Cargo Extraction Parachutes
Lockheed C-141B Starlifter Aircraft
Wake Survey
Ringslot Parachute
Airdrop System

20. ABSTRACT (Continue on reverse side if necessary and identify by block number)

Wind tunnel investigations were conducted to probe the wake of a C-141 aircraft in an airdrop configuration. A rake with twelve 5-hole yaw head probes measured velocities at various positions in the wake, and these measurements were used to compute the vorticity of the wake. In addition, motion pictures and force measurements were taken with three differently sized extraction parachute models attached to the model aircraft by three

(Continued on reverse side)

DD FORM 1 JAN 73 1473 EDITION OF 1 NOV 65 IS OBSOLETE
S/N 0102-LF-014-6601

UNCLASSIFIED

SECURITY CLASSIFICATION OF THIS PAGE (When Data Entered)

(Block 20 continued)

extraction lines of different lengths. Correlation of parachute behavior with the airflow data indicates that the vortex shed by the inboard flaps and the fuselage-wing junction causes an instability in the performance of the smallest parachute models while the performance of the larger parachute models is relatively unaffected.

Accession For
NTIS GRA&I
DTIC TAB
Unannounced
Justification
By
Distribution/
Availability Codes
Dist | Avail and/or Special
A

TABLE OF CONTENTS

LIST OF FIGURES

LIST OF TABLES

ABSTRACT

Wind tunnel investigations were conducted to probe the wake of a C-141 aircraft in an airdrop configuration. A rake with twelve 5-hole yaw head probes measured velocities at various positions in the wake, and these measurements were used to compute the vorticity of the wake. In addition, motion pictures and force measurements were taken with three differently-sized extraction parachute models attached to the model aircraft by three extraction lines of different lengths. Correlation of parachute behavior with the airflow data indicates that the vortex shed by the inboard flaps and the fuselage-wing junction causes an instability in the performance of the smallest parachute models while the performance of the larger parachute models is relatively unaffected.

ADMINISTRATIVE INFORMATION

The work reported was funded by the Army Natick Research and Development Laboratories under Military Interdepartmental Purchase Requests 79-102 and 79-404 and David W. Taylor Naval Ship Research and Development Center (DTNSRDC) Work Unit 1660-282. The C-141B aircraft model was on loan to the project from the Air Force through the Lockheed Georgia Company under Contract F09603-81-6-0443, Order Number 0002.

INTRODUCTION

Traditionally, the performance of a cargo extraction parachute in combination with an aircraft is not known until the aircraft has been built and flight tests of the cargo extraction system have been completed. A series of investigations, sponsored and administered by the Army Natick Research and Development Command, is being conducted for the purpose of reducing the cost and length of time necessary to determine the capability of an aircraft to deploy cargo in mid-flight. The goal of these investigations is to determine a method for predicting the performance of cargo extraction parachutes in the wake of any given aircraft. Aircraft wake information from wind tunnel surveys performed during the design process can be used to determine whether the proposed aircraft has the capability to airdrop cargo. When this judgment can be made in the early design process, the costs of producing airdrop-capable cargo aircraft can be reduced significantly.

During the initial investigation in the series, an attempt is made to correlate the measured performance of extraction parachute models with the wake

characteristics of an existing baseline aircraft model. This investigation was performed in a conventionally sized, low Reynolds number, subsonic wind tunnel at DTNSRDC.

The second investigation will determine the influence of wind tunnel wall proximity on aircraft wake generation and will be performed in the NASA Langley 14- by 20-ft wind tunnel. During the third investigation, Reynolds number effect will be examined with tests to be conducted in the NASA 12-ft pressure tunnel at the NASA Ames Research Center. Final validation of these investigations will be the actual flight testing of the parachutes.

In this investigation, performed in the DTNSRDC 8- by 10-ft north subsonic wind tunnel, the performance of 15-, 22-, and 28-ft ringslot parachute models was measured in the wake of a C-141B model aircraft. All models were 0.044 scale. To determine the basic model performance, parachutes were attached to a force balance located inside the model aircraft. Parachute forces were recorded and high-speed motion pictures were taken of the parachute movements. Direction and velocity of the wake flow were computed from the wake data, and an approximate computation of the vorticity of the wake flow was made using the basic vorticity equation.[1*]

MODELS, EQUIPMENT, AND TEST TECHNIQUES

Eleven models were used during the investigation: a 0.044-scale C-141B model aircraft (Figures 1 and 2),[2] an ogive cylinder (Figure 3), and nine 0.044-scale ringslot parachutes (Figure 4). The C-141B aircraft model, on loan from the Lockheed Georgia Company, served strictly as a wake generator and was configured for air drops with petal doors open and ramp door down. Four flap angle settings of 0, 10, 20, and 30 deg simulated different cargo loadings. Compressed air was ducted to the inboard engine nacelles to simulate jet engine effects[3-6] that may influence the aircraft wake in areas where the parachutes are located. Trip strips were installed on the model to ensure proper initiation of turbulent flow over the aircraft surfaces.

Three models each of the 15-, 22-, and 28-ft full-size ringslot cargo extraction parachutes were constructed at the Army Natick R&D Laboratories from nylon cargo parachute material. The models of each size were divided into two groups, by the width of the reinforcing tape between gores. Two canopies of each

---

*A complete listing of references is given on page 9.

size were constructed with narrow reinforcment tapes, types A and B. The third canopy, type C, used wider reinforcement tape to make a stiffer, sturdier model.

During the first phase of the investigation, performance of the model parachutes was measured in relatively undisturbed flow. The six types of parachute models were connected to the ogive cylinder with three different length extraction lines. Tables 1 and 2 list the significant dimensions of the parachute and suspension line models. Runs were made with dynamic pressures varying from 20 to 60 psf. The method for accurately determining the dynamic pressure is described in Appendix A.

The ogive cylinder, which was constructed at DTNSRDC, acted as a balance holder for two phases of the investigation. The cylinder was used first as a streamlined body in an attempt to measure the parachute performance in a relatively undisturbed free stream. The cylinder was then used as a mating sleeve so that the balance could be mounted inside the C-141B model.

During the second phase of the investigation, a survey of the wake generated by the C-141B model was taken in the areas where the parachutes were located. A rake of twelve 5-hole flow angularity probes (Figure 5) mounted on the model support system was used to determine velocities and flow directions in the wake. The model support system enabled the rake to traverse 50 in. in the streamwise X-direction and 24 in. in the vertical Z-direction while the tunnel dynamic pressure was at 60 psf, which dramatically reduced the time necessary to complete the survey. Pressure measurements at various spanwise Y-positions were achieved by repositioning the entire model support system and by orienting the rake so that as each data point was recorded the 12 probes took recordings at 1-in. increments over an 11-in. span in the Y-direction. Three pairs of planes (X = constant) were surveyed where the canopies would be located when the parachutes are attached to the three different extraction lines. The planes of each pair were separated by one inch, as each probe station was in the vertical and lateral directions. The method used to reduce these wake rake data is presented in Appendix B.

During the final phase of the investigation, the model parachutes were connected to the strain gauge balance in the C-141B model while motion pictures were taken. Each parachute type was connected to all three extraction lines, including two of the 28-ft models, simultaneously.

Usually, six-component balances are mounted on a sting support with the "live end" facing into the free stream. The experimental body is then mounted over the

balance. Measuring the forces generated by the extraction parachute models employed a different mounting method. The ogive cylinder served as a balance holder positioning the balance to face "live end" downstream. The parachute extraction lines, made of braided 50-lb test monofilament line, were attached to the balance "live end." Measurements of axial force, side force, and vertical force were possible; however, moments were not measureable because the extraction line was flexible and the extraction-line, balance-connection joint was a hook preventing any moment transfer from the parachute models. The angular deflections of the parachutes from directly behind the balance were calculated trigonometrically from the force data.

Figures 6 through 8 illustrate the arrangement of equipment and models during the three phases of the investigation.

DISCUSSION OF RESULTS

Analysis of the films indicates that the 15-ft parachute models are unstable in all cases studied. The different versions had no fixed, steady position in the aircraft wake at any of the three extraction line lengths. The parachutes moved laterally up to 56 scale feet. The 22- and 28-ft parachute models can be grouped into one category except for the 28-ft C type. These models when subjected to the wake either were not fully inflated or were pulsed (diameter varied at a constant frequency), signifying that the models were either squidding or that some basic instability existed in the parachute model. The 22- and 28-ft parachute models were also steady except for instances where the canopies were partially inflated. The canopies of the two 28-ft models never fully inflated at the same time, except when the free-stream velocity was extremely low at the beginning and end of each point. The failure of the parachute to inflate and the pulsing phenomenon are unknown. It is possible that the models were not constructed to operate at the free-stream velocity used in this investigation.

The Y-Z velocity plots (Figure 9) indicate in a physical sense the flow of air in a particular X-plane. A vortex seems to be located from 2 to 3 in. outboard of the wing-fuselage juncture. Between the vortex and the fuselage centerline, there is a strong upwash and inboard flow. The strength of this flow increases as the flap deflections increase. Similarly, outboard of the vortex location a significant downwash region intensifies as the flap deflection increases. Despite

the different flap settings, the general description of the flow remains the same. As flap deflection increases the velocity vector magnitudes increase; consequently, the flow patterns become more clearly defined. The X-velocity component plots (Figure 10), in combination with the Y-Z velocity plots, give a view of the total velocity at each point. Note that the vector scales of the plots are very different. The X-velocity component scale is length (grid units) = (X-component velocity in ft/sec - 100)/100; the Y-Z velocity component scale is length (grid units) = 10 ft/sec/grid.

Vorticity plots of these regions are shown in Figures 11 and 12. The components were computed using the expressions:

$$\Omega_x \doteq \frac{\Delta W}{\Delta y} - \frac{\Delta V}{\Delta z}$$

$$\Omega_y \doteq \frac{\Delta u}{\Delta z} - \frac{\Delta W}{\Delta x}$$

$$\Omega_z \doteq \frac{\Delta V}{\Delta x} - \frac{\Delta u}{\Delta y}$$

where Ω_x = x-component of vorticity
Ω_y = y-component of vorticity
Ω_z = z-component of vorticity
Δu = x-velocity component (streamwise)
ΔV = y-velocity component (spanwise)
ΔW = z-velocity component (vertical)
Δx = streamwise distance from the ramp door
Δy = spanwise distance from the ramp door
Δz = vertical distance from the ramp door

The plots (Figures 11 and 12) indicate areas of viscous interaction and their relative intensities.

The grid system of the plots in Figures 9 through 12 is laid out so that the origin of the axis is at the center of the ramp door of the C-141B model. The point of origin of each vector corresponds to the position of the actual probe related to the aircraft model in the wind tunnel. The value of the vector's magnitude is given by the scale located in the heading of each plot.

Force data taken while the parachutes were attached to the ogive cylinder and to the C-141B model further support the assertion that the parachute models were not constructed to be tested at this free-stream velocity. A typical drag coefficient for a ringslot parachute is 0.55 within a range of 0.45 to 0.65.[7] The drag coefficients, 0.10 to 0.46 (Figure 13), were consistently below this range. Only the C-type parachutes approach this lower limit of the range.

CONCLUSIONS AND RECOMMENDATIONS

In analyzing the results of this investigation, several assumptions are made:

1. The aircraft wake generated is approximately symmetric about the vertical plane that encompasses the centerline of the aircraft.

2. Because the flow mapping was made without the parachutes in the flow, the plots do not show the actual flow in which these parachutes are behaving, but show a related flow.

3. The wake is steady over a timed average but changes on an instantaneous basis.

4. The configuration of model parachutes attached to a model aircraft by a flexible line has an inherent stability based on a continuous X-velocity component.

The translational motions of the 15-ft models may be explained by the velocity patterns plotted by the rake data. The only obvious difference in the 15-ft parachute models and the larger parachute models is their size. The difference in model behavior may be because the 15-ft models are small and do not occupy the area where the wing-fuselage vortex pattern originates when directly behind the fuselage in what would be considered a stable position. The 15-ft parachutes follow the vortex pattern that is indicated by the vorticity plots and, more distinctly, outlined by the velocity plots. The instantaneous changes in the aircraft wake are significant enough to force the parachute model from a stable position into the vortex flow where it moves outside its range of stability. The larger parachute models also experience the same instantaneous wake changes; however, their occupation of both wing-fuselage vortex centers and the restoring forces that these models create are strong enough to prevent an unstable departure.

Although the wake mapping seems accurate and the high-speed films capture the behavior of the parachute models, the scaling of the parachute models may not have

been accurate. Subsequent tests should be conducted to determine the type of parachute model that would best simulate performance. Originally, the models were to be vacuum bag molded from fiberglass-reinforced plastic; however, the cost of this process was prohibitive. The plots of the drag coefficients in Figure 13 indicate that most of the drag coefficients of the parachute models were below the generally accepted range of 0.45 to 0.65. The plots indicate that the type-C parachutes have higher drag coefficients than models with narrower reinforcement tapes. Cloth parachute models should be refined to prevent squidding in all cases and to raise the drag coefficients. The parachute performance resulting from this investigation supports the conclusions of Weber and Garrard:[8]

> "The stiffness of the parachute did not strongly influence stability characteristics, and, in fact, stiffer models appeared to perform more like full-size parachutes than did more flexible models."

At each configuration point during this investigation, 10 to 12 samples of data were taken at 0.5-sec intervals. Because the parachutes were in a highly dynamic situation, a higher or continuous sampling rate could have recorded information that would have provided more insight into parachute model performance. Consideration should also be given to using a continuous data collection method for the parachute force data.

REFERENCES

1. Roberson, J.A. and C.T. Crowe, "Engineering Fluid Mechanics," Houghton Mifflin Co., Boston (1975), p. 103.

2. Cleveland, F.A. and R.D. Gilson, "Development Highlights of the C-141 Starlifter," Journal of Aircraft, Vol. 2, No. 4 (1965), pp. 248-287.

3. Goodrick, T.F., "Wind Tunnel Studies of the Pressure Distribution and the Flow in the Wake of the Lockheed C-141A Starlifter Jet Transport Aircraft," University of Minnesota (Aug 1967).

4. Ribner, H.S., "Field of Flow About a Jet and Effects of Jets on Stability of Jet Propelled Airplanes," Report NACA/ACR No. 16C13 (1946).

5. Squire, H.B. and J. Trouncer, "Round Jet in a General Stream," British Aeronautical Research Committee, Report and Memorandum No. 1974 (Jan 1944).

6. "Jane's All the World's Aircraft," McGraw-Hill Book Co., New York (1967), pp. 535-536.

7. "United States Air Force Parachute Handbook," Report WADC TR 55-265 (Dec 1956), p. 2-1-17.

8. Weber, T. and W.L. Garrard, "Effects of Flexibility on Stability of Small Ribbon Parachutes," Journal of Aircraft, Vol. 19, No. 8 (1982), pp. 692-694.

PRECEDING PAGE BLANK-NOT FILMED

APPENDIX A
DETERMINATION OF DYNAMIC PRESSURE

Determining the accurate dynamic pressure (and hence speed) of the free-stream flow in the north subsonic wind tunnel requires several correction factors. Incompressible dynamic pressure is the difference between the total head pressure and static pressure of the flow. This pressure was measured with a piezometer ring during this investigation. The piezometer ring measures the difference in pressure of the flow at two locations on the wind tunnel circuit. One of four static taps was located on each wall in the settling chamber in the same plane perpendicular to the tunnel X-axis. The velocity of the air in the settling chamber is very low, providing the equivalent of total head pressure on a pitot static tube. The second location of the static taps is in the contraction cone just ahead of the test section.

Two factors are used to adjust the pressure differences measured by the piezometer ring to provide an accurate value for the dynamic pressure at the model. The blocking factor adjusts the dynamic pressure for the effects of the presence of the model, support system, and any of the other gear in the test section that decreases the area available for air to flow and thus increases the dynamic pressure.

$$BF = \frac{1 + \text{Model Area} + \text{Equipment Area}}{4 \times \text{Test Section Area}}$$

The correlation factor relates the measurement taken by the piezometer ring to the dynamic pressure in the test section. This correction is necessary because the piezometer ring does not measure the dynamic pressure gradient upstream of the test section which has been correlated previously to the dynamic pressure of various locations in the test section.

The equation relating dynamic pressure to the pressure measured by the piezometer ring is:

$$\Delta q = p * BF * CF$$

where q = free-stream dynamic pressure, $1/2\ V^2$

Δp = pressure difference measured by piezometer ring

BF = blocking factor

CF = correlation factor

PRECEDING PAGE BLANK-NOT FILMED

APPENDIX B
WAKE RAKE DATA REDUCTION

The wake mapping was performed with a rake of 12 pitot-static angularity probes. These probes are essentially cylinders with pressure taps located in the hemispherical tip that permit pressure differences over the tip to be measured. The pressure difference measured by the central tap on the probe tip and ring of static taps downstream on the cylinder is the dynamic pressure at the probe. The equations which govern the data reduction and Figures B.1 through B.3 are included to indicate the pressure tap arrangement of the probe and the sign conventions used to reduce data.*

$$\varepsilon = \left[\frac{\Delta P_{1,2}}{P_T - P_S} + a + b \left(\frac{\Delta P_{3,4}}{P_T - P_S} \right) \right] c$$

$$\sigma = \left[\frac{\Delta P_{3,4}}{P_T - P_S} + k + l \left(\frac{\Delta P_{1,2}}{P_T - P_S} \right) \right] m$$

$$q = \frac{P_T - P_S}{1 + A + B(\varepsilon^2 + \sigma^2)}$$

ε = vertical deflection angle, deg

σ = horizontal deflection angle, deg

$\Delta P_{1,2}$ = difference in pressure measured in taps 1 and 2 $(P_1 - P_2)$ psf

$\Delta P_{3,4}$ = difference in pressure measured in taps 3 and 4 $(P_3 - P_4)$ psf

$P_T - P_S$ = dynamic pressure $(P_{total} - P_{static})$ psf

a = constant to account for shift in reading at $\sigma = \varepsilon = 0$

k = constant to account for shift in reading at $\sigma = \varepsilon = 0$

b = coefficient correcting influence of pressure reading of horizontal deflection taps

l = coefficient correcting influence of pressure reading of vertical deflection taps

*Work reported by M.L. Cook ("Wind Tunnel Freestream Flow Survey at the Mounting Location of the X-Wing Model Rotor," DTNSRDC/TM-16-80/02, Jan 1982).

PRECEDING PAGE BLANK-NOT FILMED

c = coefficient converting pressure readings into degrees of vertical deflection, deg

m = coefficient converting pressure readings into degrees of horizontal deflection, deg

q = dynamic pressure or velocity parameter, psf

A = constant to correct for constant deficiency between actual q and measured q

B = coefficient to account for losses due to deflection angles

TABLE 1 - PARACHUTE CHARACTERISTICS

Parachute Diameter		Type	Canopy Weight	Suspension Line Average Length
Full Scale	Model Scale			
ft	in		grams	in
15	7.5	A	7.5	5.9
15	7.0	B	7.8	5.7
15	7.6	C	7.6	6.0
22	11.3	A	20.1	9.0
22	11.2	B	20.0	8.9
22*	-	C	-	-
28	14.7	A	23.7	12.7
28	15.0	B	23.7	12.7
28	14.1	C	22.5	12.5

*Destroyed during investigation.

TABLE 2 - EXTRACTION LINES

Extraction Line Length	
Full Scale	Model Scale
ft	in
60	31.7
90	47.5
120	63.4

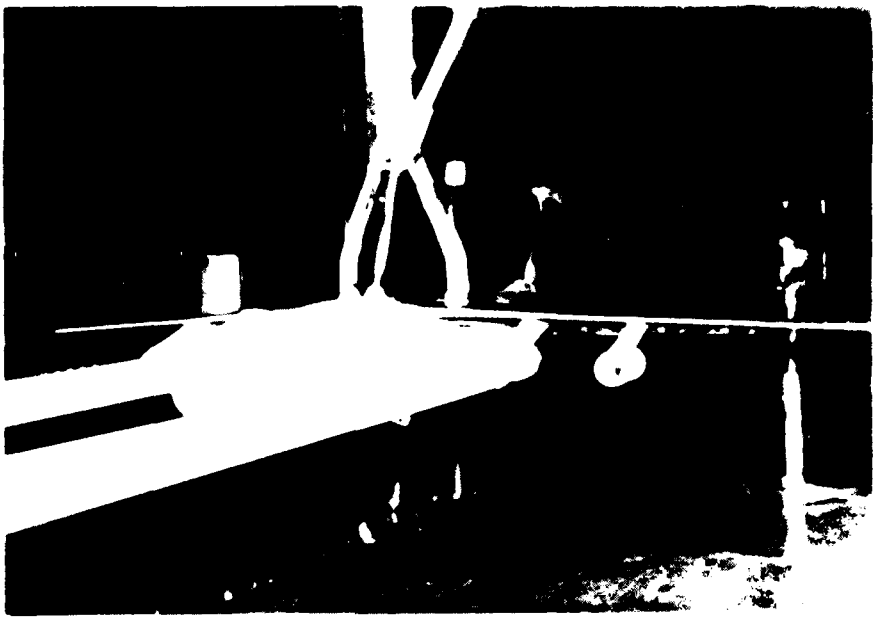

Figure 1 - C-141B Model Installation and Motion Picture Camera

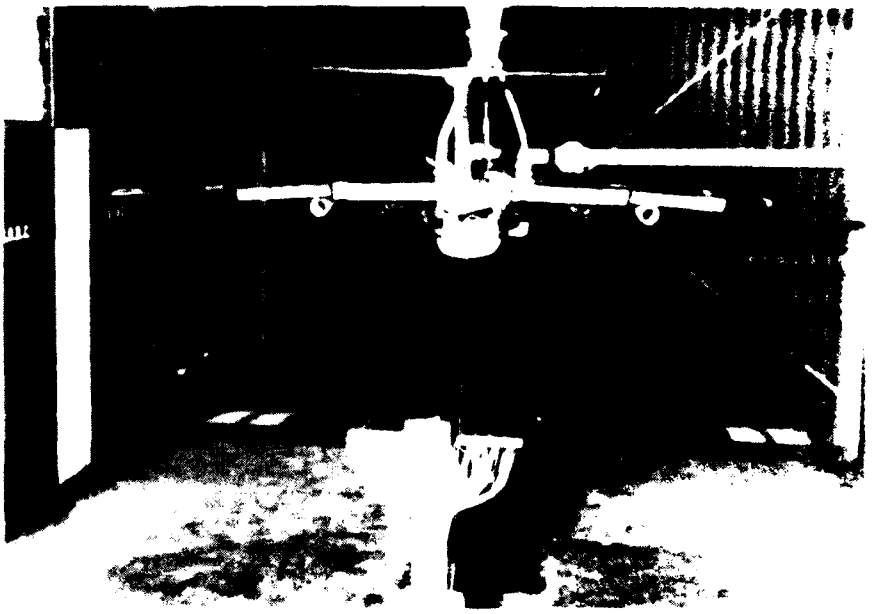

Figure 2 - C-141B Model and Cable Rake

PRECEDING PAGE BLANK-NOT FILMED

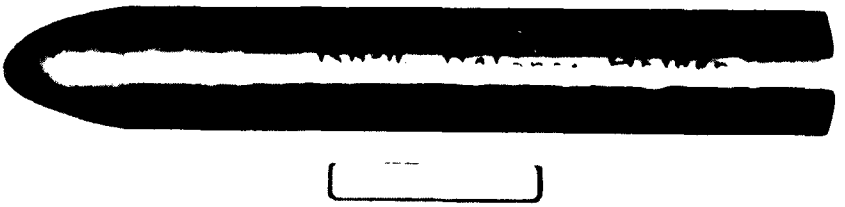

Figure 3 - Ogive Cylinder

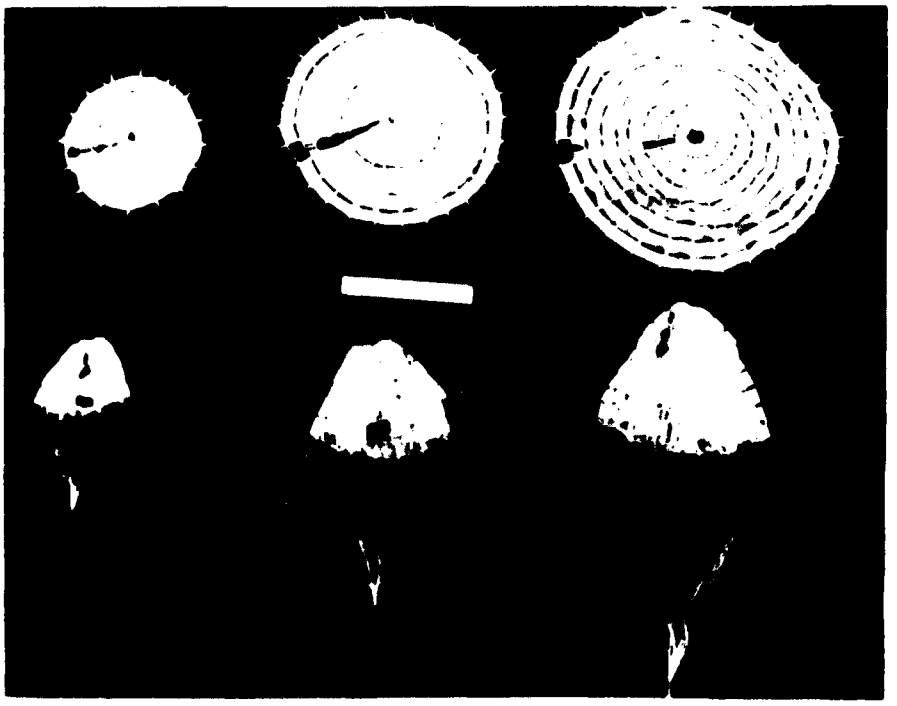

Figure 4 - Parachute Models

PRECEDING PAGE BLANK-NOT FILMED

PRECEDING PAGE BLANK-NOT FILMED

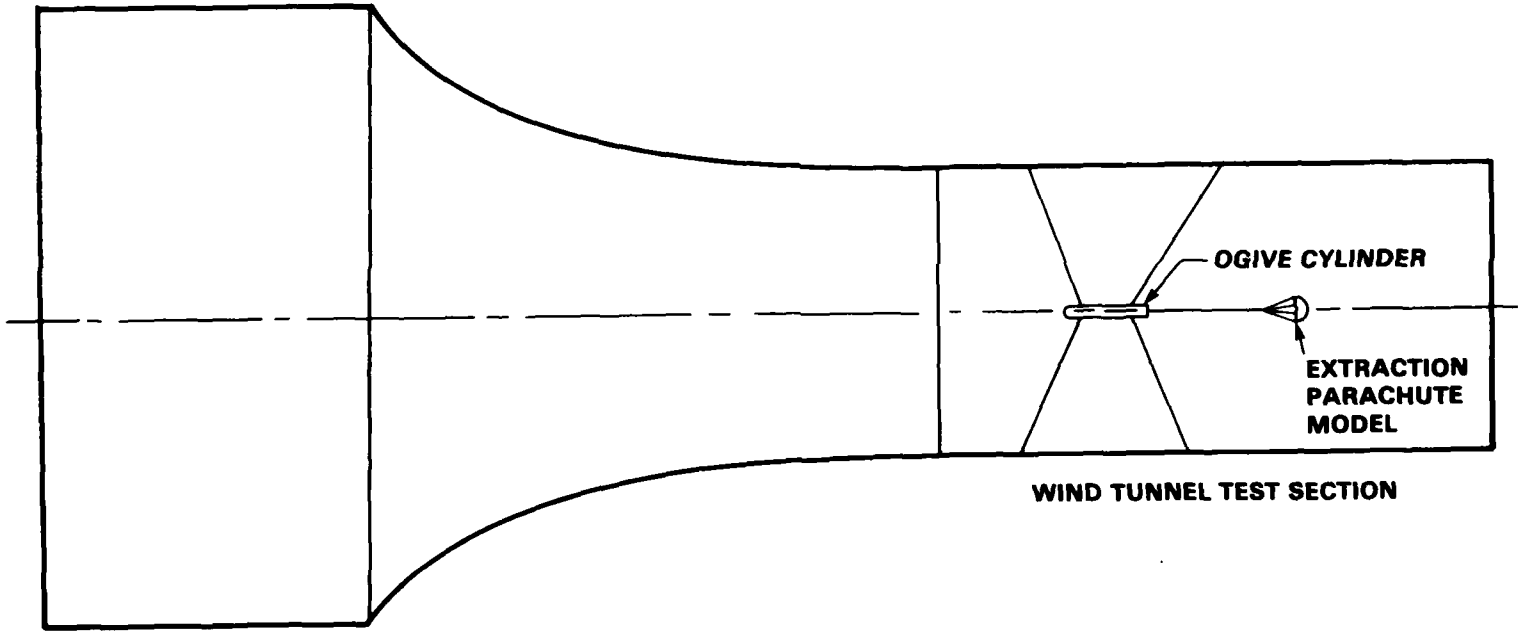

Figure 6 - Ogive Cylinder and Parachute Model (Phase I)

PRECEDING PAGE BLANK-NOT FILMED

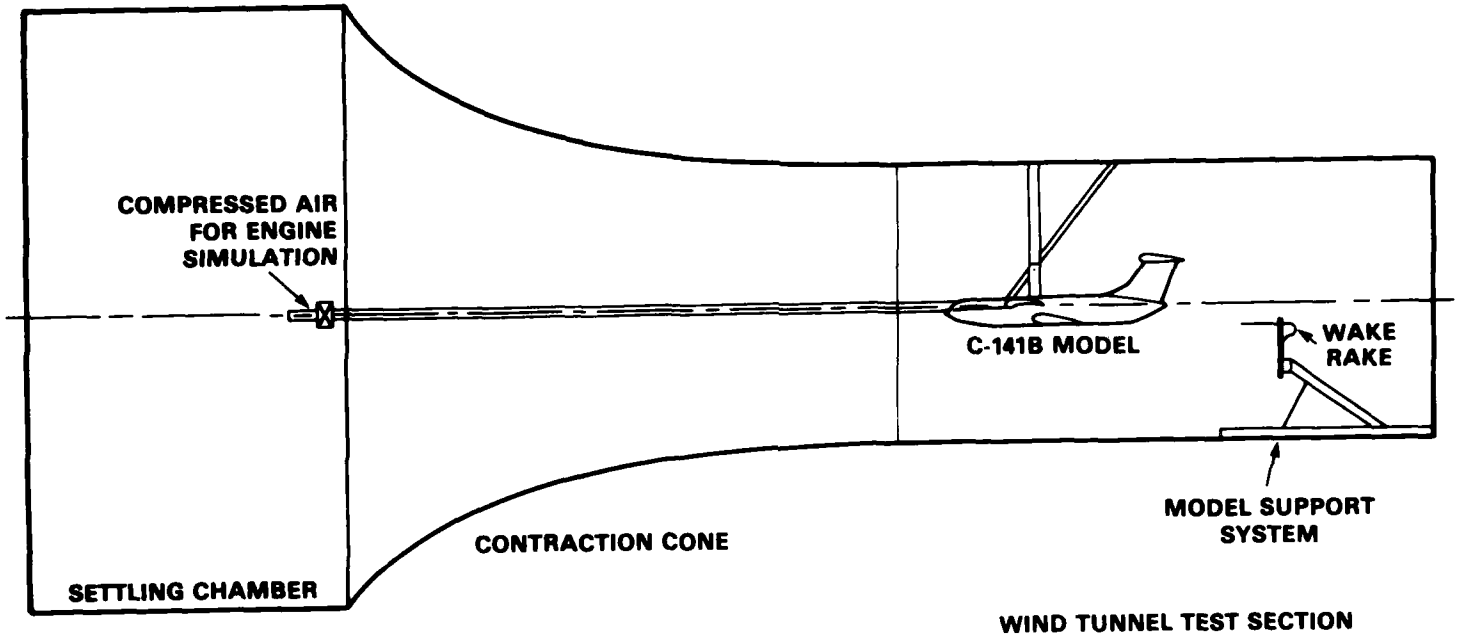

Figure 7 - C-141B Model and Wake Rake (Phase II)

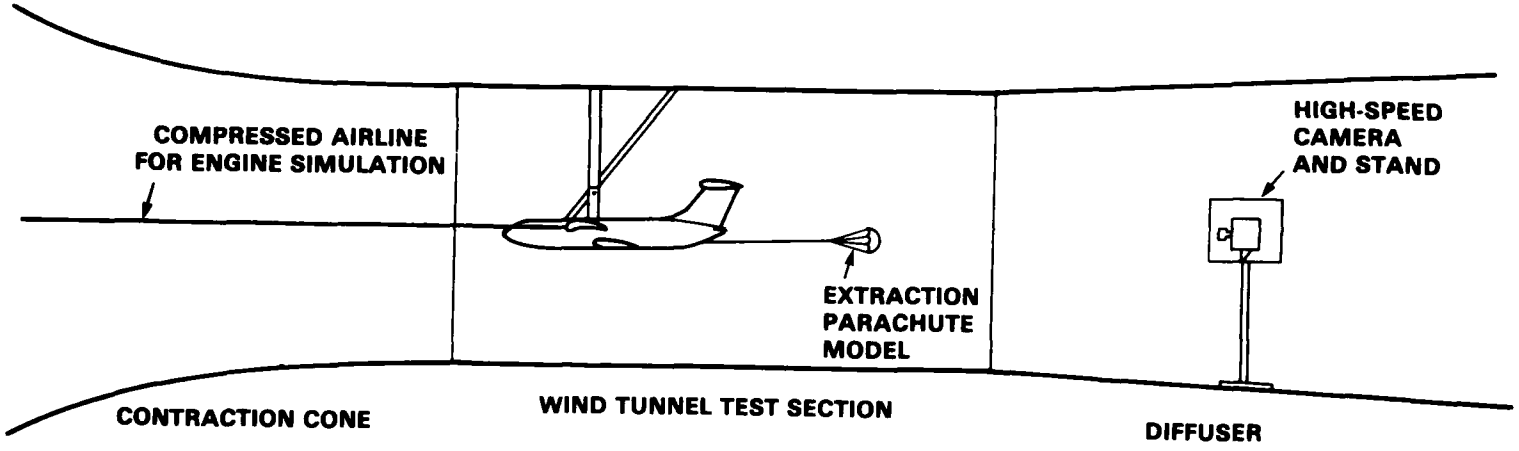

Figure 8 - C-141B Model, Parachute Model, and Motion Picture Camera (Phase III)

Figure 9 - Y-Z Velocity Component Plot of C-141B Wake: Varying X Distance and Flap Angle Setting (V_{Tunnel} = 200 ft/sec, Vector Magnitude 10 ft/sec/grid)

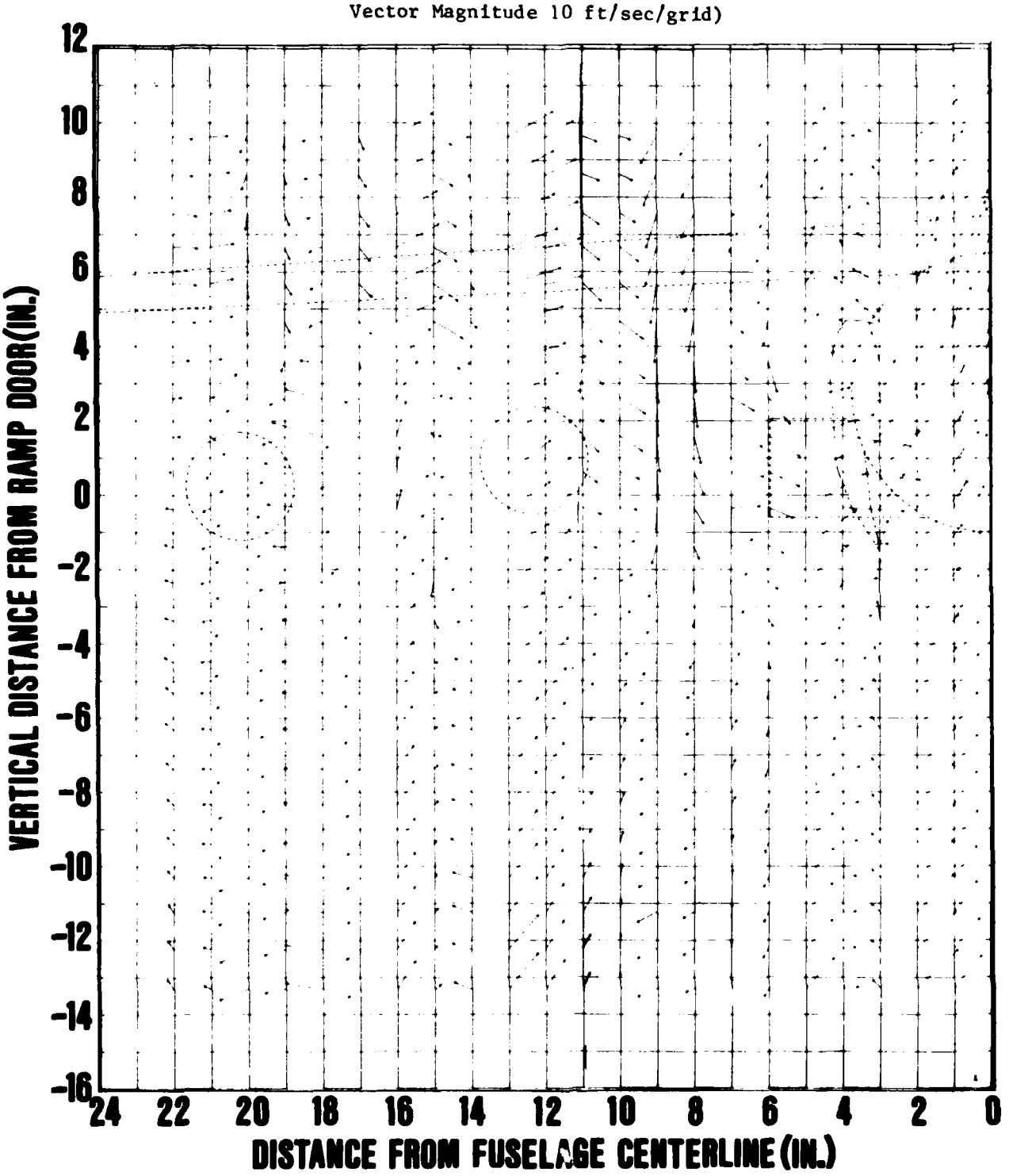

Figure 9a - X Position = 38.2 in. Downstream from Ramp Door; Flap Setting = 0 deg

Figure 9 (Continued)

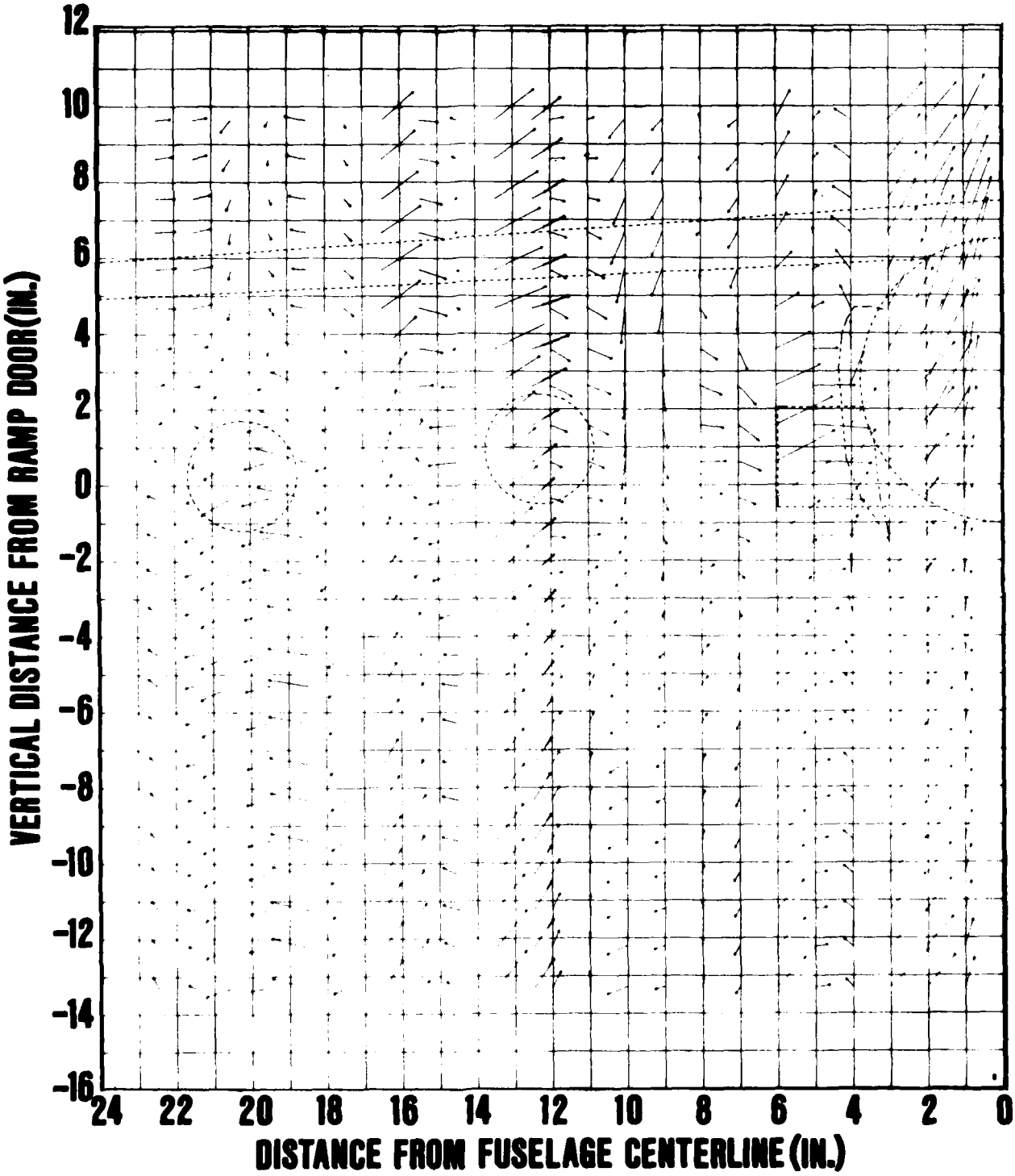

Figure 9b - X Position = 56.8 in. Downstream from Ramp Door; Flap Setting = 0 deg

Figure 9 (Continued)

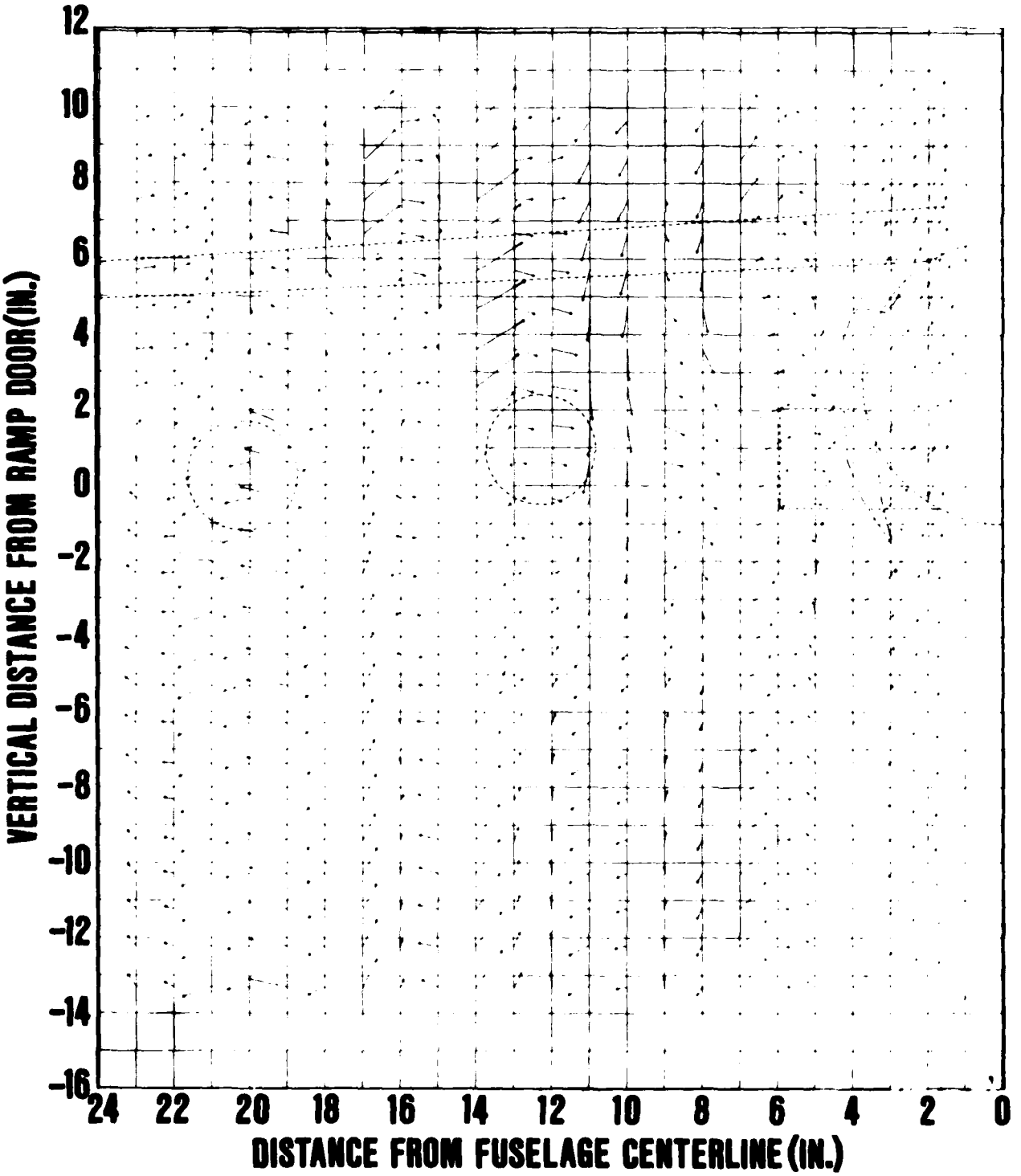

Figure 9c - X Position = 76.3 in. Downstream from Ramp Door; Flap Setting = 0 deg

Figure 9 (Continued)

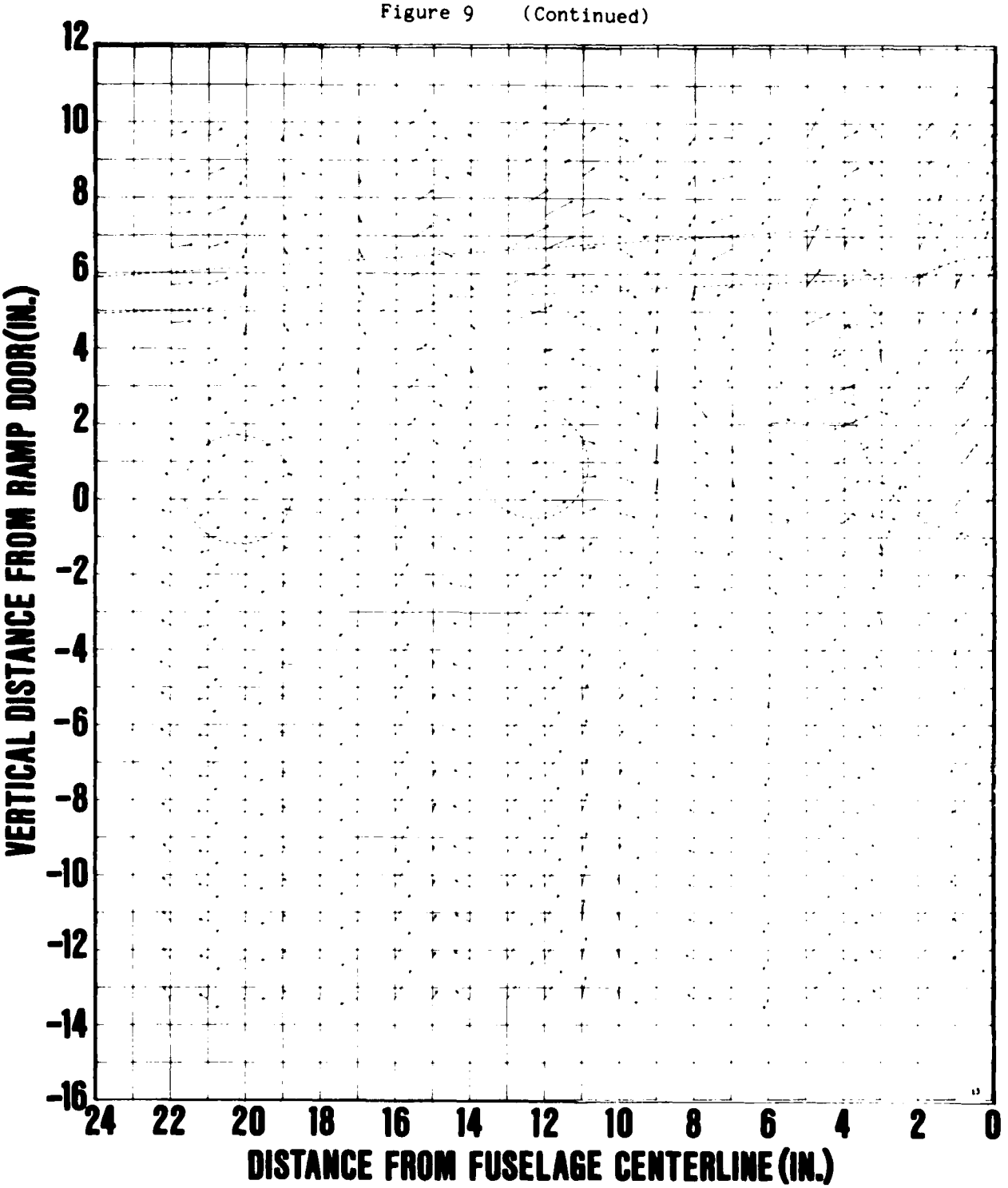

Figure 9d - X Position = 38.2 in. Downstream from Ramp Door; Flap Setting = 0 deg; No Thrust Simulation

Figure 9 (Continued)

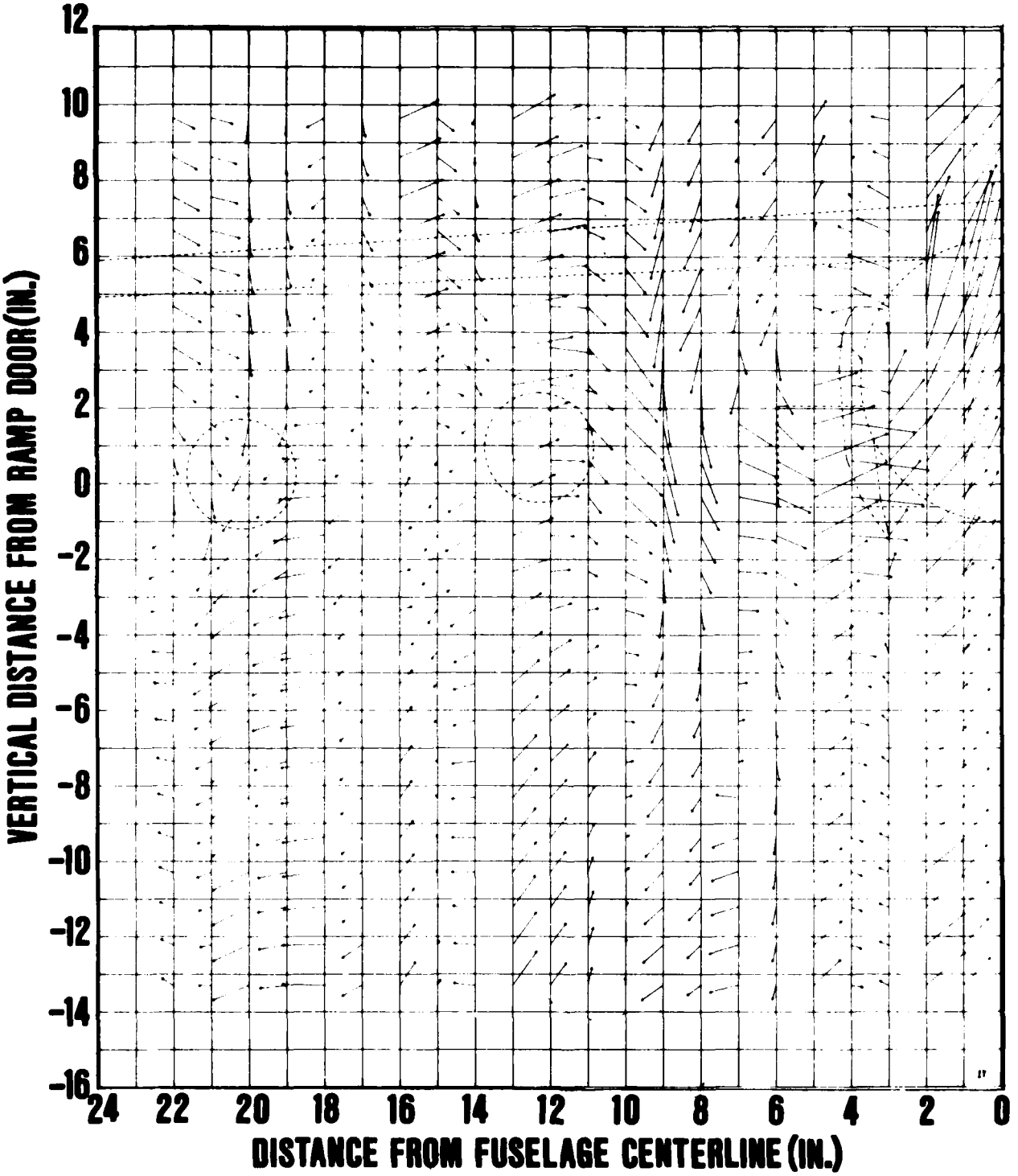

Figure 9e - X Position = 38.2 in. Downstream from Ramp Door; Flap Setting = 10 deg

Figure 9 (Continued)

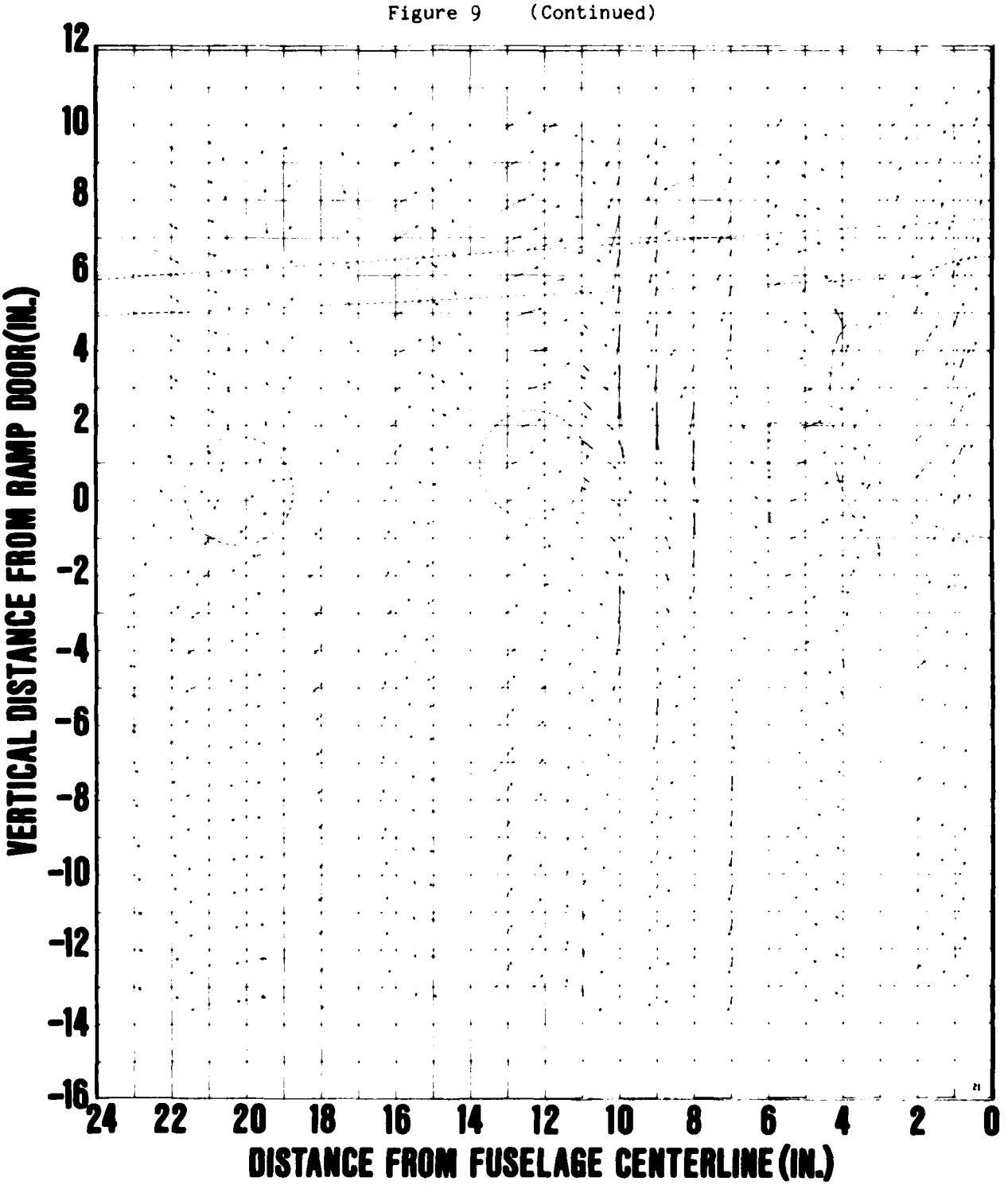

Figure 9f - X Position = 56.8 in. Downstream from Ramp Door; Flap Setting = 10 deg

Figure 9 (Continued)

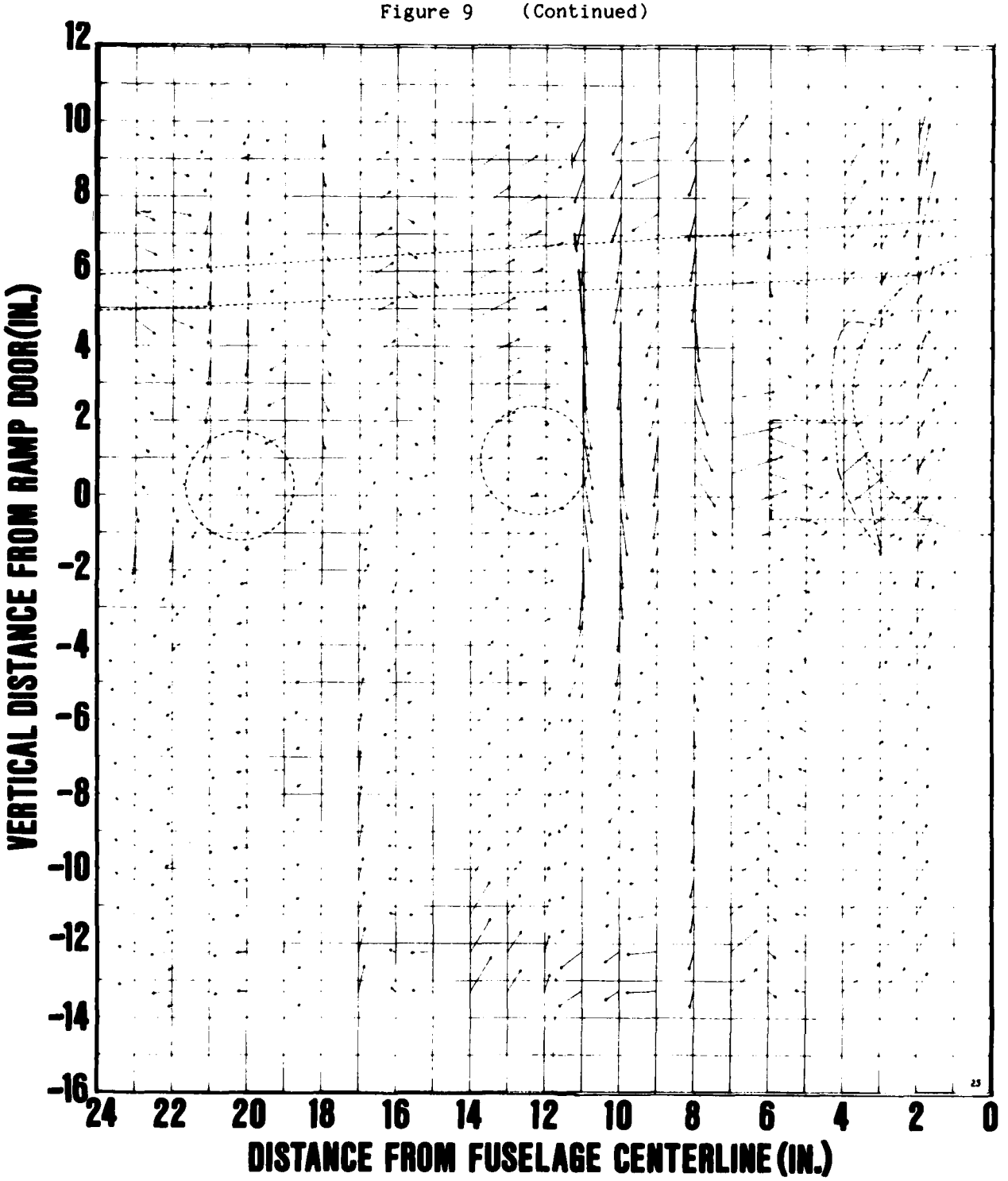

Figure 9g - X Position = 76.3 in. Downstream from Ramp Door;
Flap Setting = 10 deg

Figure 9 (Continued)

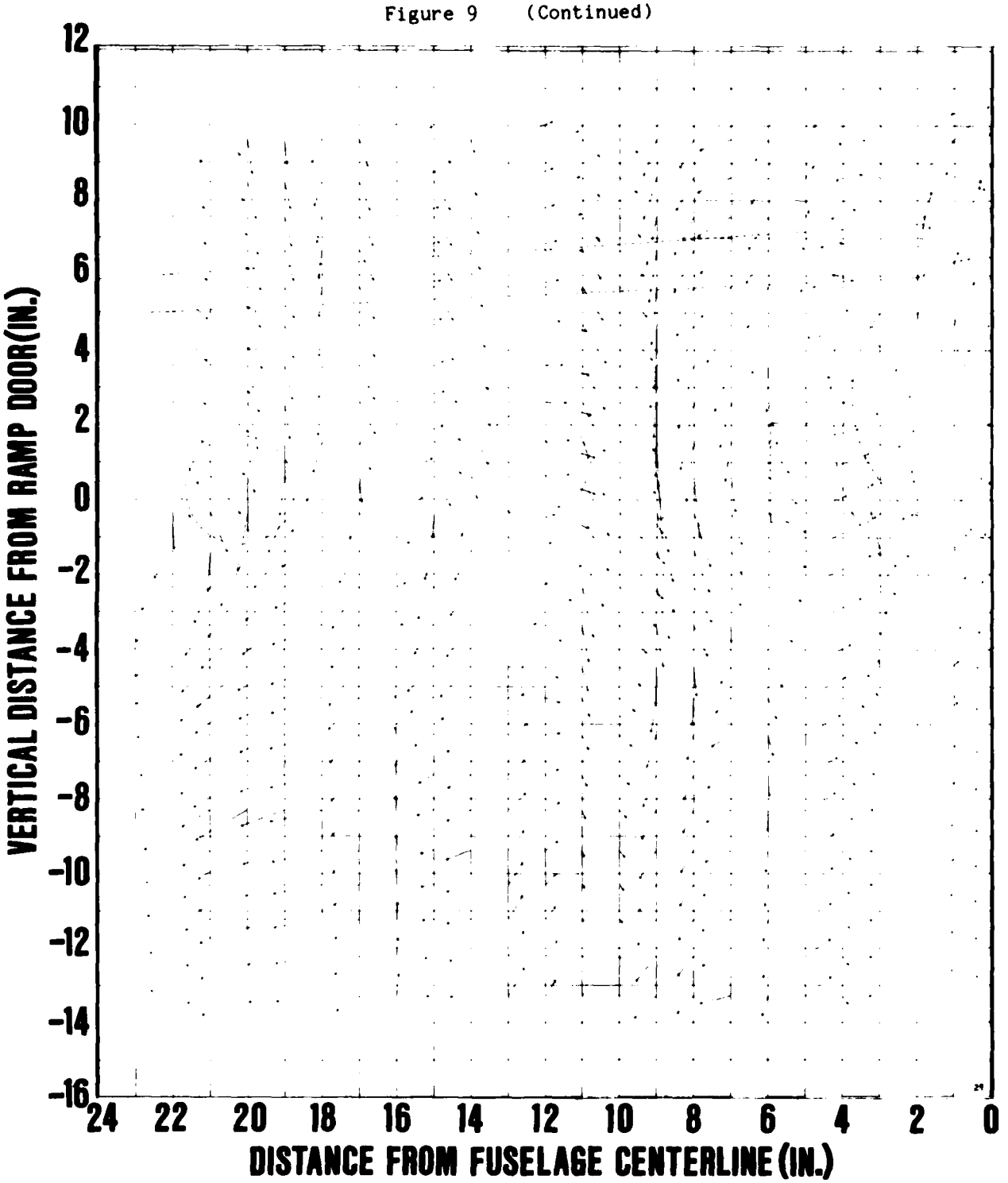

Figure 9h - X Position = 38.2 in. Downstream from Ramp Door;
Flap Setting = 20 deg

Figure 9 (Continued)

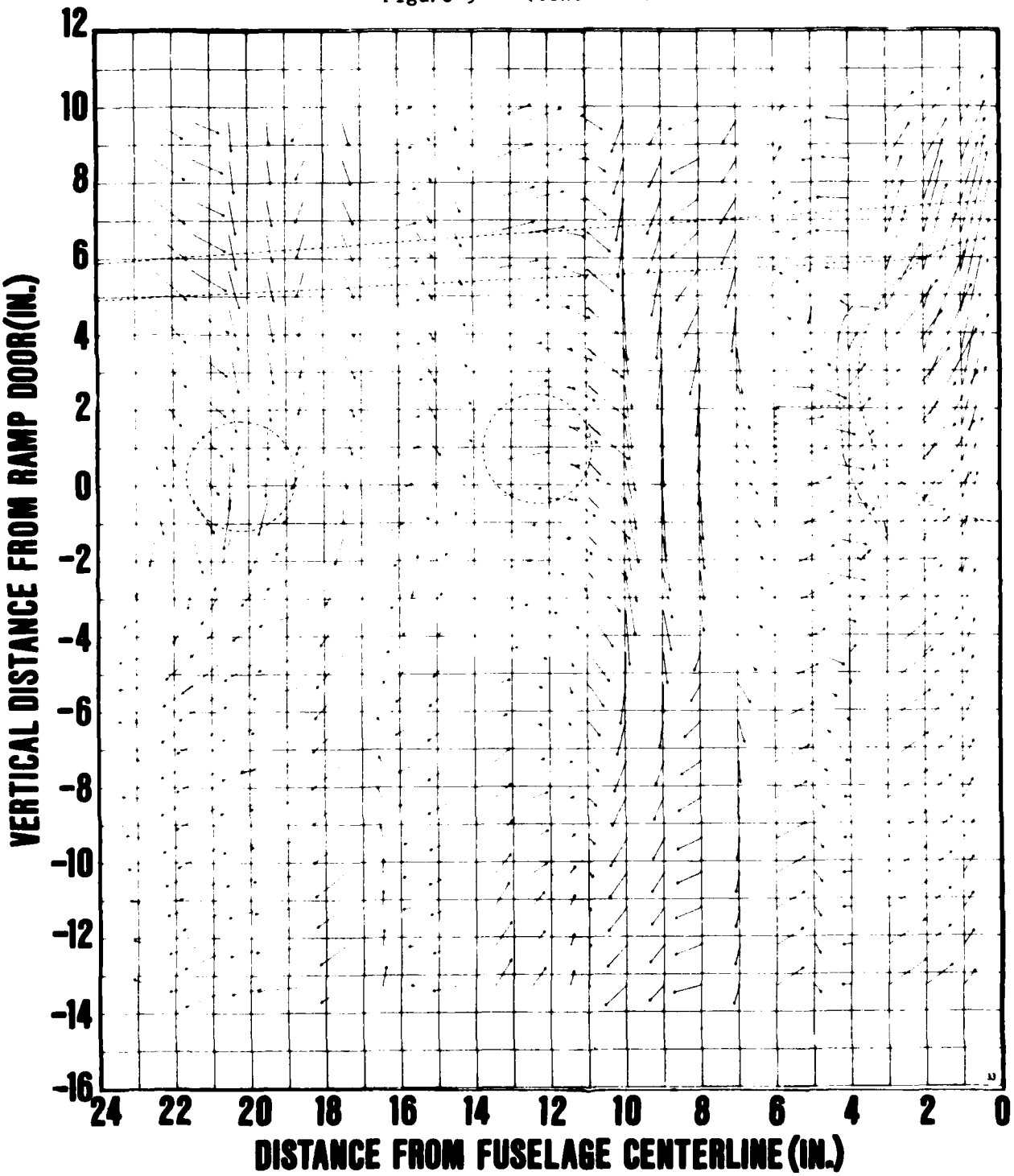

Figure 9i - X Position = 56.8 in. Downstream from Ramp Door;
Flap Setting = 20 deg

Figure 9 (Continued)

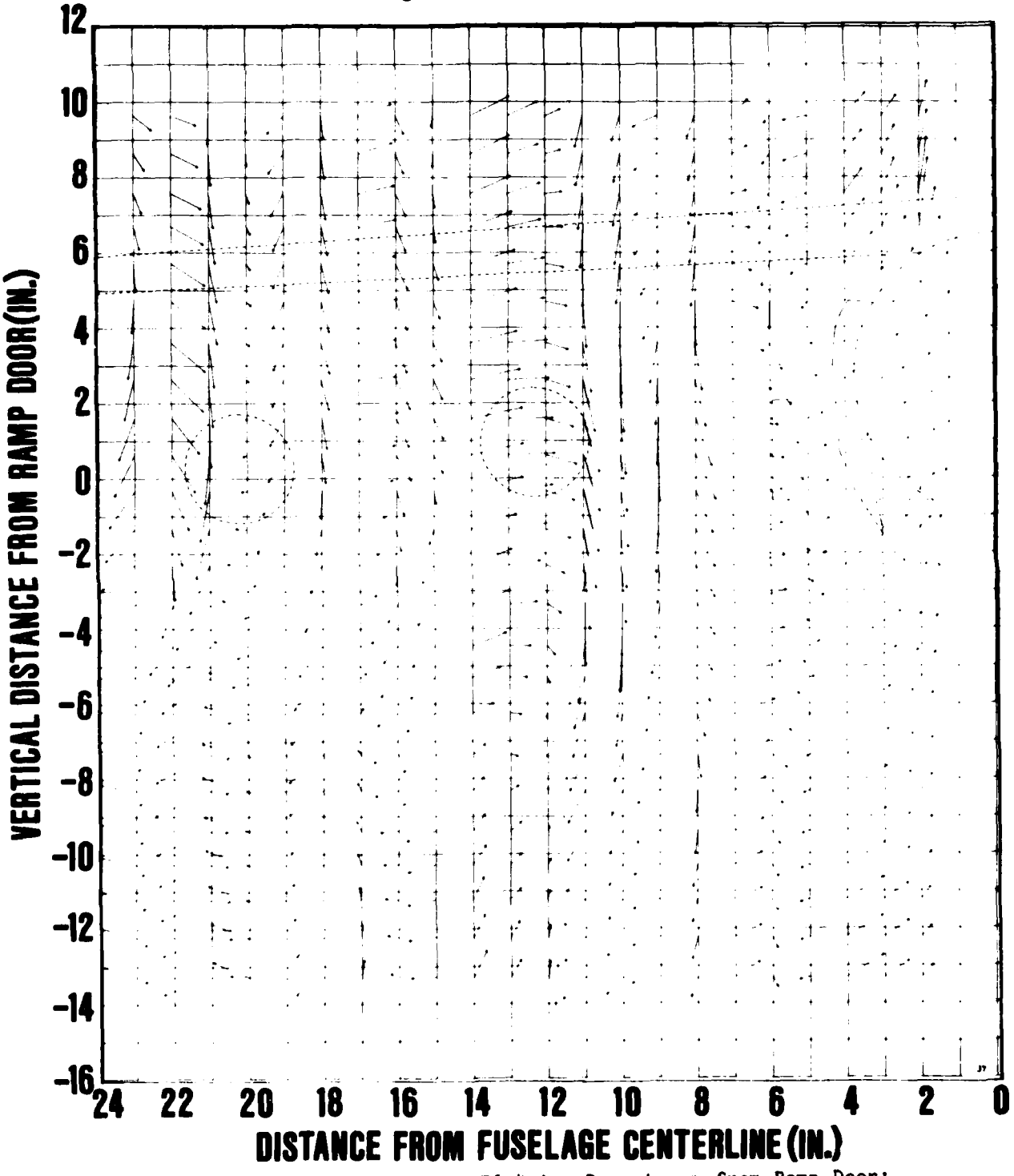

Figure 9j - X Position = 76.4 in. Downstream from Ramp Door; Flap Setting = 20 deg

Figure 9 (Continued)

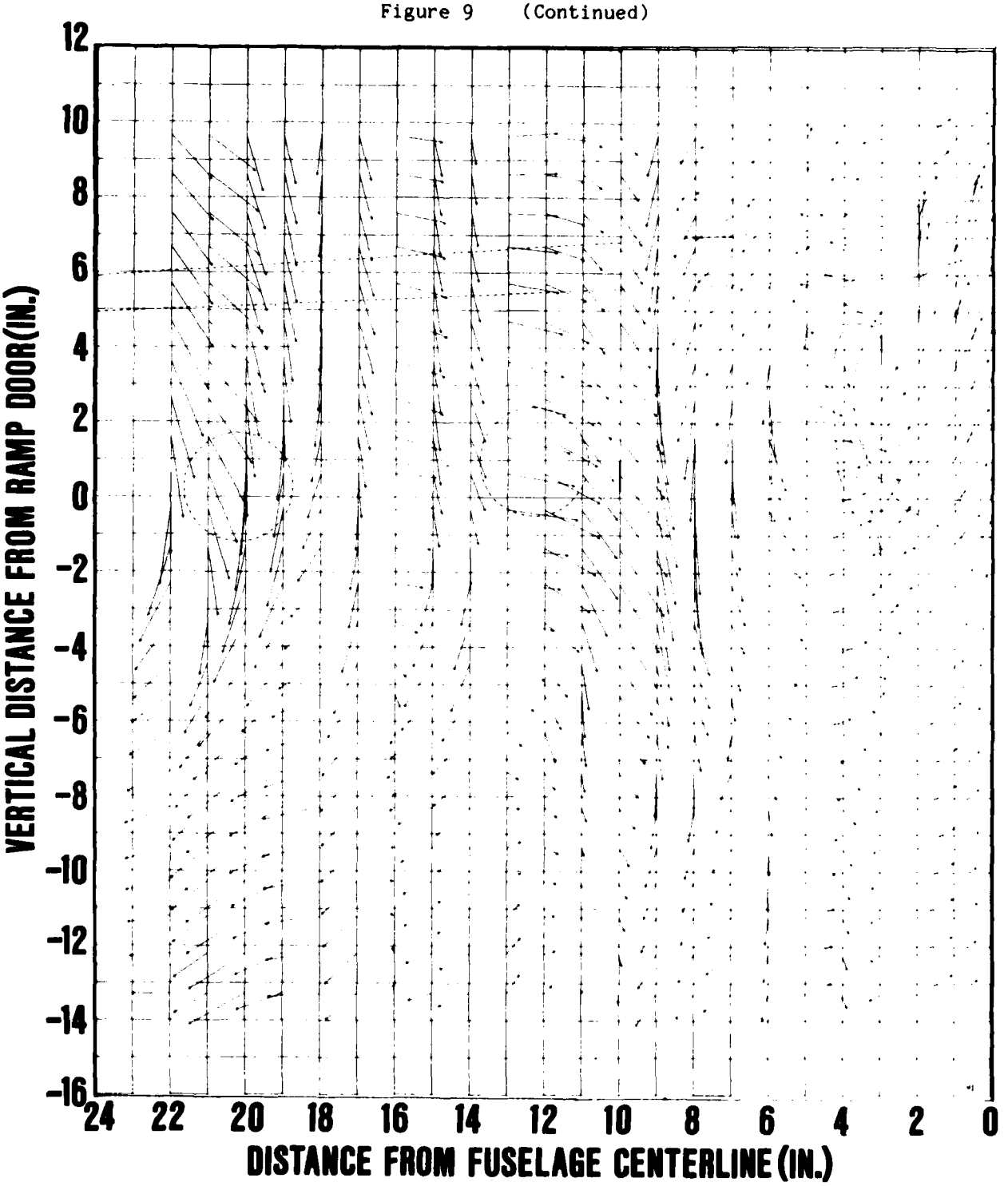

Figure 9k - X Position = 38.2 in. Downstream from Ramp Door; Flap Setting = 30 deg

Figure 9 (Continued)

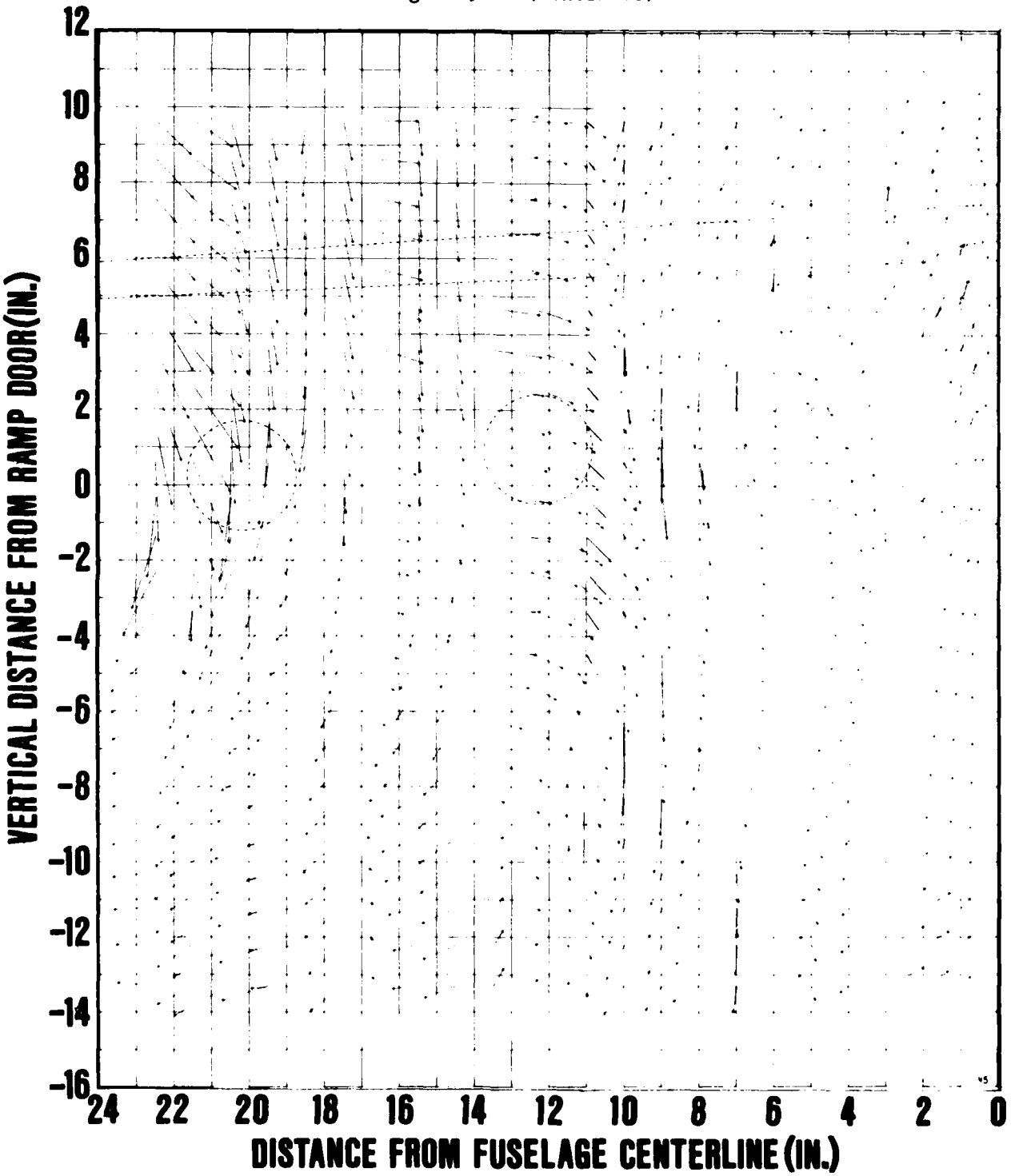

Figure 91 - X Position = 56.8 in. Downstream from Ramp Door; Flap Setting = 30 deg

Figure 9 (Continued)

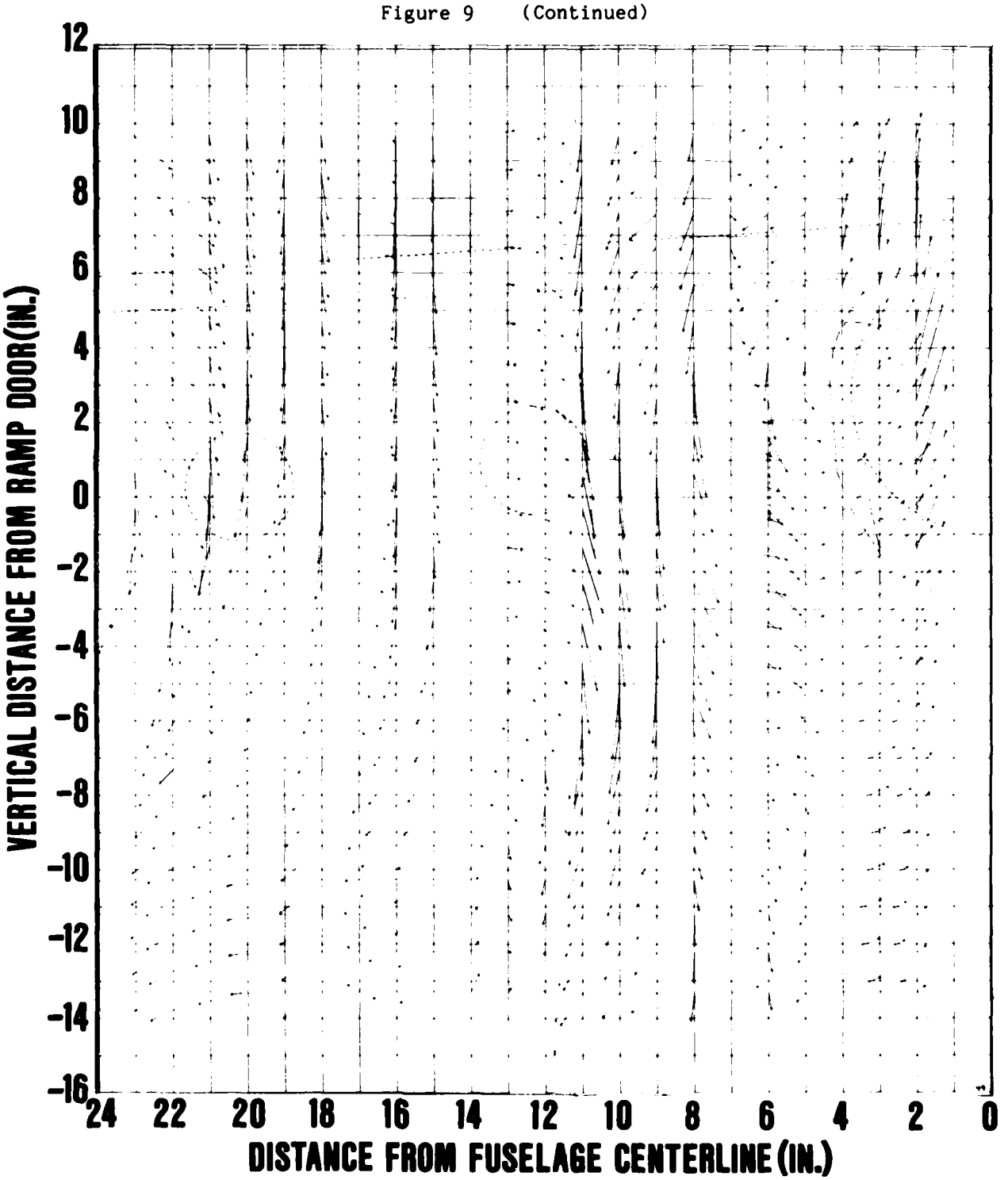

Figure 9m - X Position = 76.3 in. Downstream from Ramp Door;
Flap Setting = 30 deg

Figure 9 (Continued)

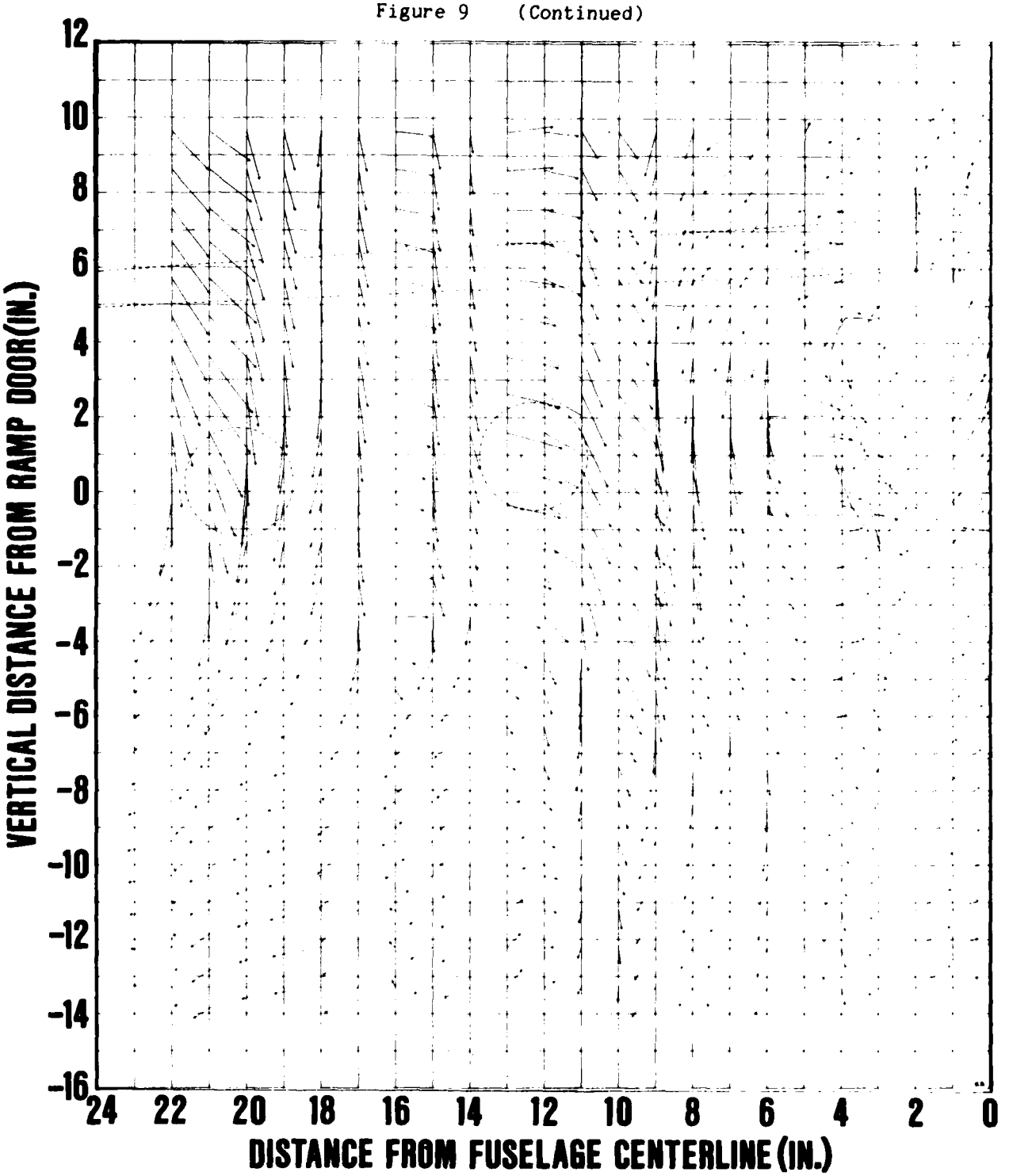

Figure 9n - X Position = 38.2 in. Downstream from Ramp Door; Flap Setting = 30 deg; No Thrust Simulation

Figure 10 - X Velocity Component Plot of C-141B Wake; Varying X Distance and Flap Angle Setting (V_{Tunnel} = 200 ft/sec, Vector Magnitude 100 ft/sec/grid + 100 ft/sec with Positive Downstream Direction to Left)

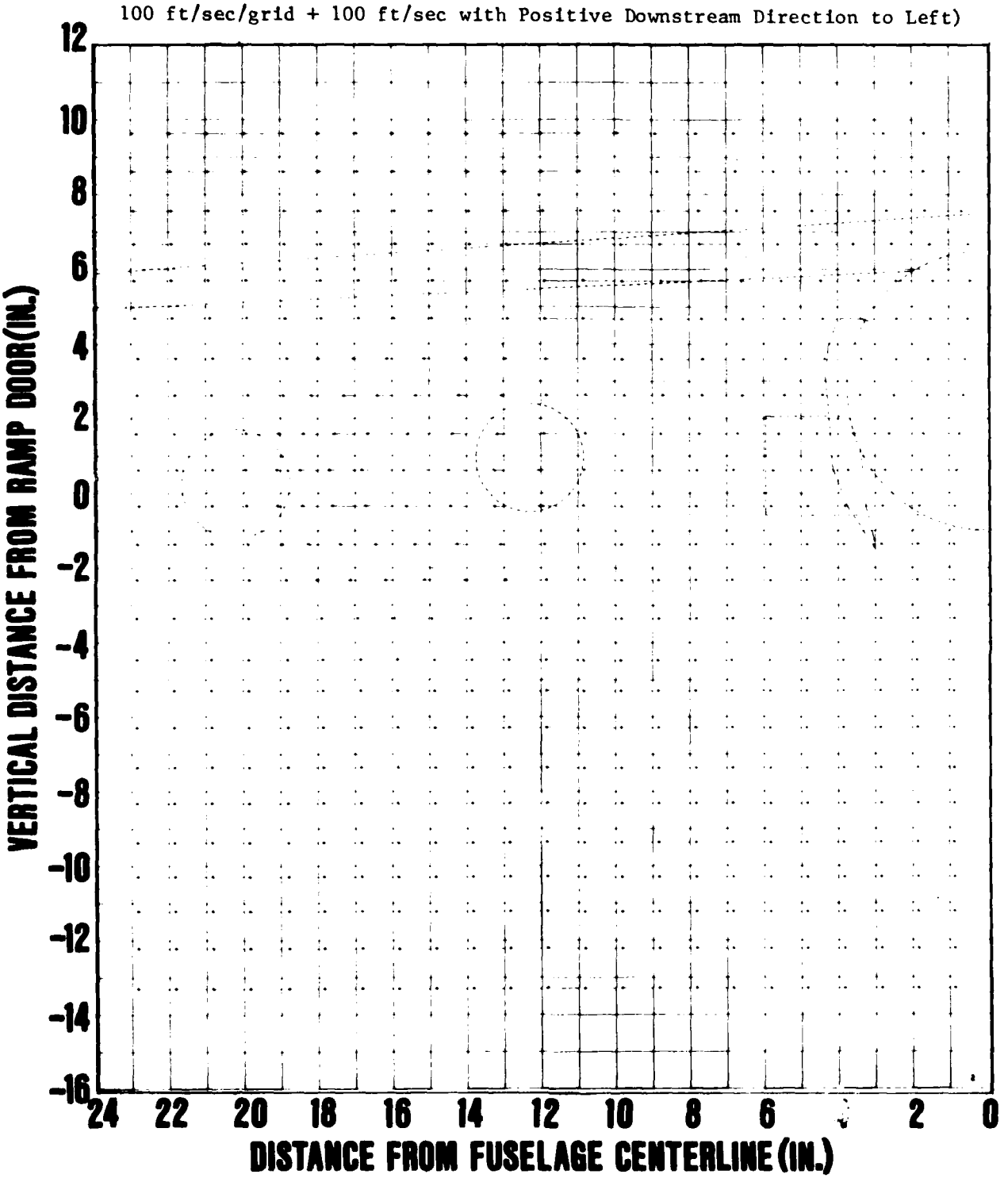

Figure 10a - X Position = 38.2 in. Downstream from Ramp Door; Flap Setting = 0 deg

Figure 10 (Continued)

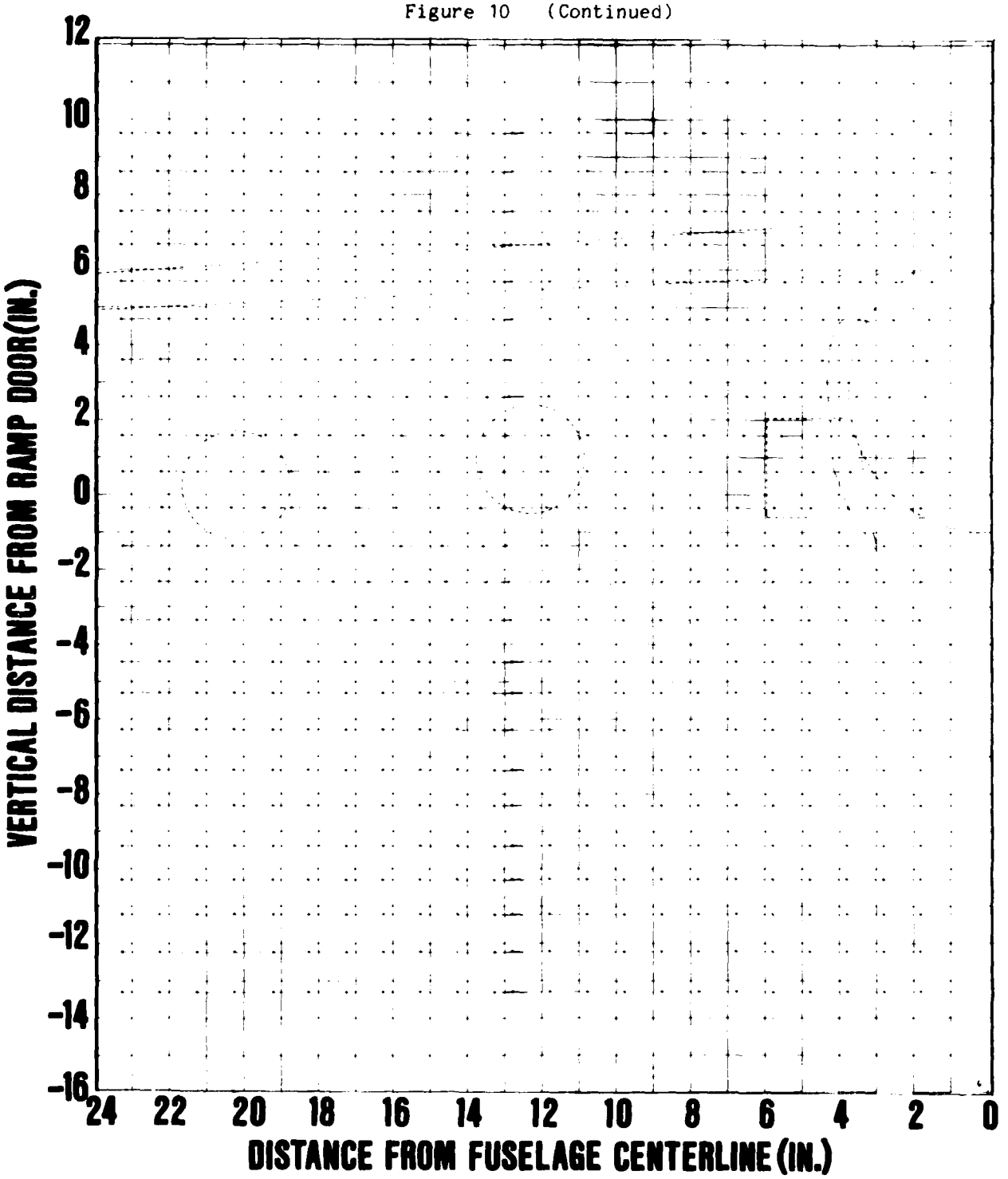

Figure 10b - X Position = 56.8 in. Downstream from Ramp Door; Flap Setting = 0 deg

Figure 10 (Continued)

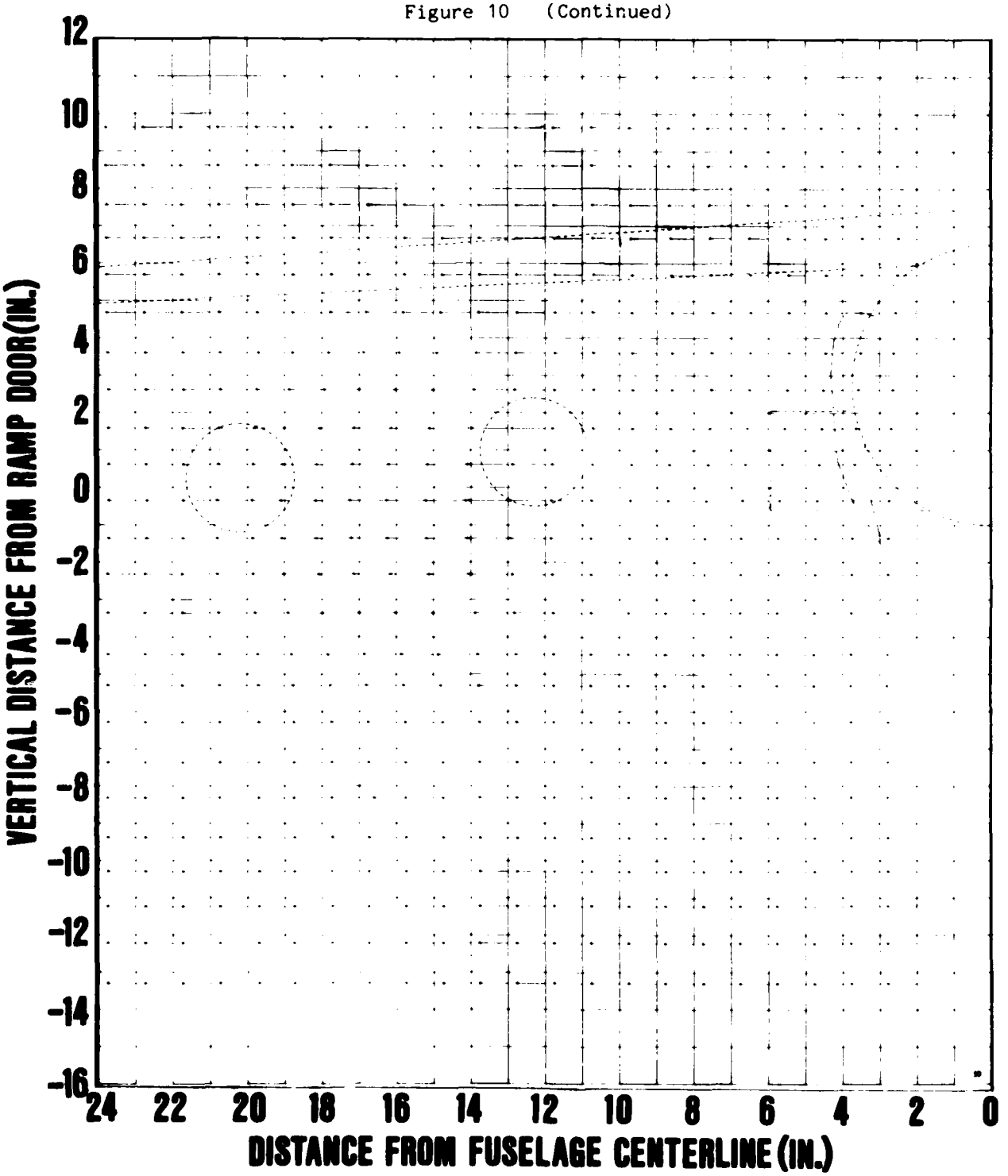

Figure 10c - X Position = 76.3 in. Downstream from Ramp Door;
Flap Setting = 0 deg

Figure 10 (Continued)

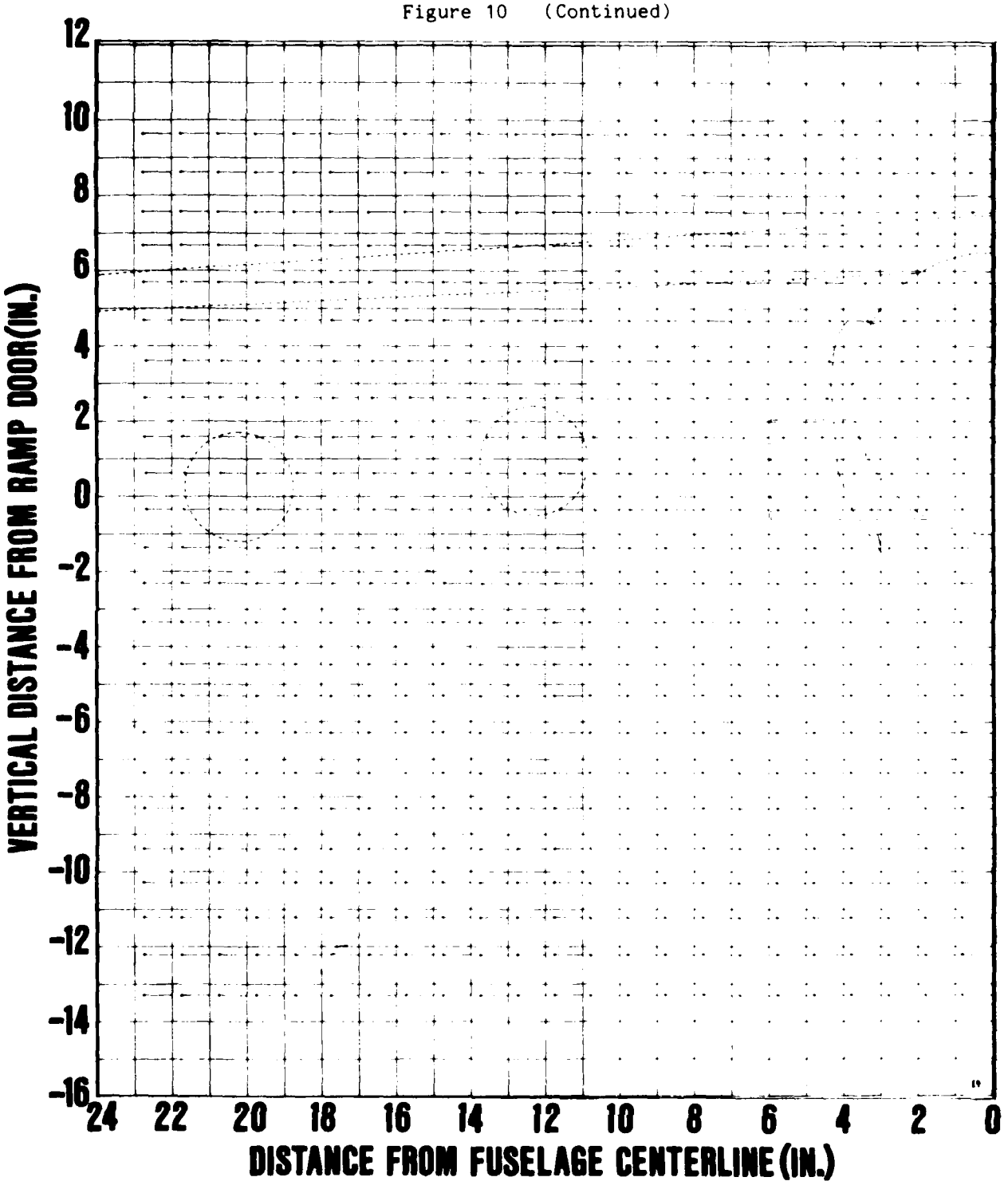

Figure 10d - X Position = 38.2 in. Downstream from Ramp Door;
Flap Setting = 0 deg; No Thrust Simulation

Figure 10 (Continued)

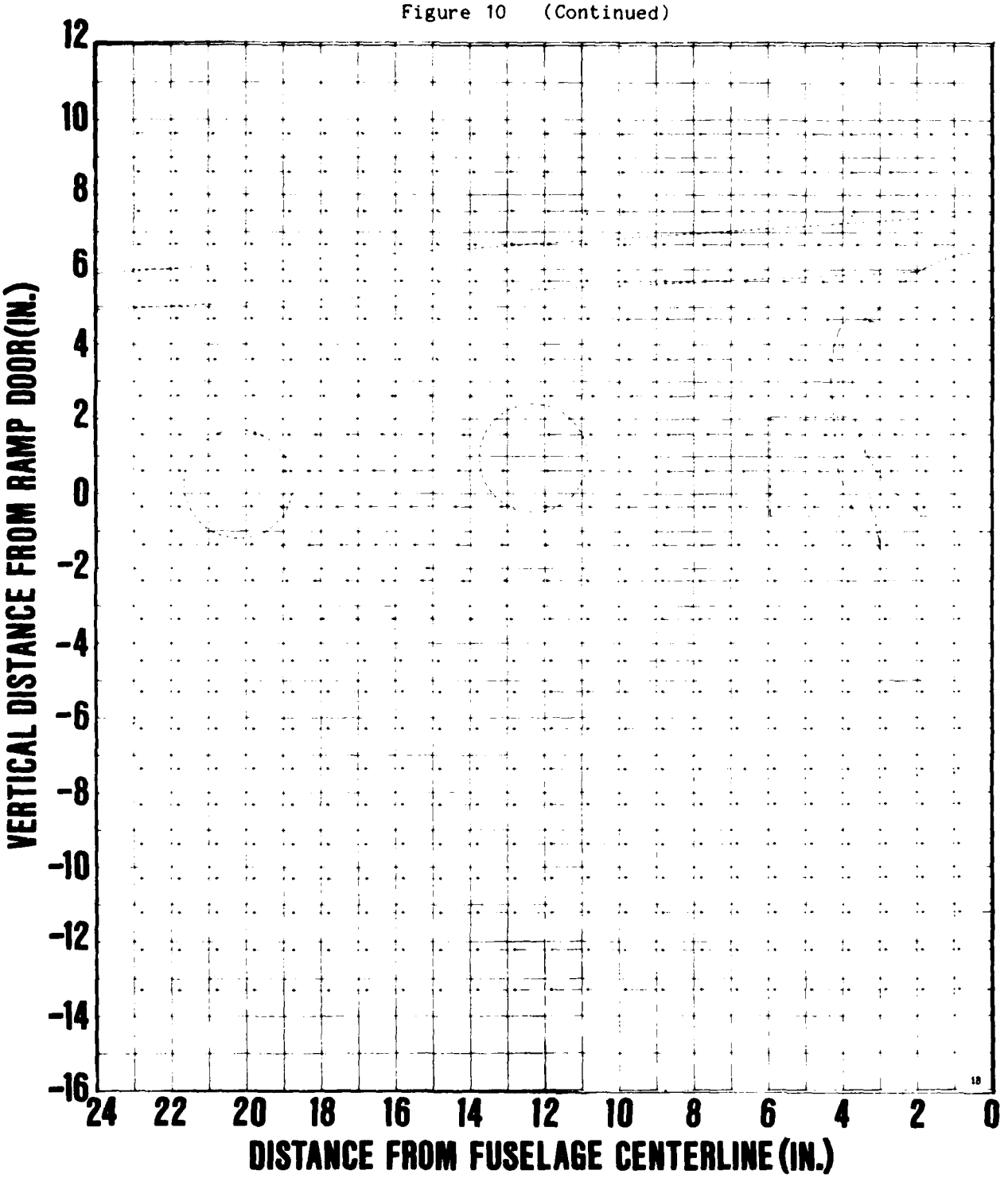

Figure 10e - X Position = 38.2 in. Downstream from Ramp Door;
Flap Setting = 10 deg

Figure 10 (Continued)

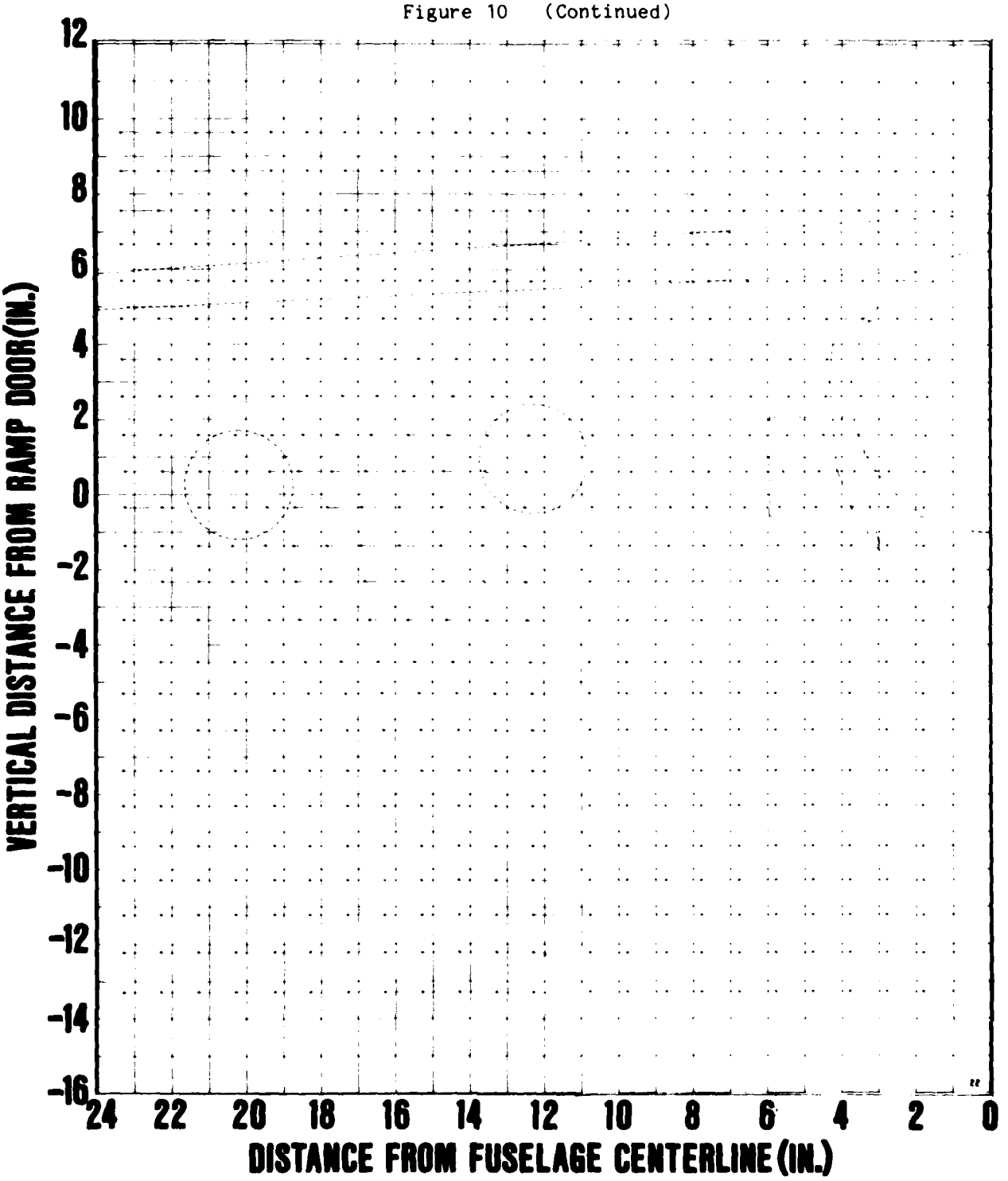

Figure 10f - X Position = 56.8 in. Downstream from Ramp Door; Flap Setting = 10 deg

Figure 10 (Continued)

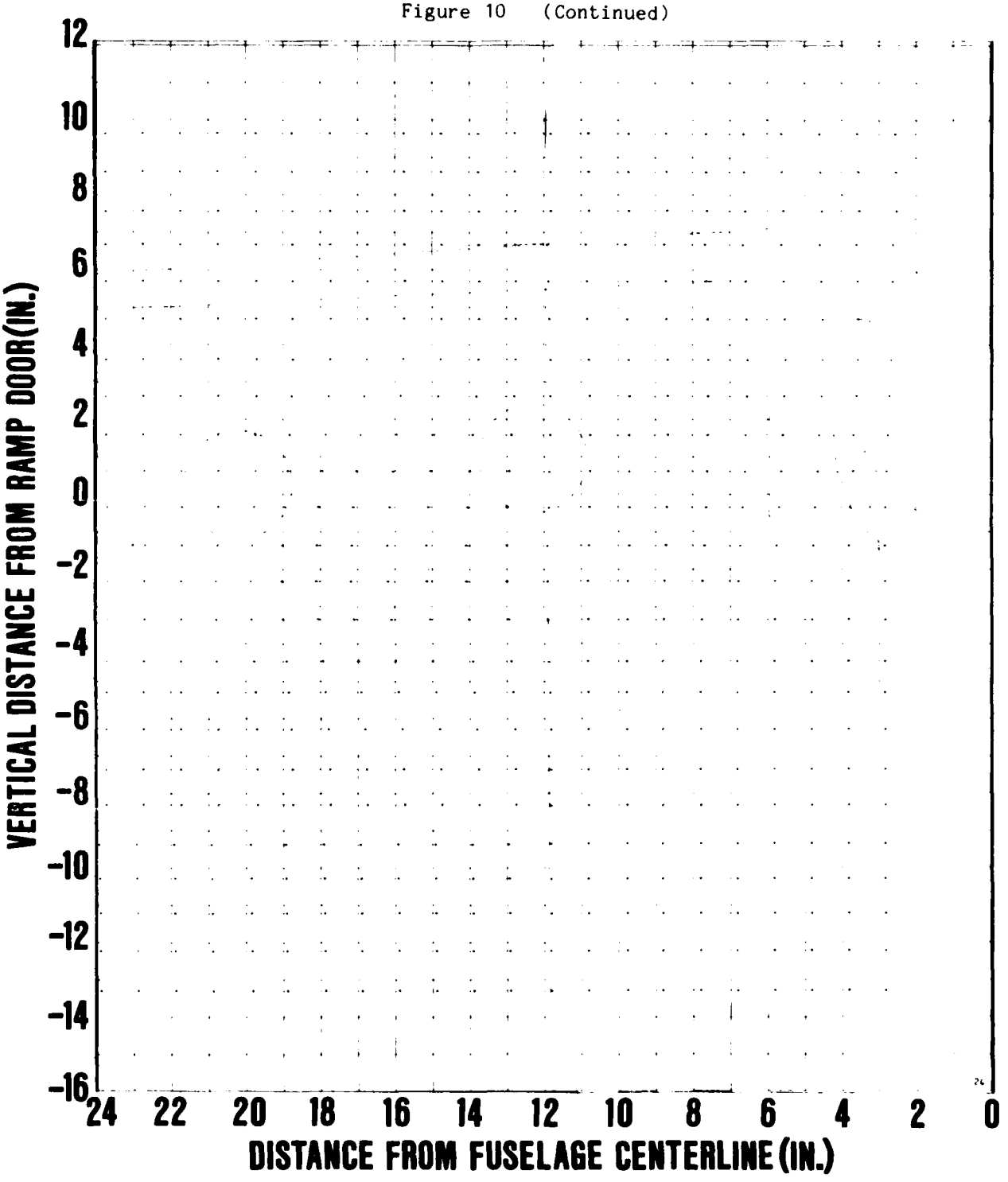

Figure 10g - X Position = 76.3 in. Downstream from Ramp Door;
Flap Setting = 10 deg

Figure 10 (Continued)

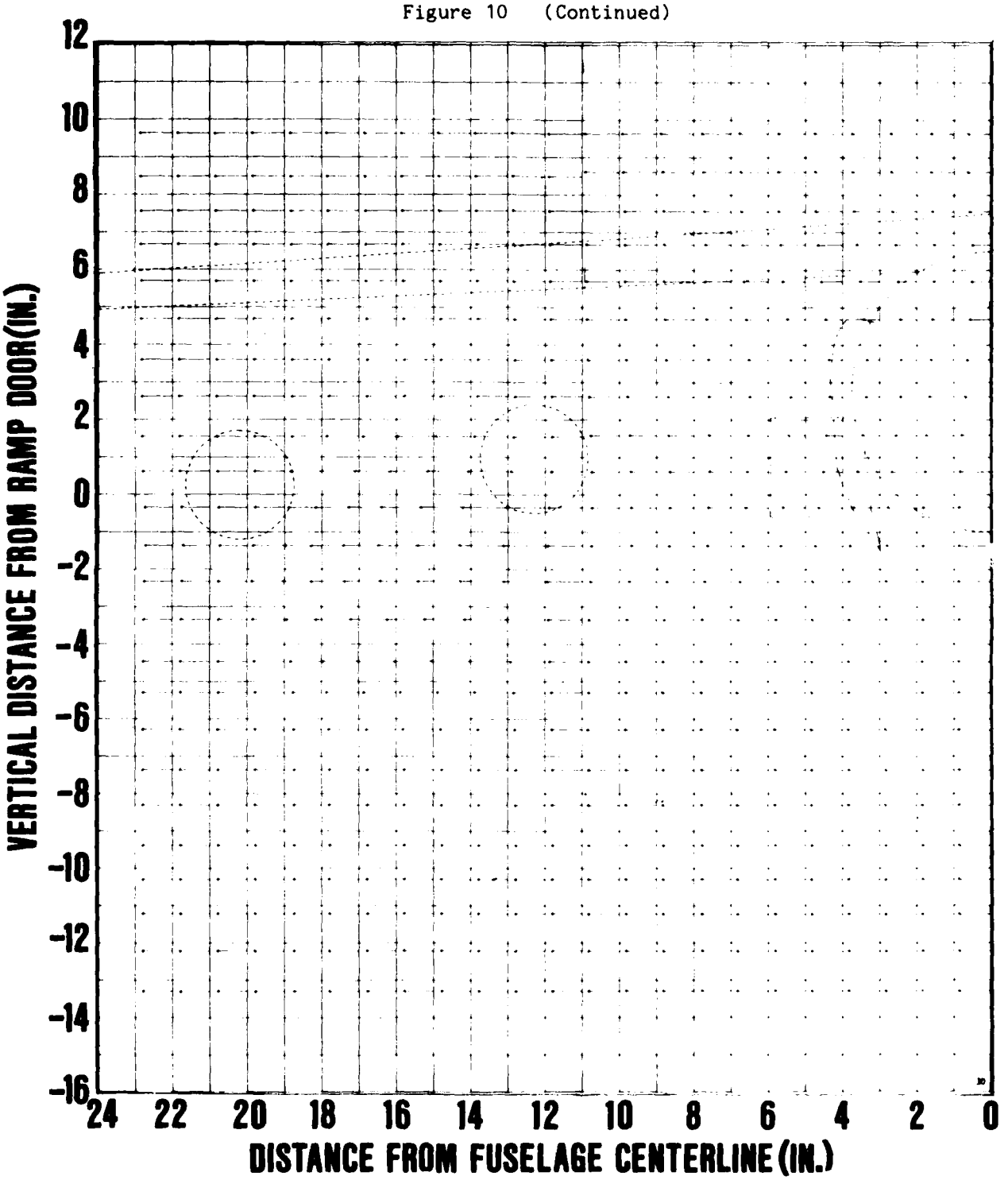

Figure 10h - X Position = 38.2 in. Downstream from Ramp Door;
Flap Setting = 20 deg

Figure 10 (Continued)

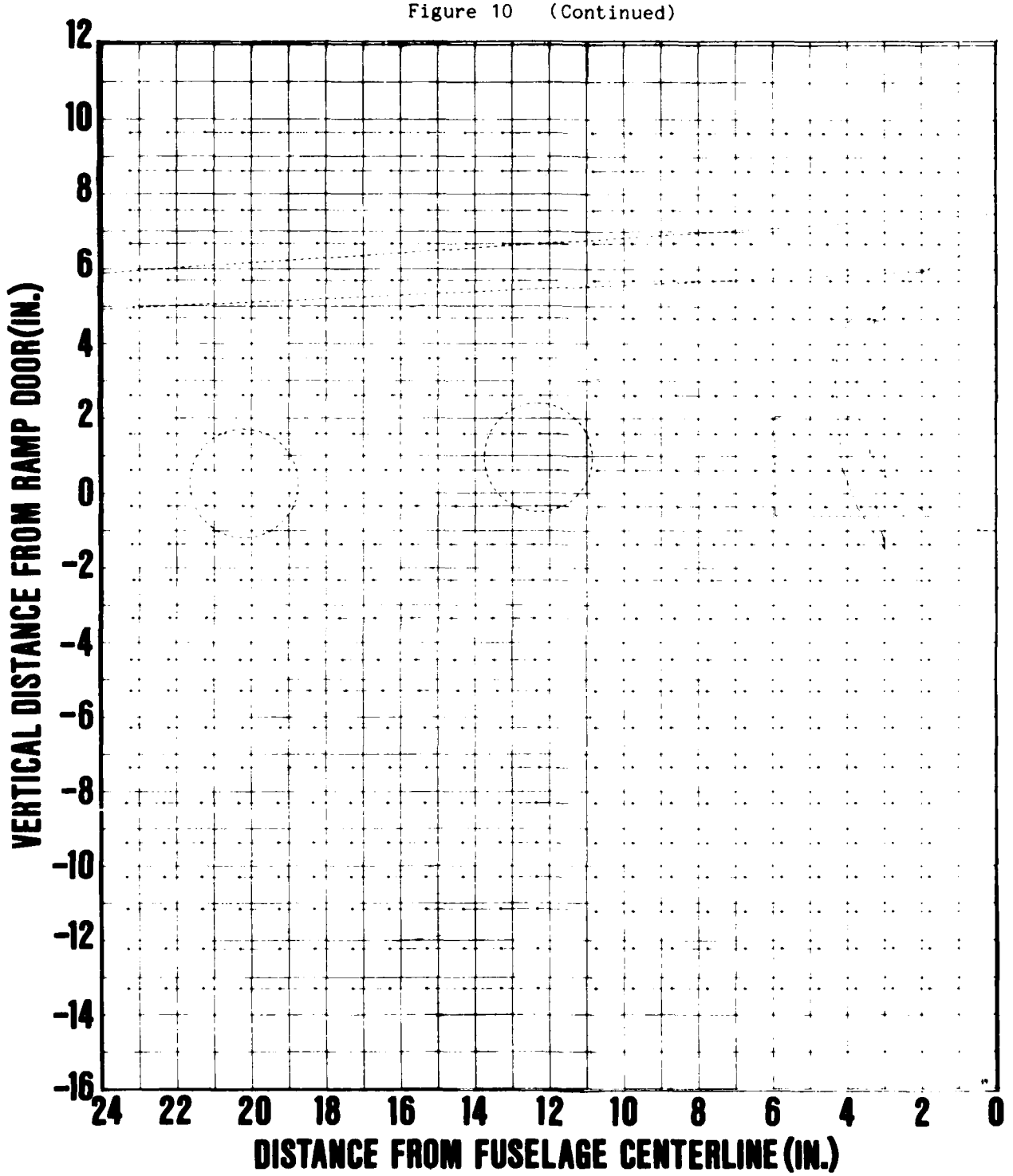

Figure 10i - X Position = 56.8 in. Downstream from Ramp Door; Flap Setting = 20 deg

Figure 10 (Continued)

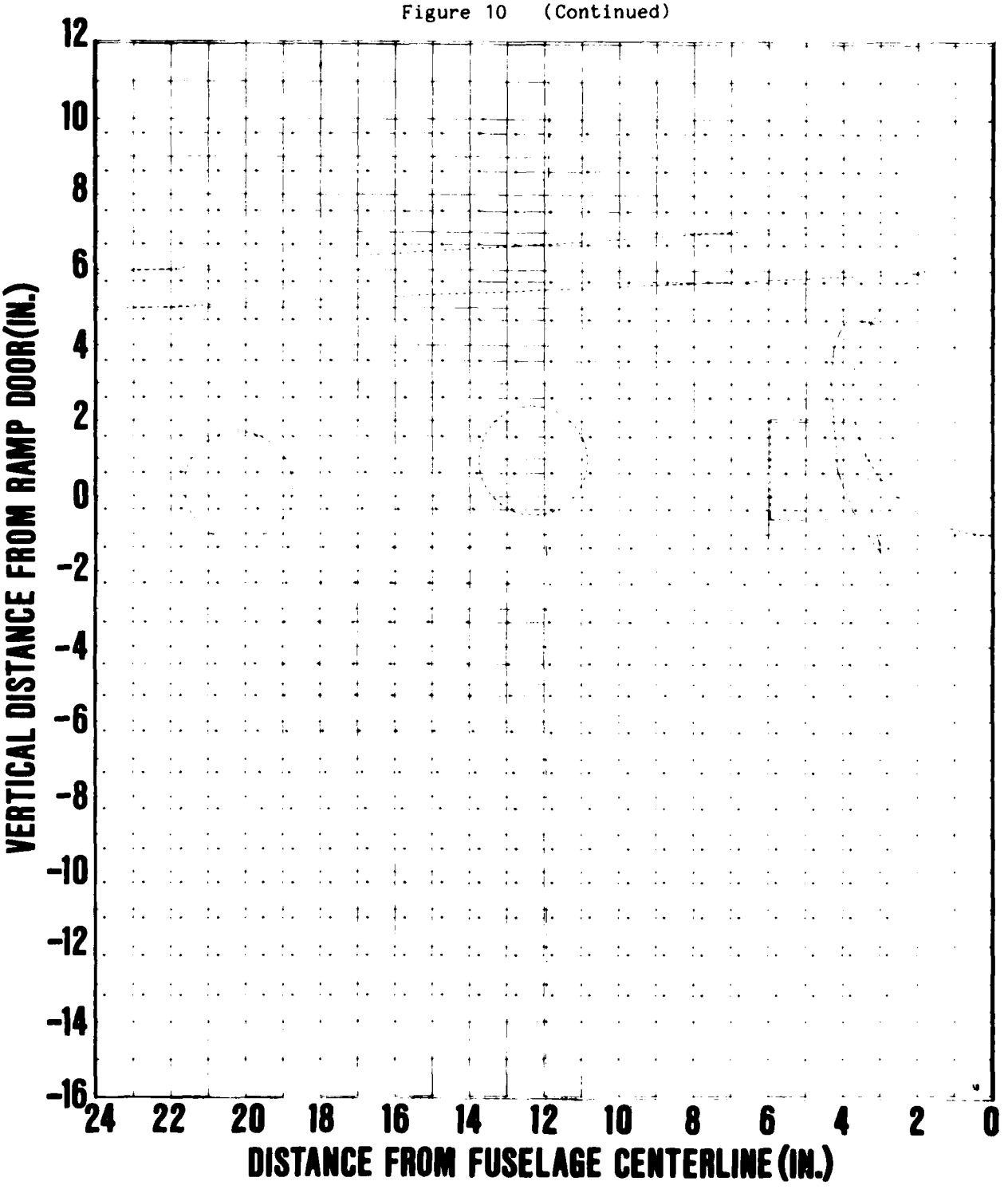

Figure 10j - X Position = 76.4 in. Downstream from Ramp Door; Flap Setting = 20 deg

Figure 10 (Continued)

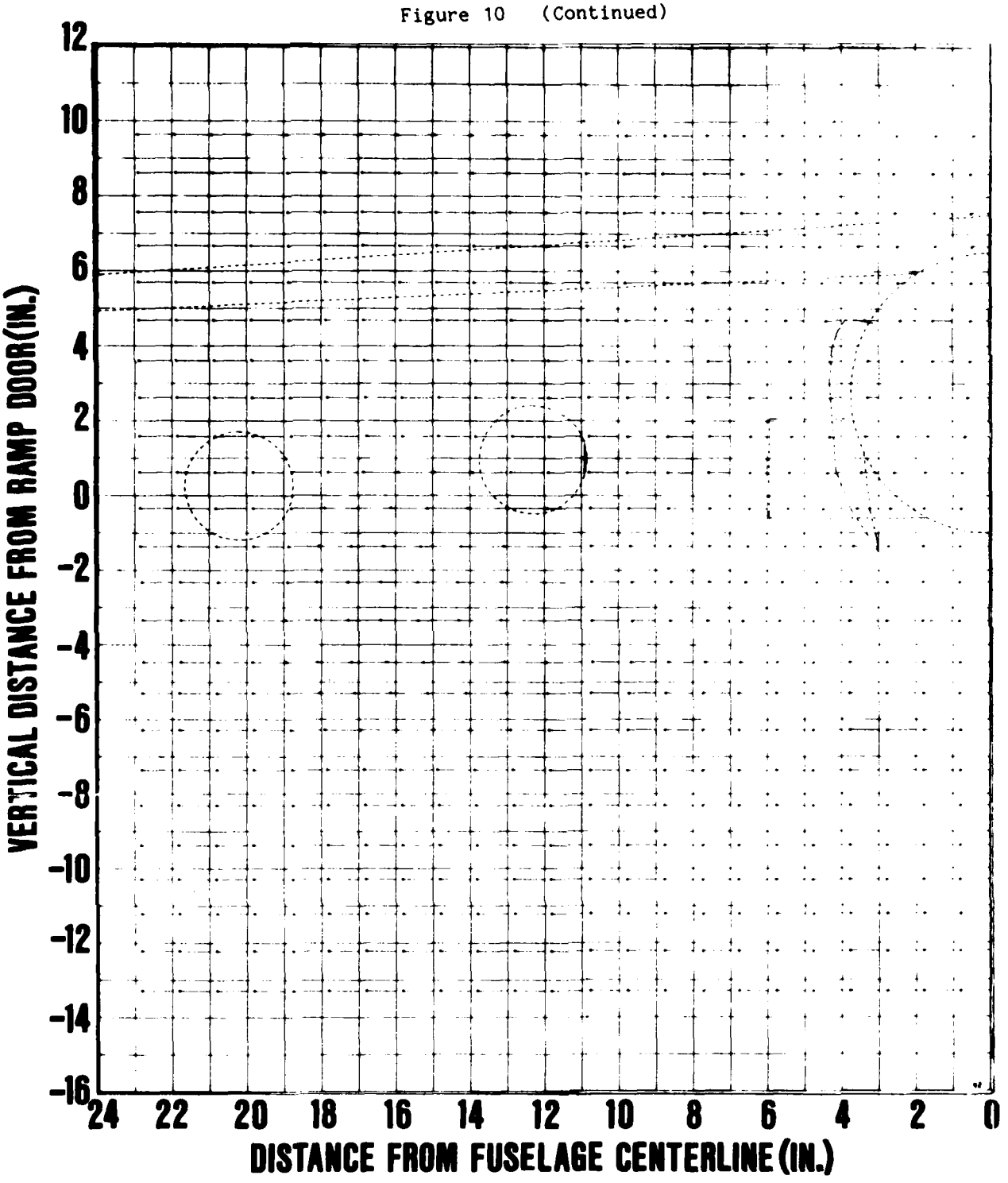

Figure 10k - X Position = 38.2 in. Downstream from Ramp Door;
Flap Setting = 30 deg

Figure 10 (Continued)

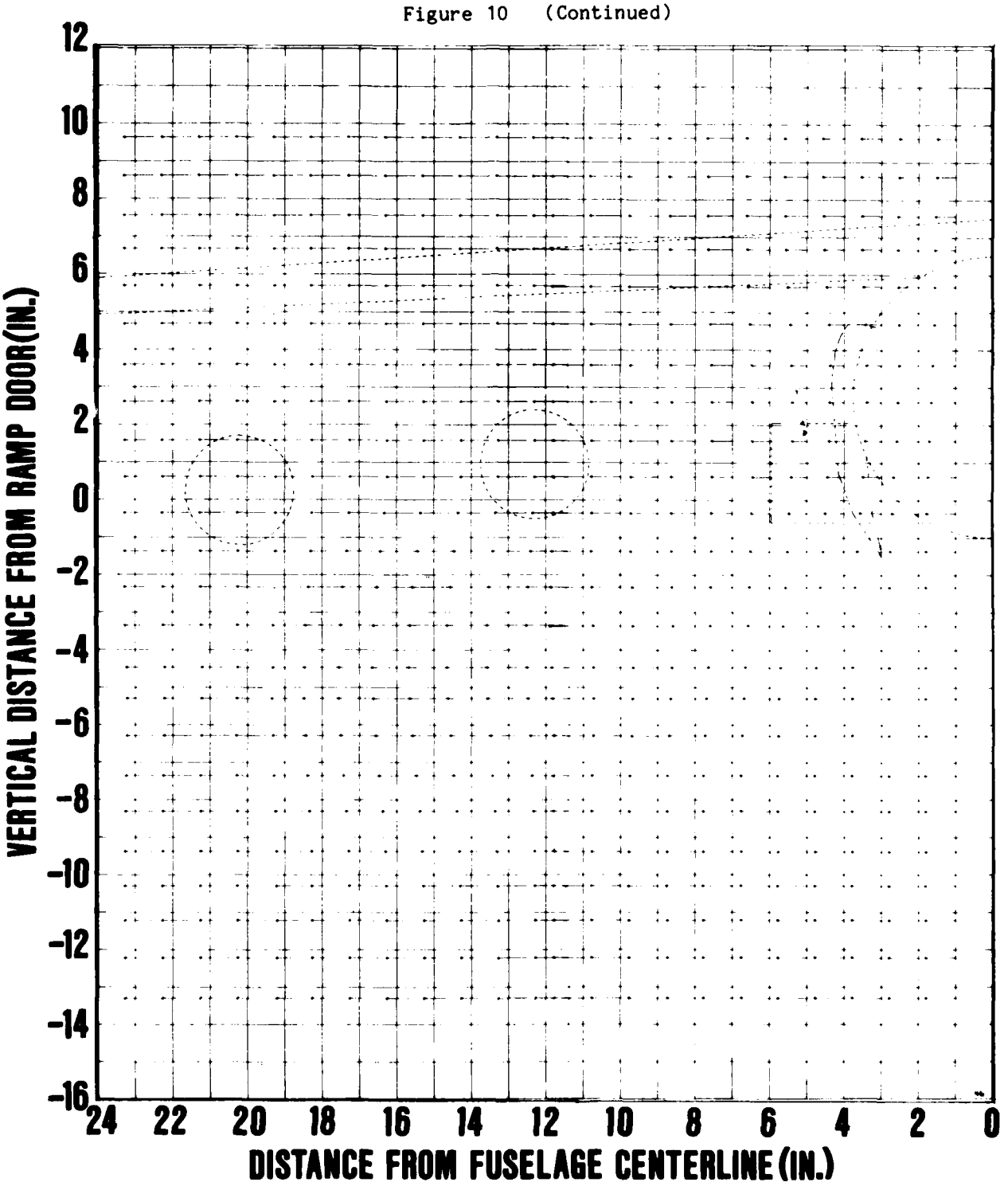

Figure 101 - X Position = 56.8 in. Downstream from Ramp Door;
Flap Setting = 30 deg

Figure 10 (Continued)

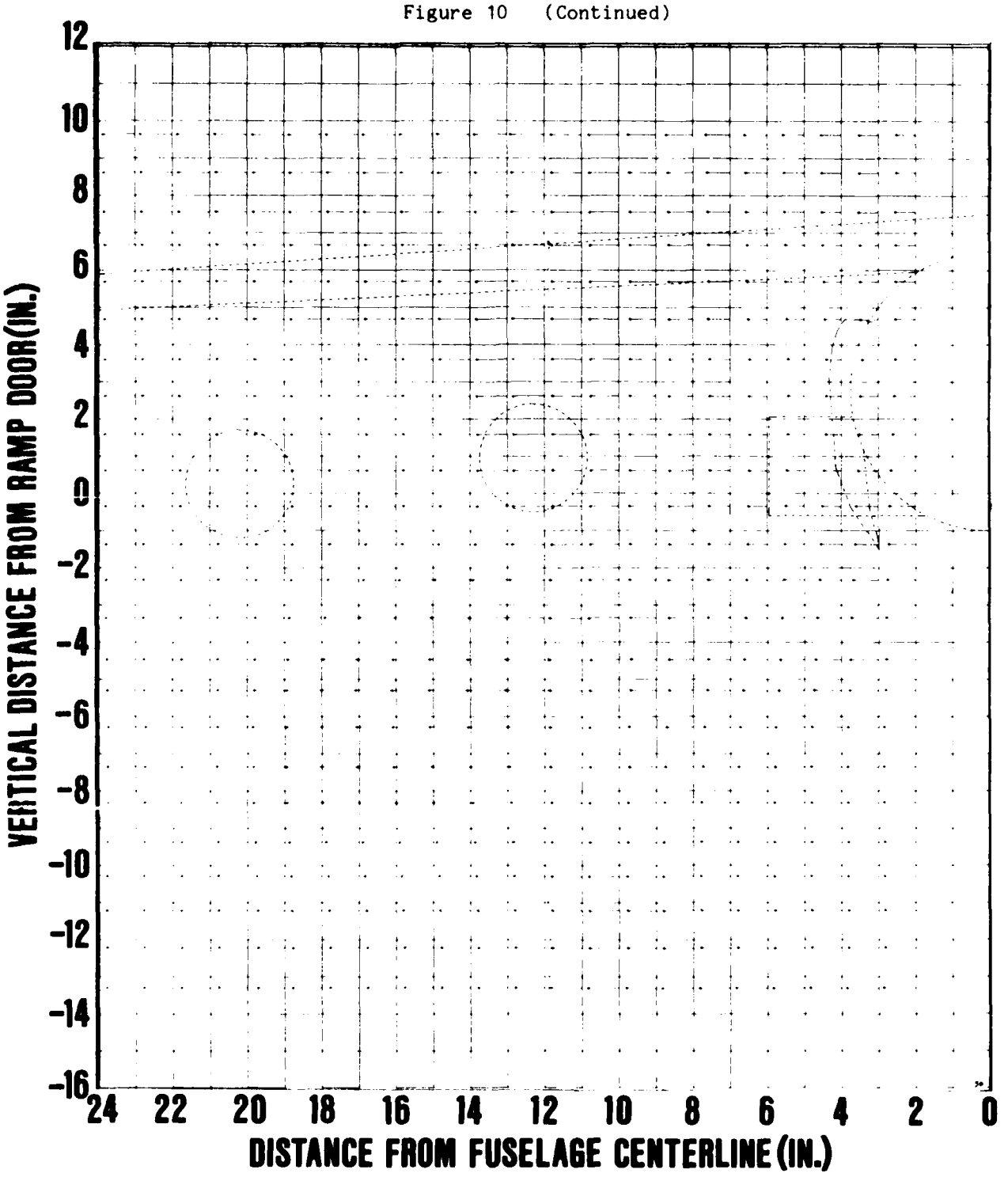

Figure 10m - X Position = 76.3 in. Downstream from Ramp Door;
Flap Setting = 30 deg

Figure 10 (Continued)

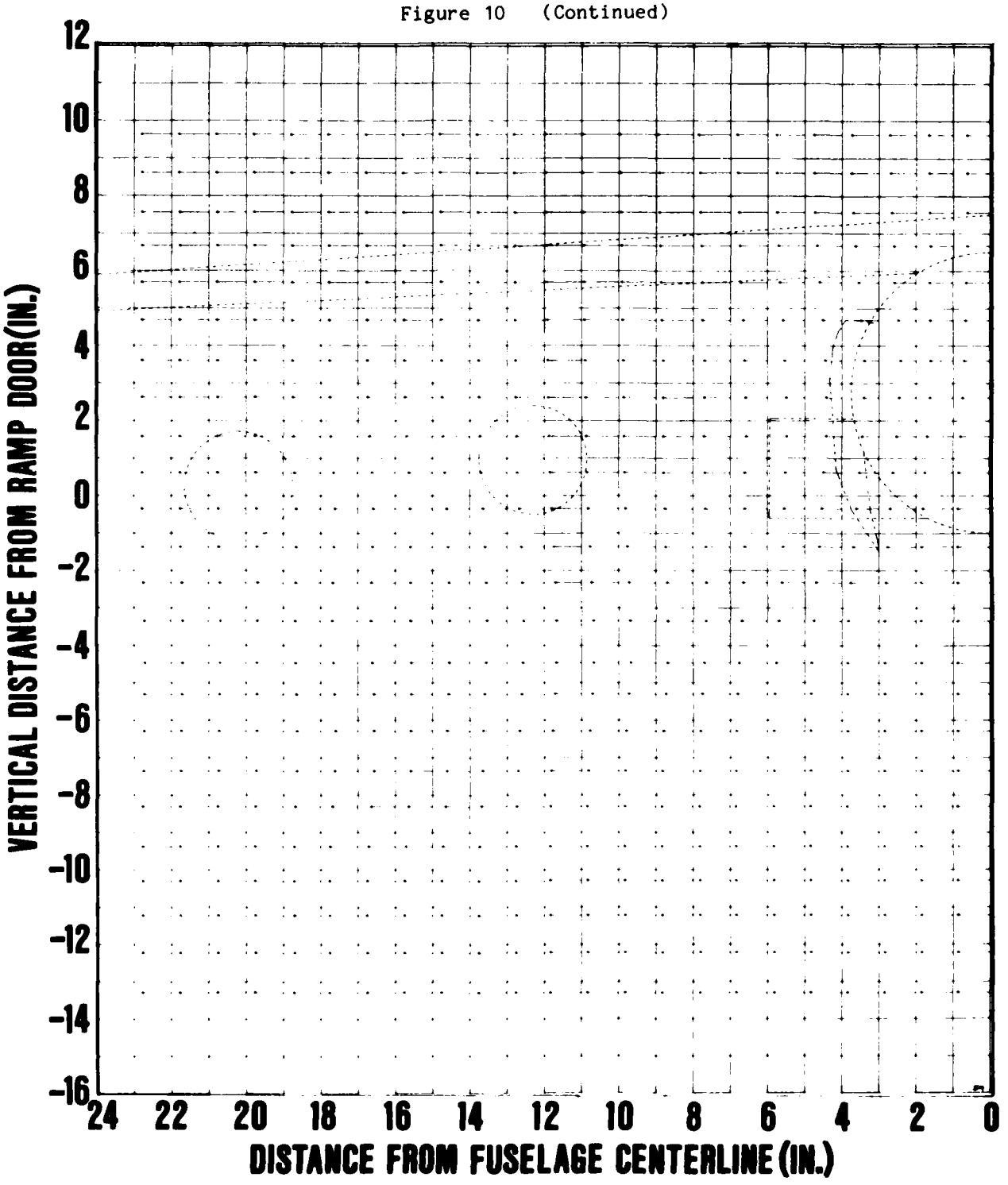

Figure 10n - X Position = 38.2 in. Downstream from Ramp Door;
Flap Setting = 30 deg; No Thrust Simulation

Figure 11 - Y-Z Vorticity Component Plot of C-141B Wake; Varying X Distance and Flap Angle Setting (V_{Tunnel} = 200 ft/sec, Vector Magnitude Y Component 100 ft/sec/grid, Z Component 150 ft/sec/grid)

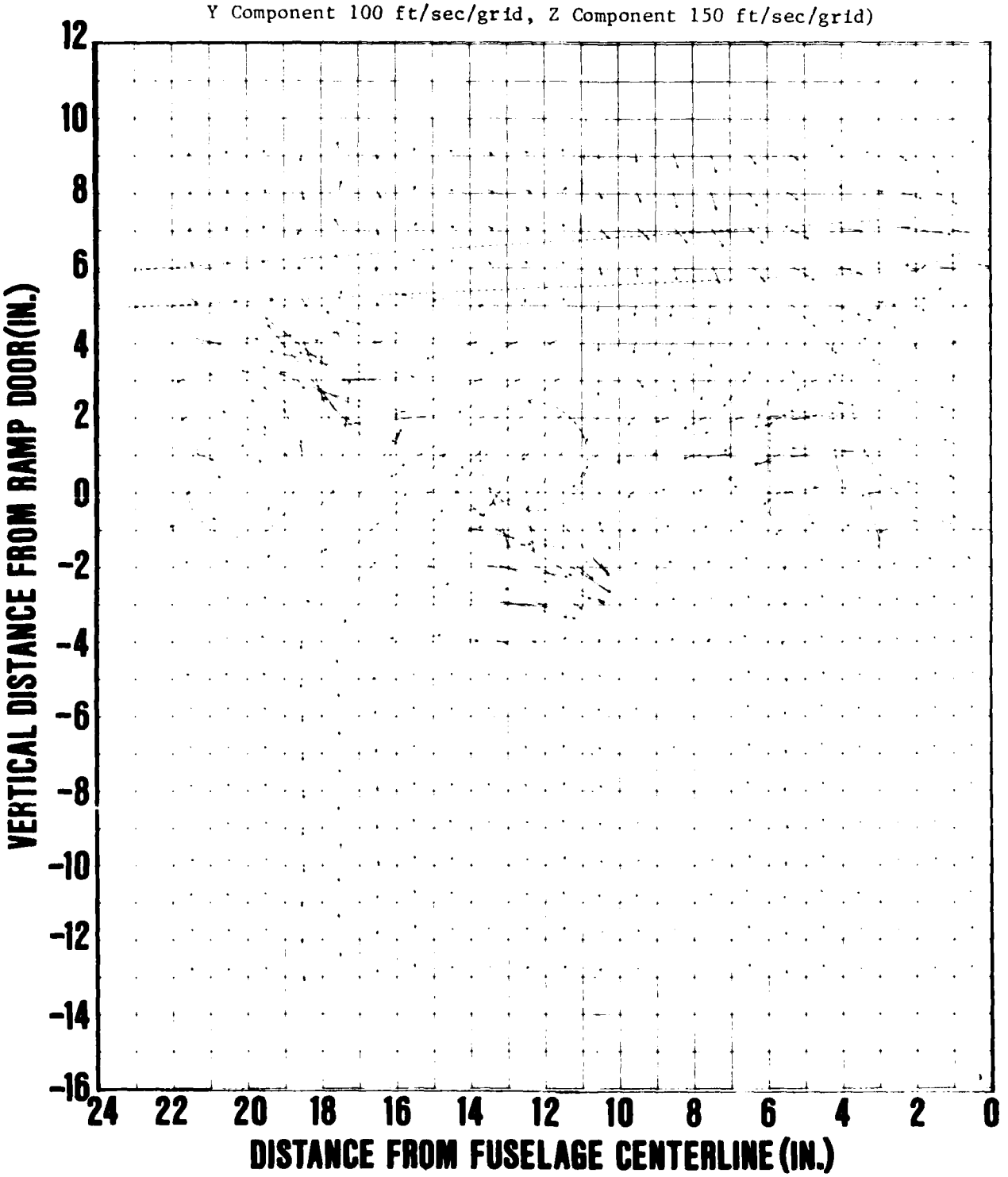

Figure 11a - X Position = 38.7 in. Downstream from Ramp Door; Flap Setting = 0 deg

Figure 11 (Continued)

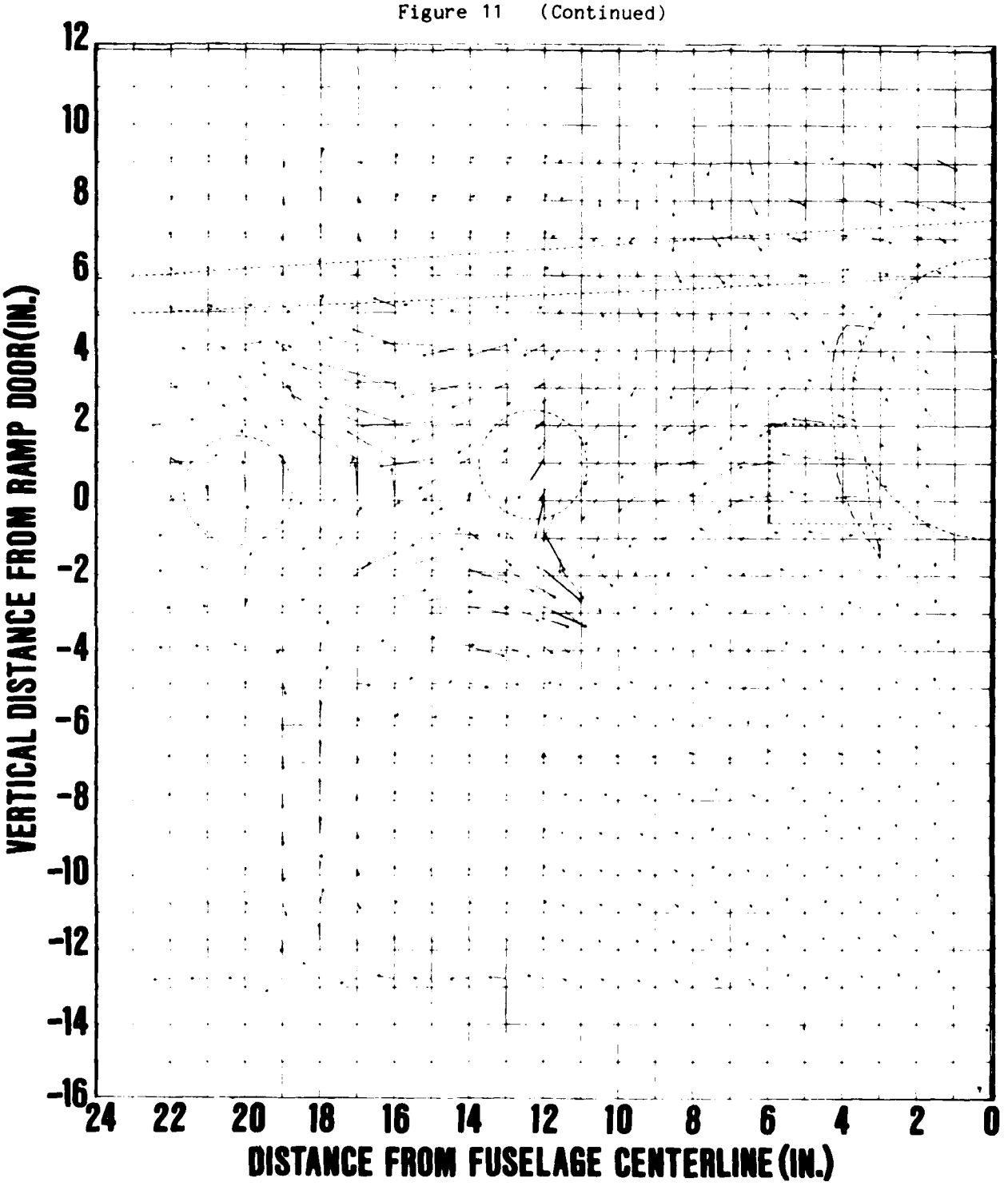

Figure 11b - X Position = 57.2 in. Downstream from Ramp Door;
Flap Setting = 0 deg

Figure 11 (Continued)

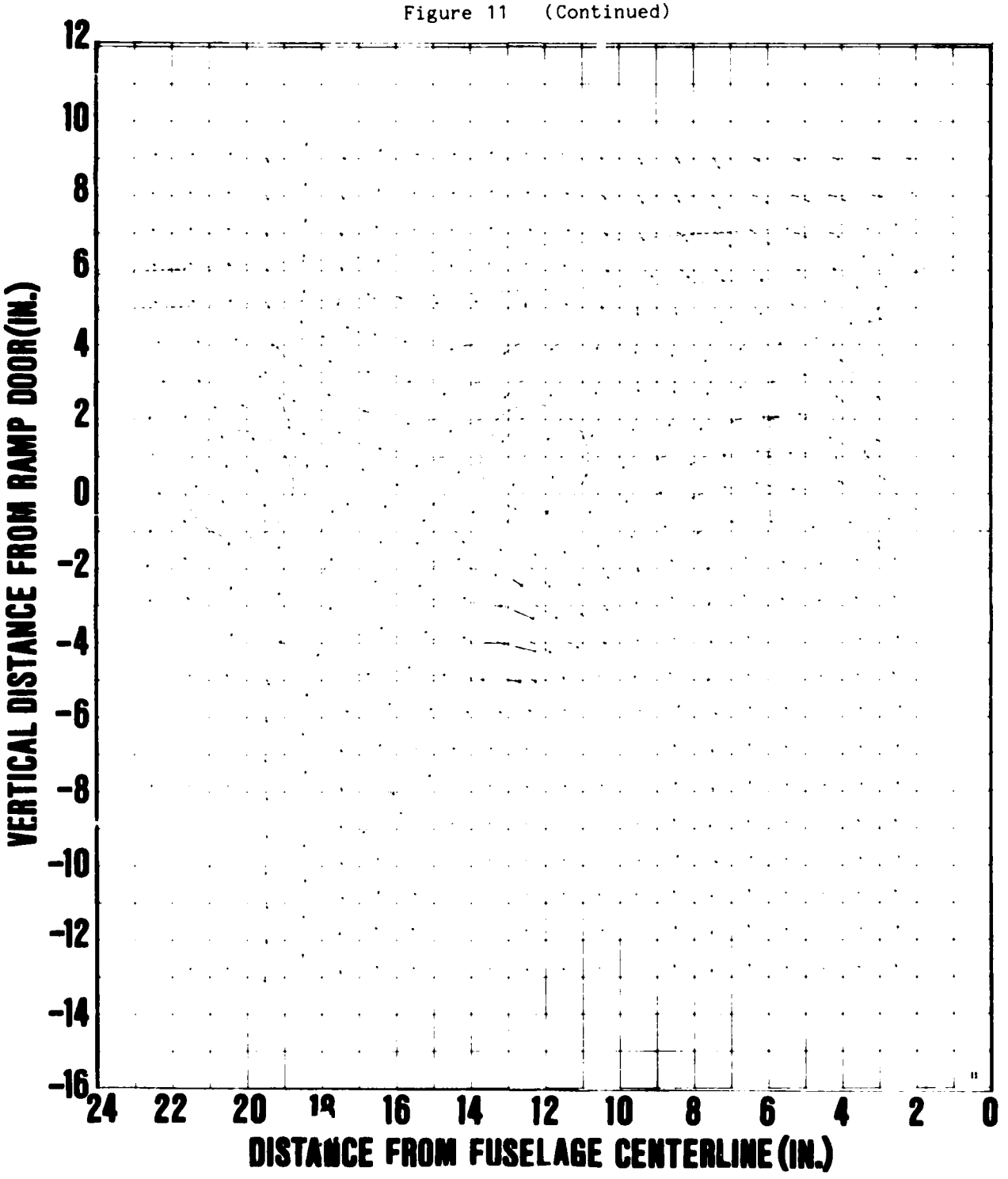

Figure 11c - X Position = 76.8 in. Downstream from Ramp Door;
Flap Setting = 0 deg

Figure 11 (Continued)

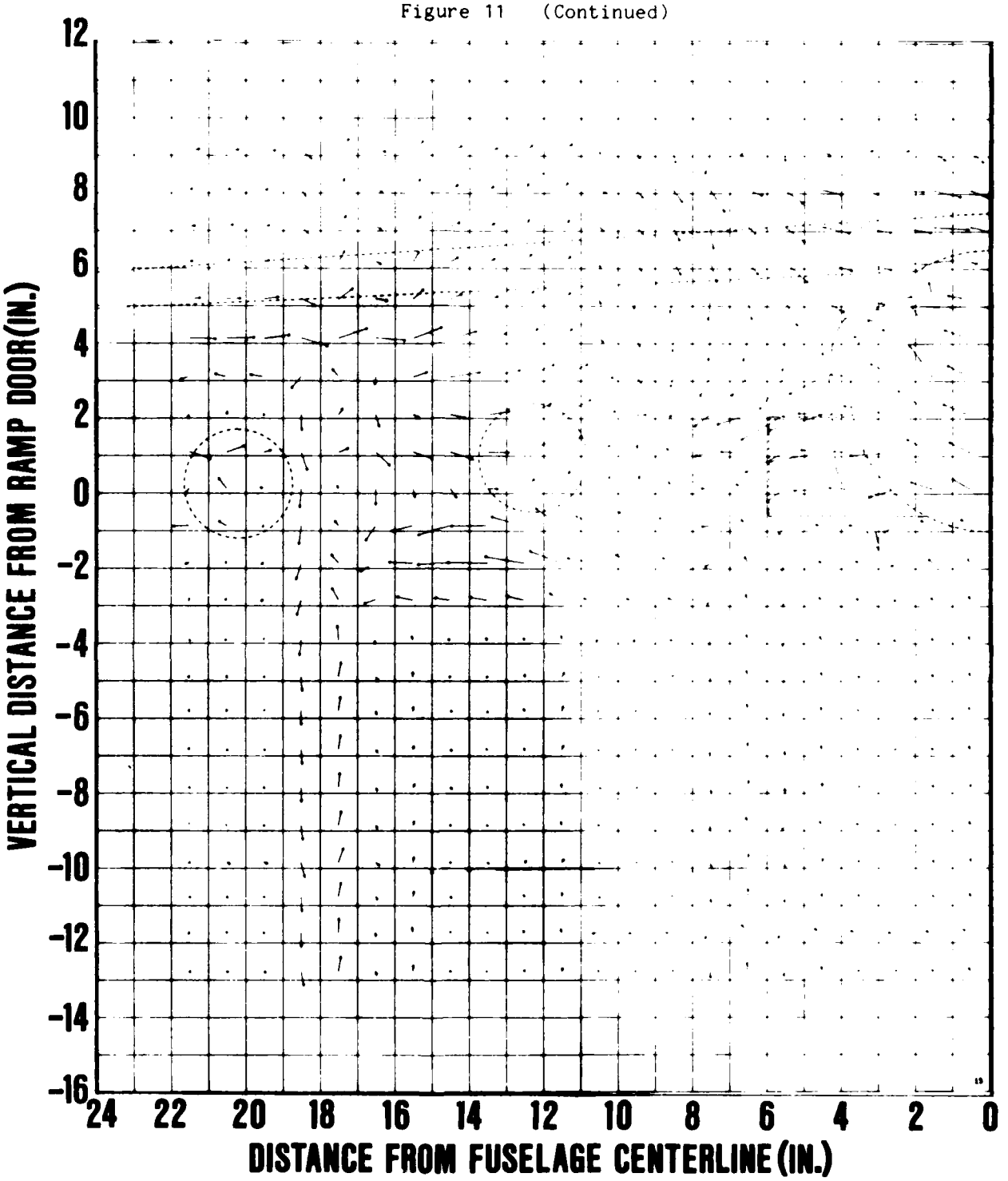

Figure 11d - X Position = 38.7 in. Downstream from Ramp Door;
Flap Setting = 0 deg; No Thrust Simulation

Figure 11 (Continued)

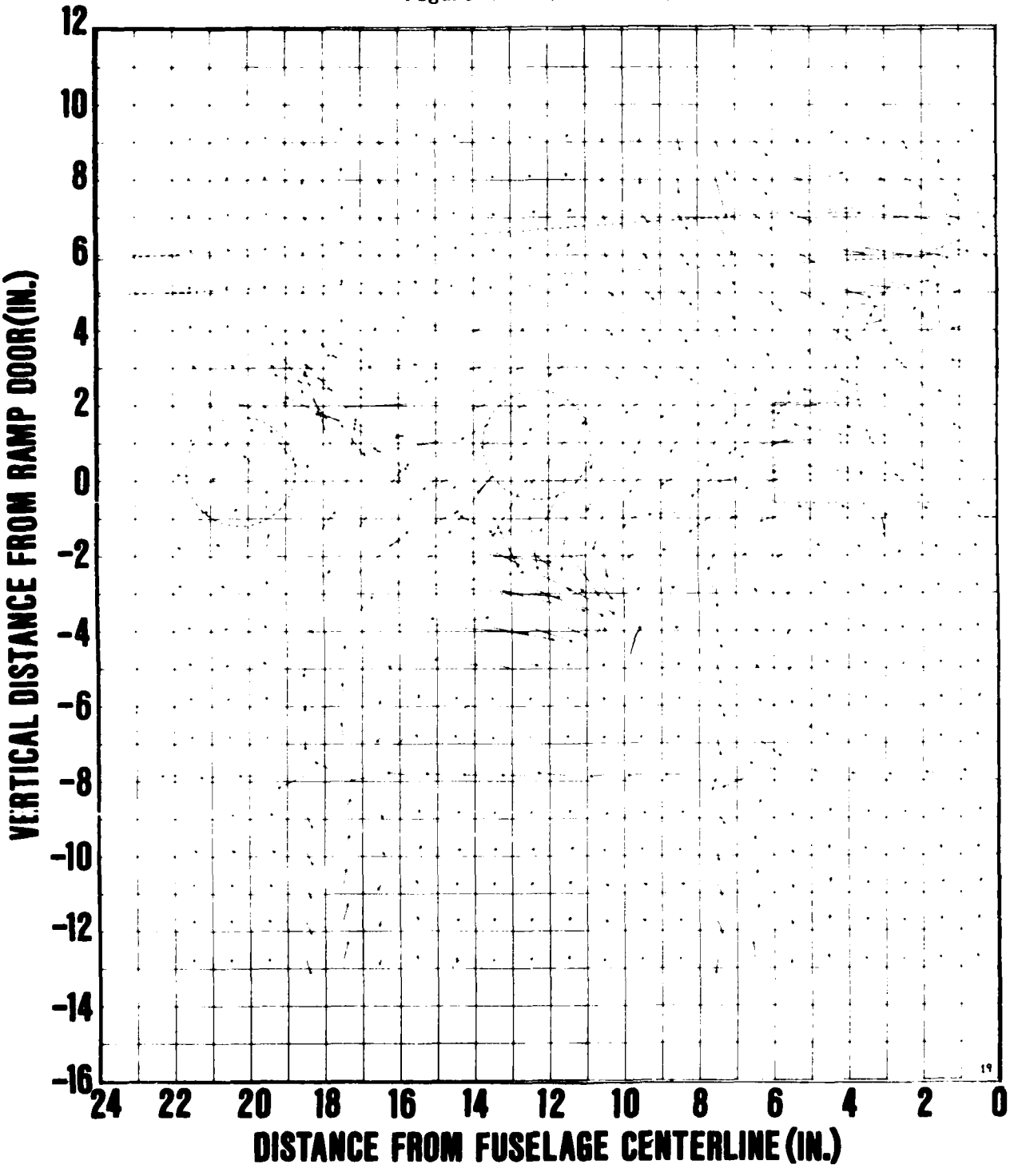

Figure 11e - X Position = 38.7 in. Downstream from Ramp Door;
Flap Setting = 10 deg

Figure 11 (Continued)

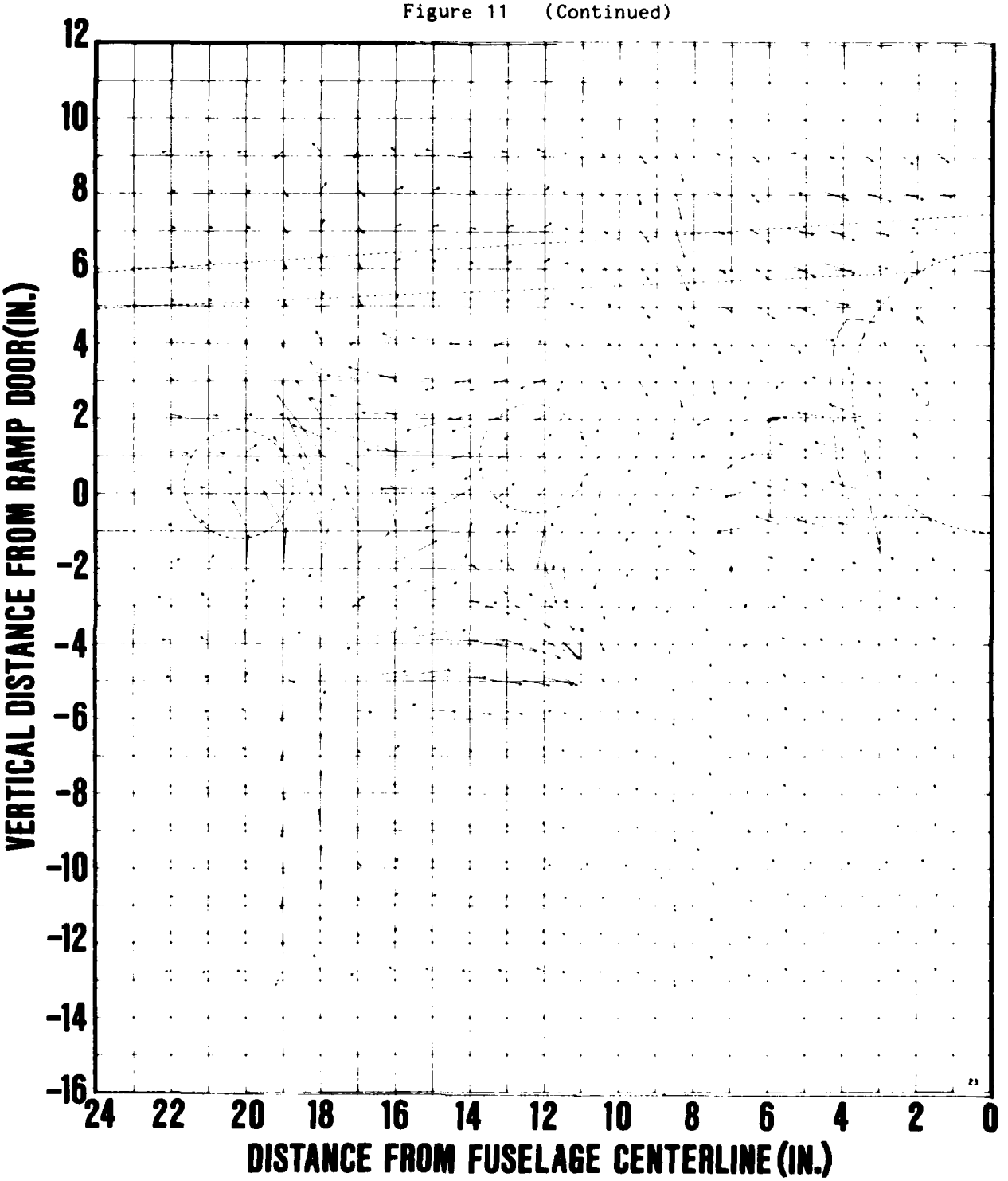

Figure 11f - X Position = 57.3 in. Downstream from Ramp Door;
Flap Setting = 10 deg

Figure 11 (Continued)

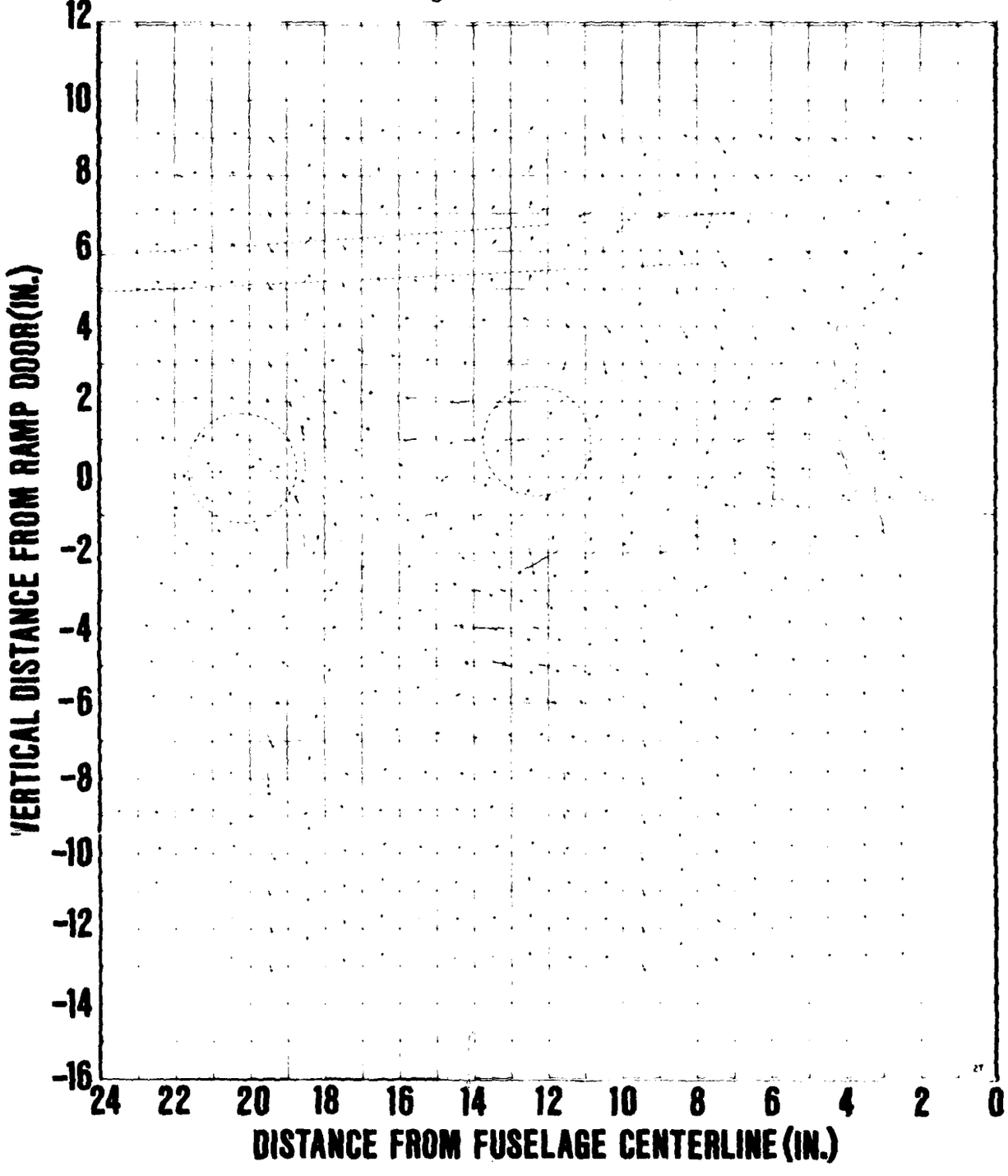

Figure 11g - X Position = 76.8 in. Downstream from Ramp Door;
Flap Setting = 10 deg

Figure 11 (Continued)

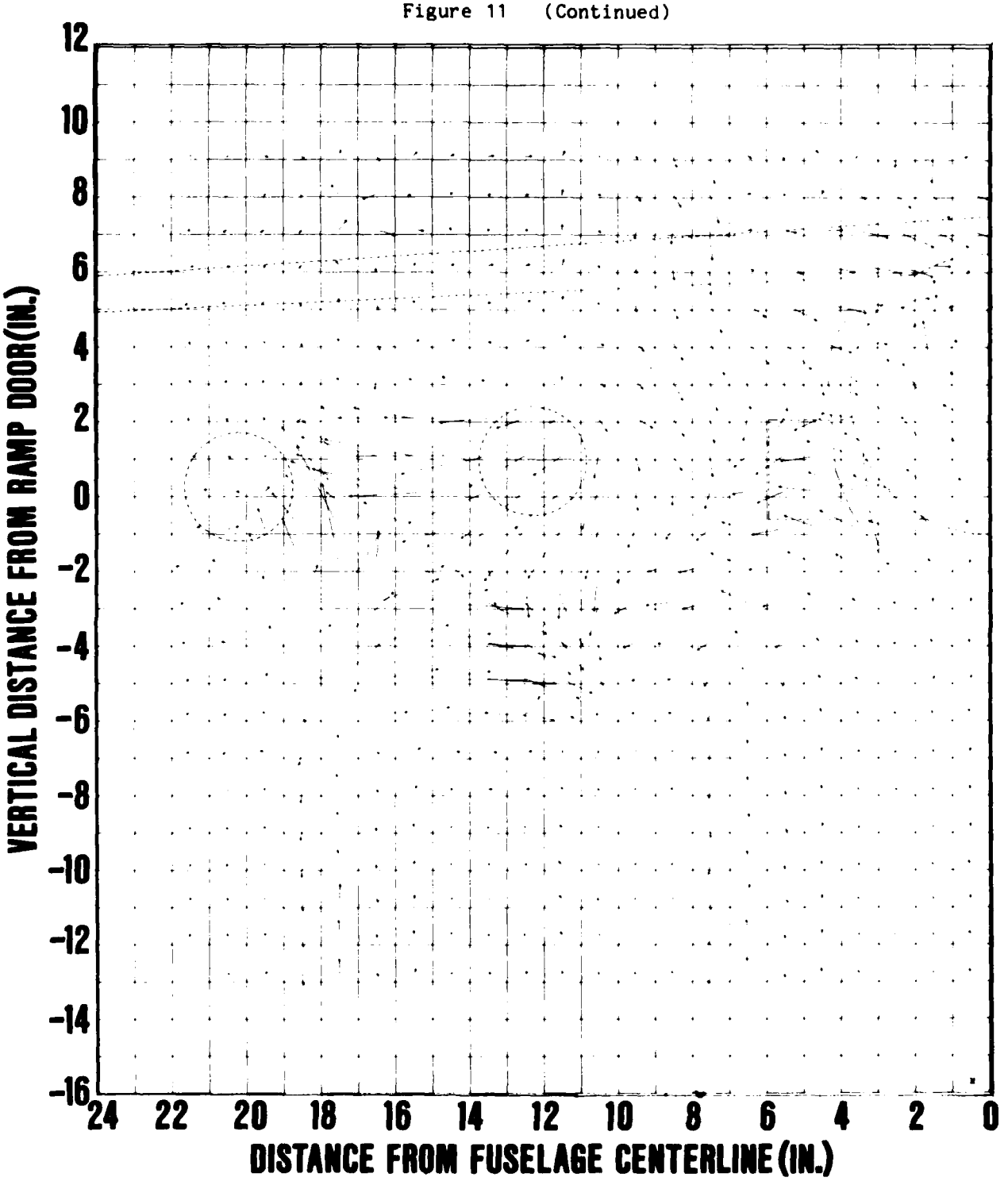

Figure 11h - X Position = 38.7 in. Downstream from Ramp Door; Flap Setting = 20 deg

Figure 11 (Continued)

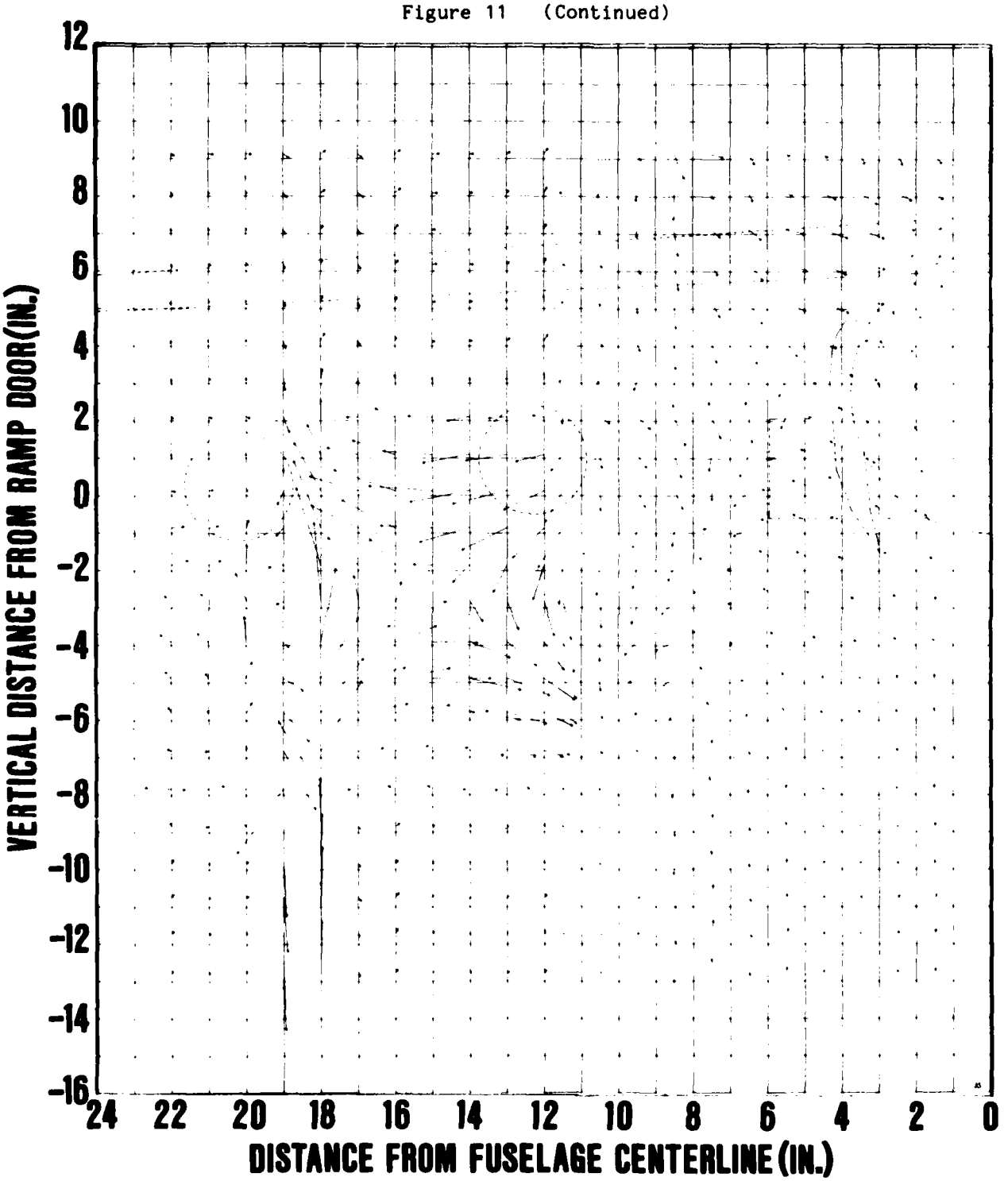

Figure 11i - X Position = 57.3 in. Downstream from Ramp Door;
Flap Setting = 20 deg

Figure 11 (Continued)

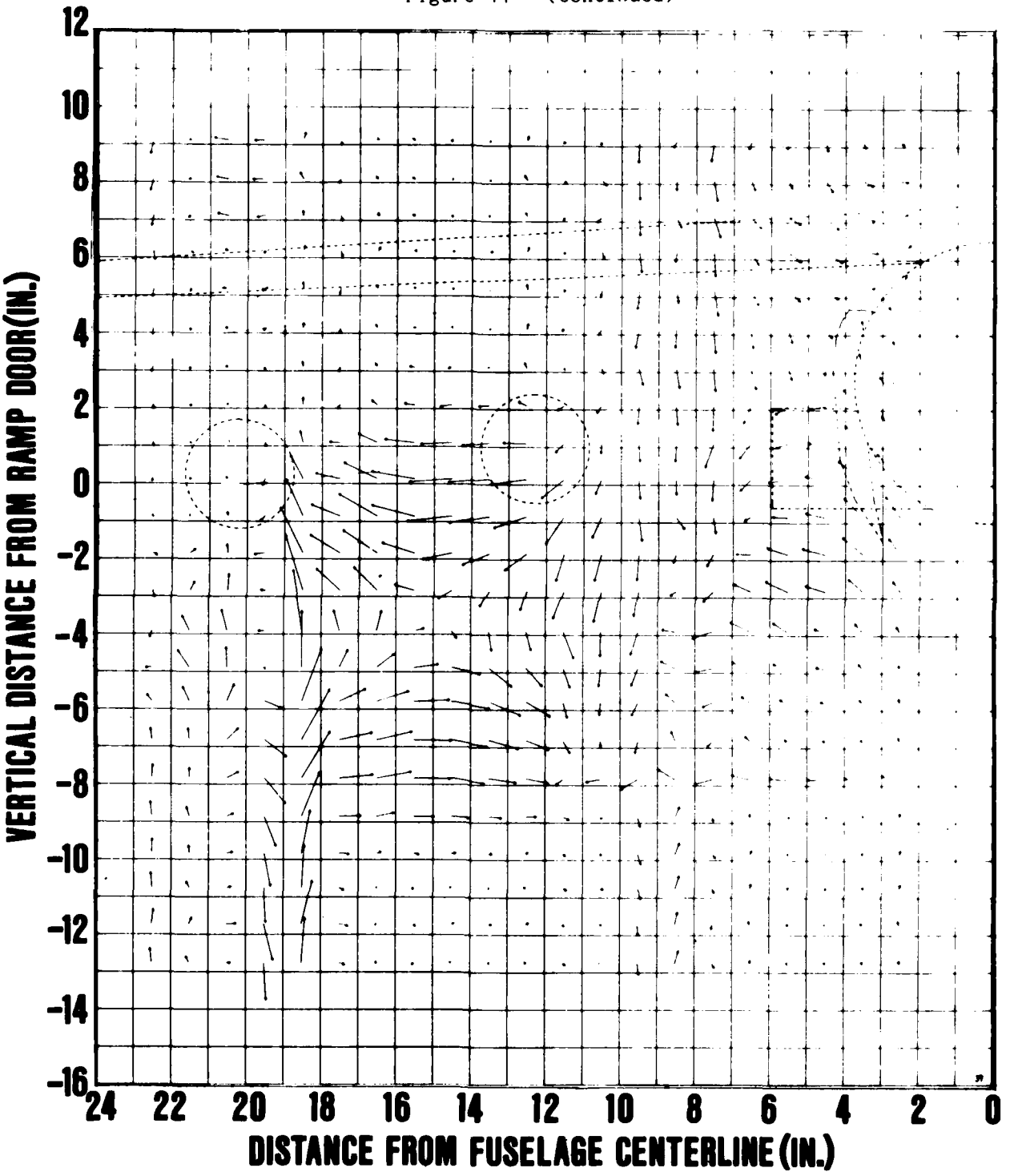

Figure 11j - X Position = 76.9 in. Downstream from Ramp Door;
Flap Setting = 20 deg

Figure 11 (Continued)

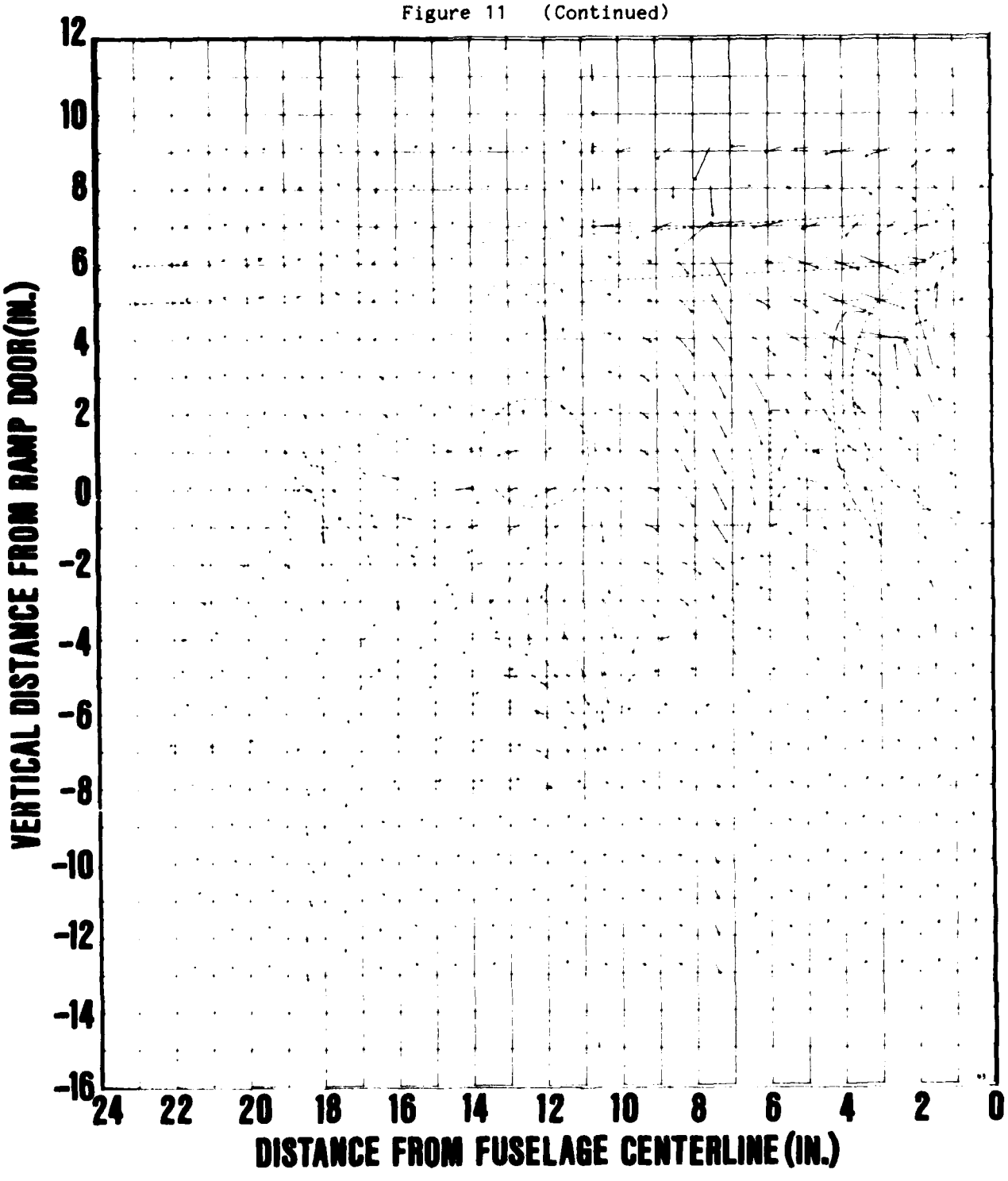

Figure 11k - X Position = 38.7 in. Downstream from Ramp Door;
Flap Setting = 30 deg

Figure 11 (Continued)

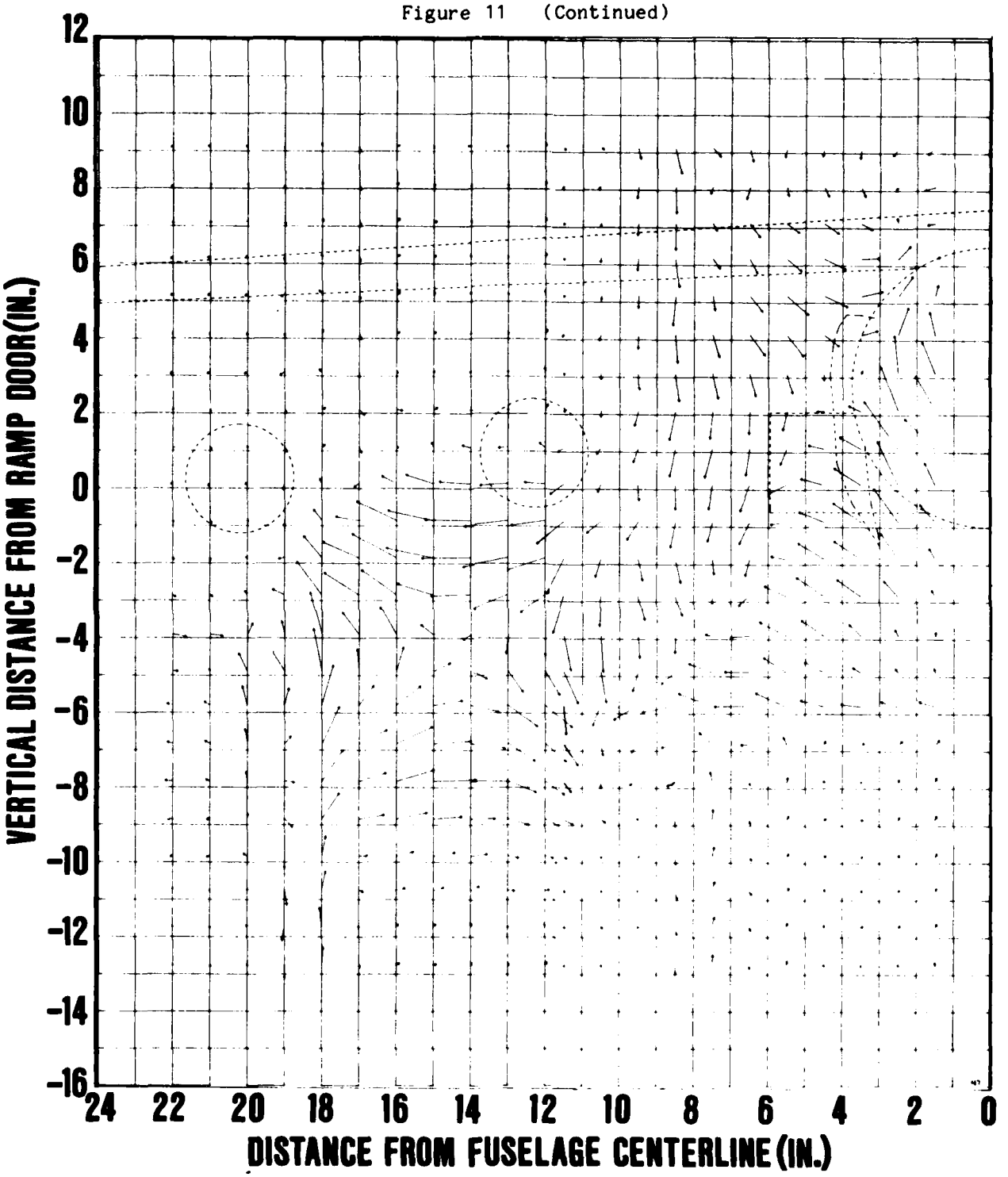

Figure 111 - X Position = 57.3 in. Downstream from Ramp Door;
Flap Setting = 30 deg

Figure 11 (Continued)

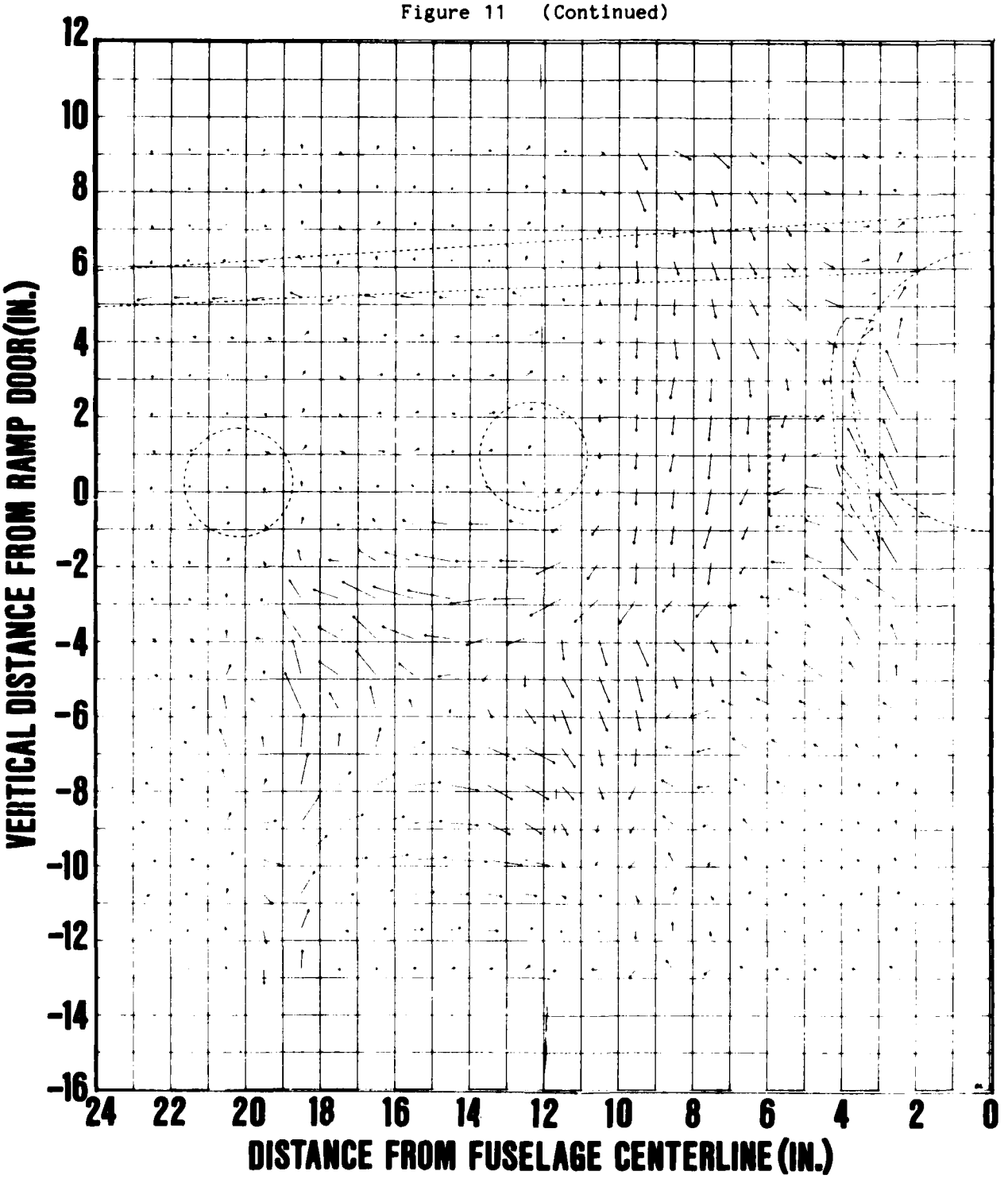

Figure 11m - X Position = 76.6 in. Downstream from Ramp Door;
Flap Setting = 30 deg

Figure 11 (Continued)

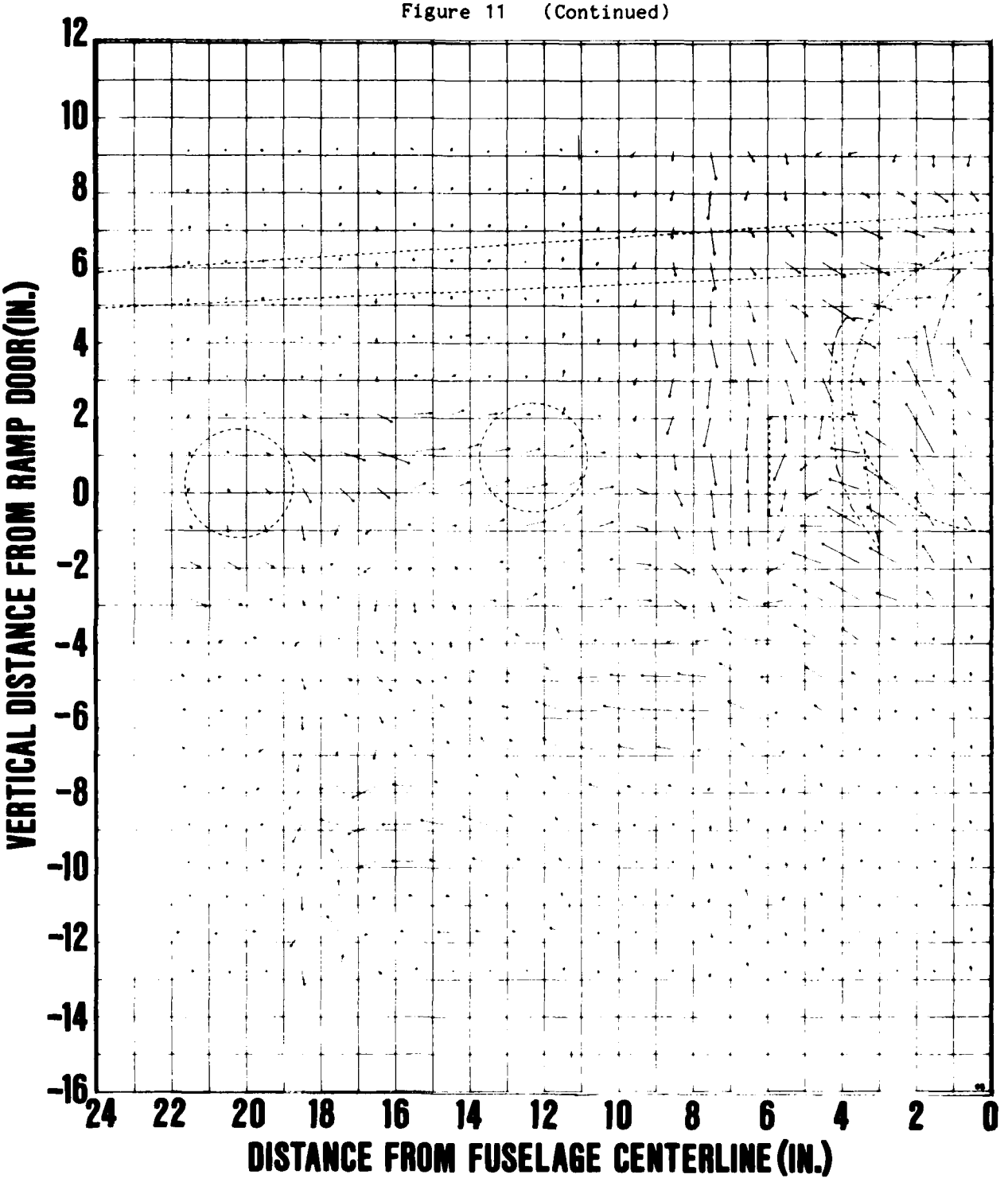

Figure 11n - X Position = 38.7 in. Downstream from Ramp Door; Flap Setting = 30 deg; No Thrust Simulation

Figure 12 - X Vorticity Component Plot of C-141B Wake; Varying X Distance and Flap Angle Setting (V_{Tunnel} = 200 ft/sec, Vector Magnitude 100 ft/sec/grid)

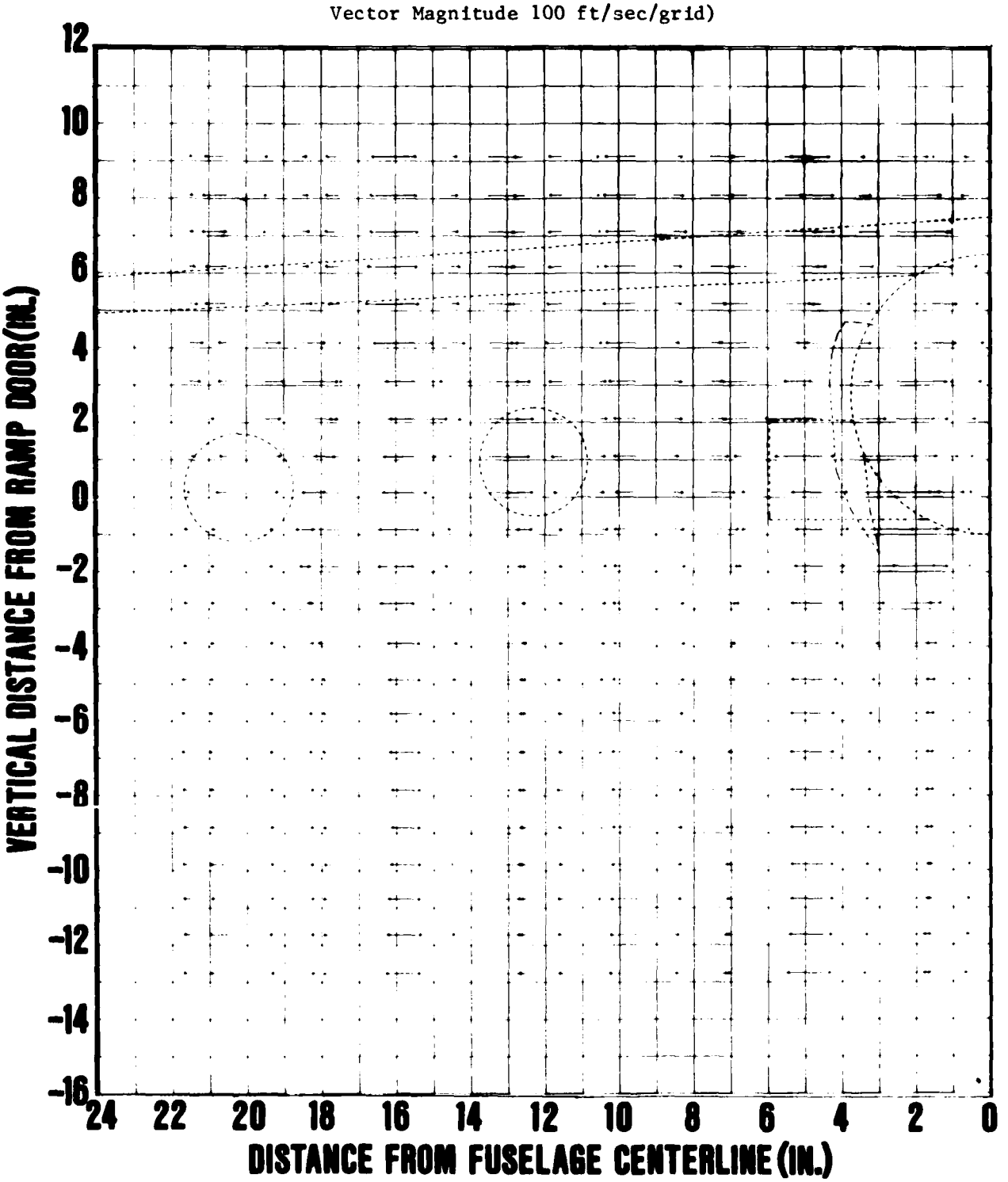

Figure 12a - X Position = 38.7 in. Downstream from Ramp Door; Flap Setting = 0 deg

Figure 12 (Continued)

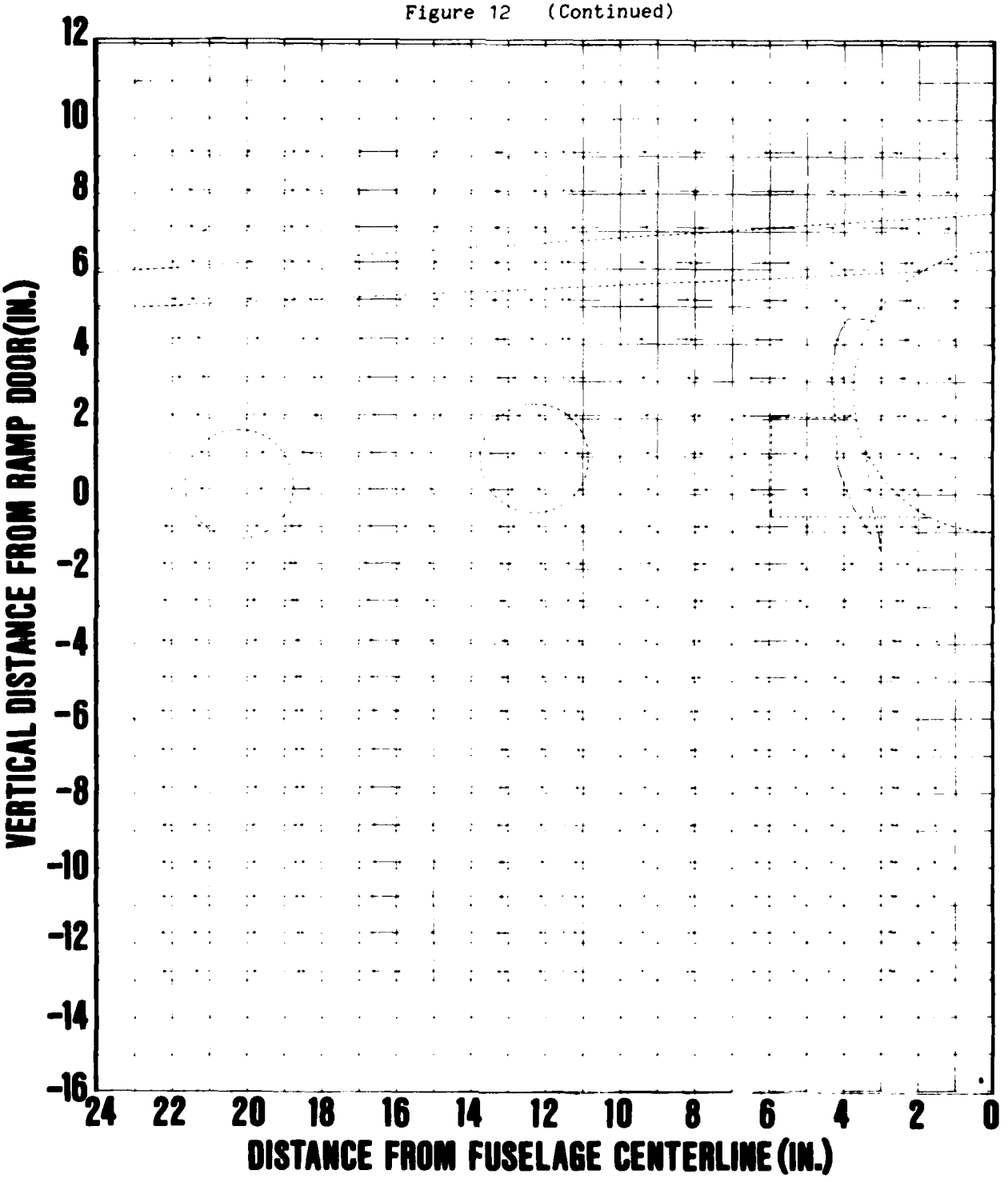

Figure 12b - X Position = 57.2 in. Downstream from Ramp Door;
Flap Setting = 0 deg

Figure 12 (Continued)

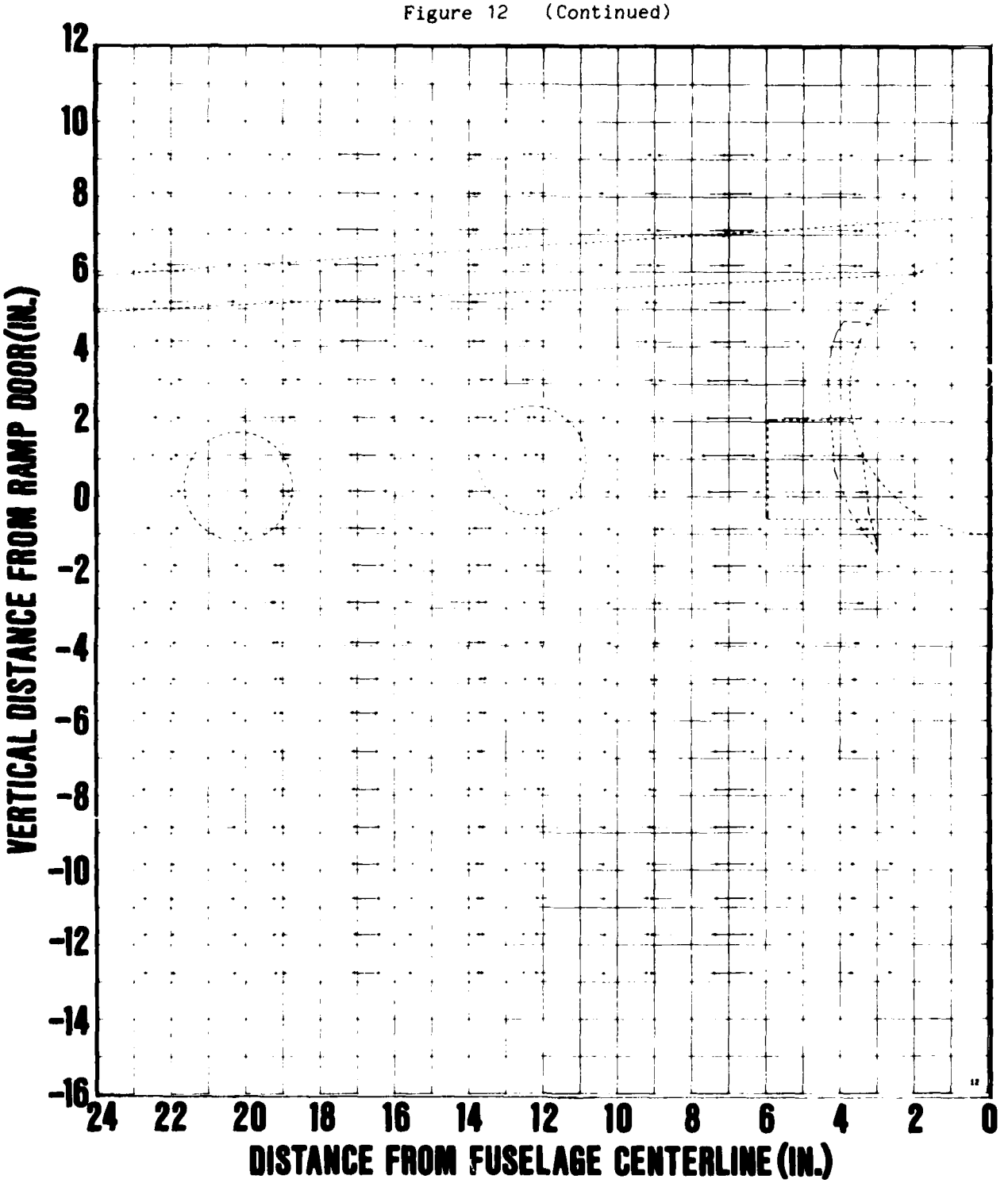

Figure 12c - X Position = 76.8 in. Downstream from Ramp Door;
Flap Setting = 0 deg

Figure 12 (Continued)

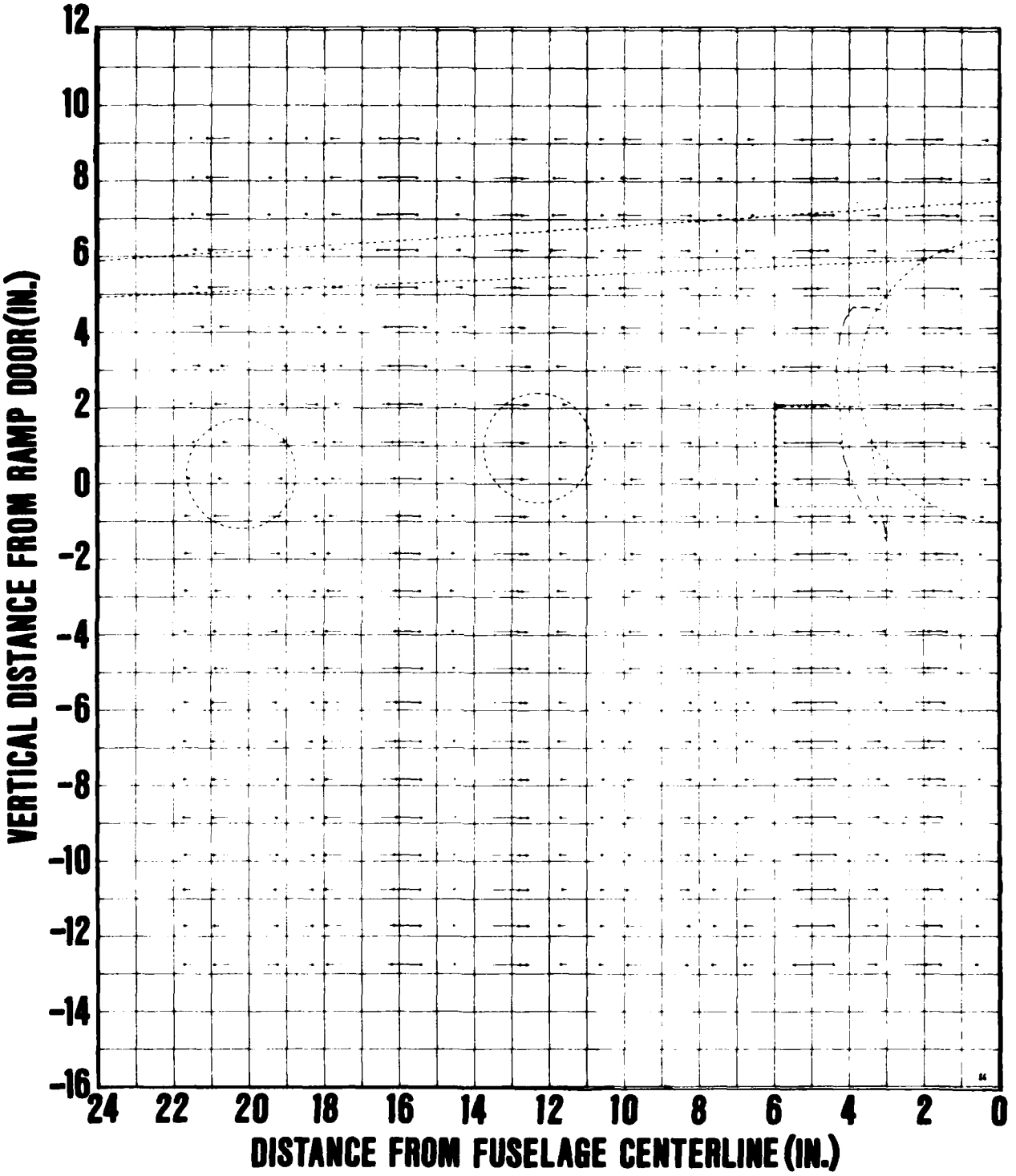

Figure 12d - X Position = 38.7 in. Downstream from Ramp Door;
Flap Setting = 0 deg; No Thrust Simulation

Figure 12 (Continued)

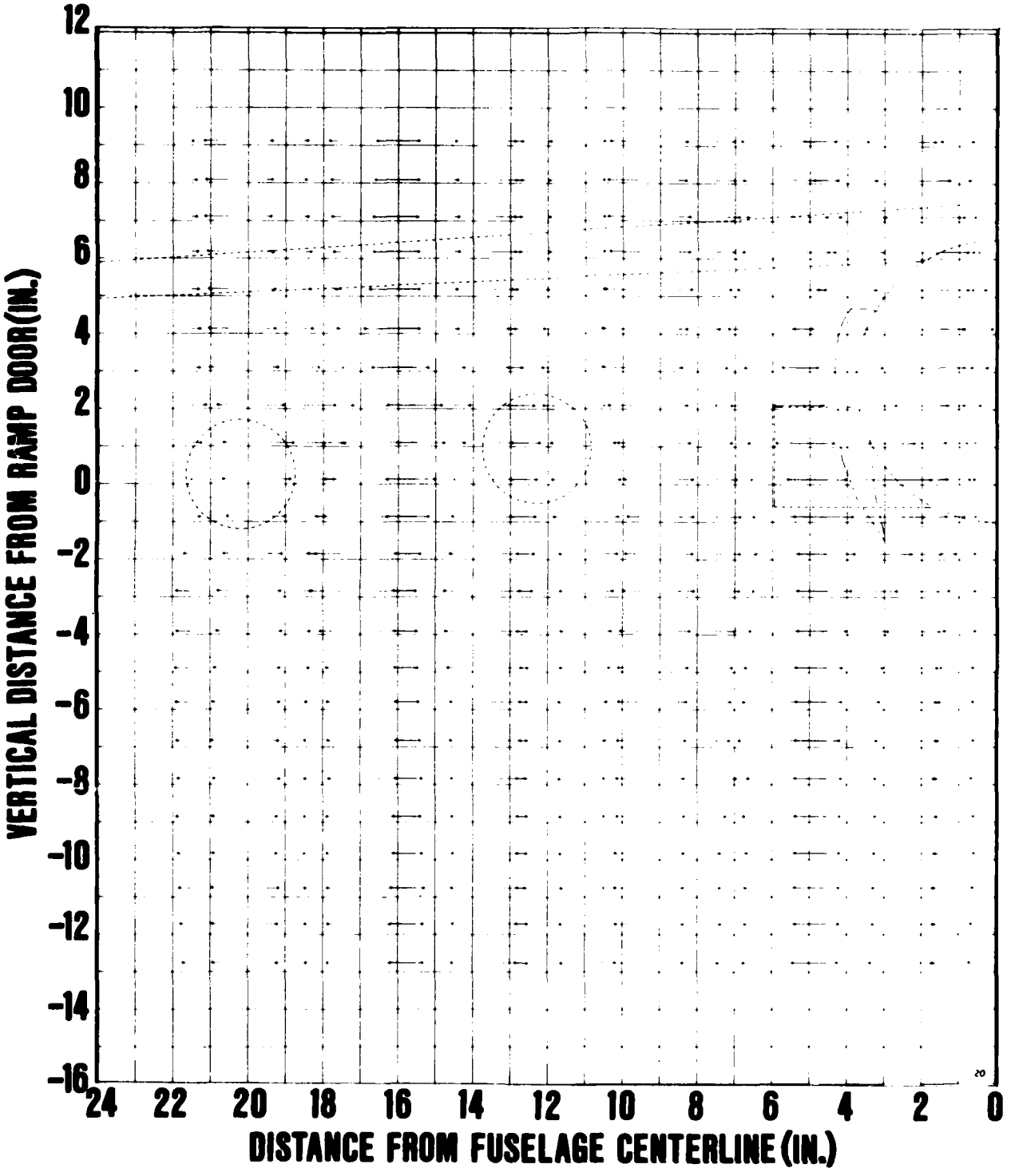

Figure 12e - X Position = 38.7 in. Downstream from Ramp Door;
Flap Setting = 10 deg

Figure 12 (Continued)

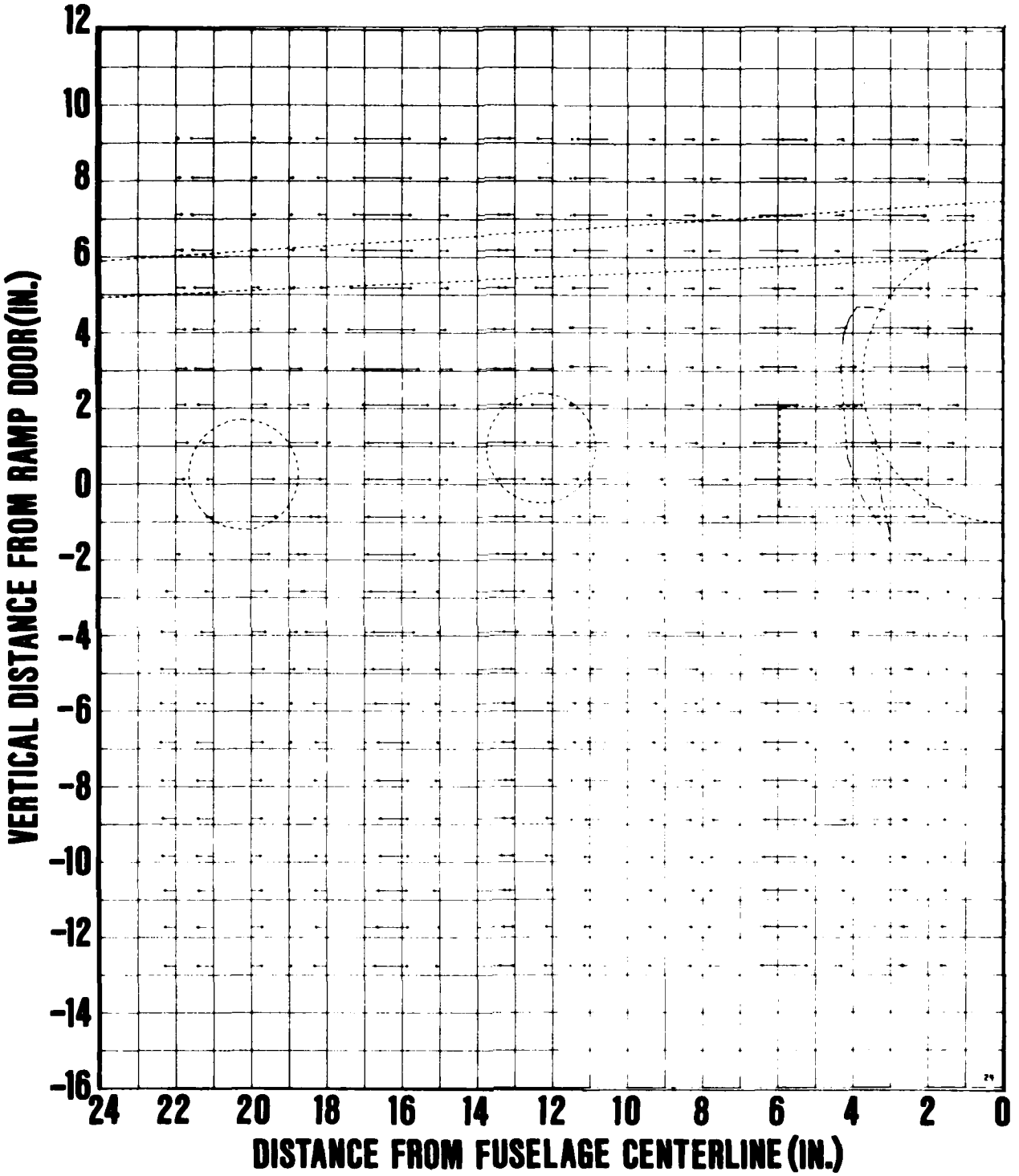

Figure 12f - X Position = 57.3 in. Downstream from Ramp Door;
Flap Setting = 10 deg

Figure 12 (Continued)

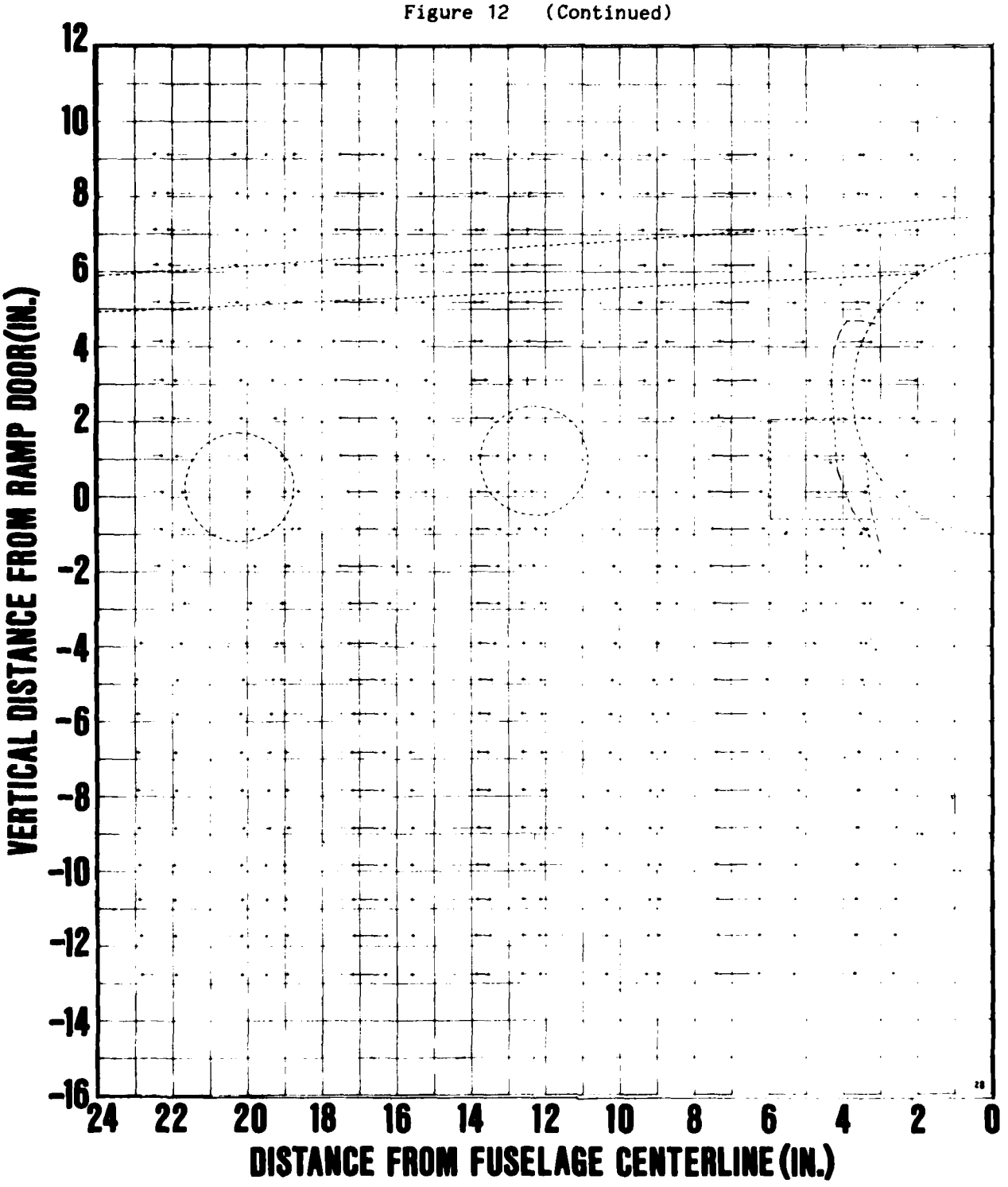

Figure 12g - X Position = 76.8 in. Downstream from Ramp Door;
Flap Setting = 10 deg

Figure 12 (Continued)

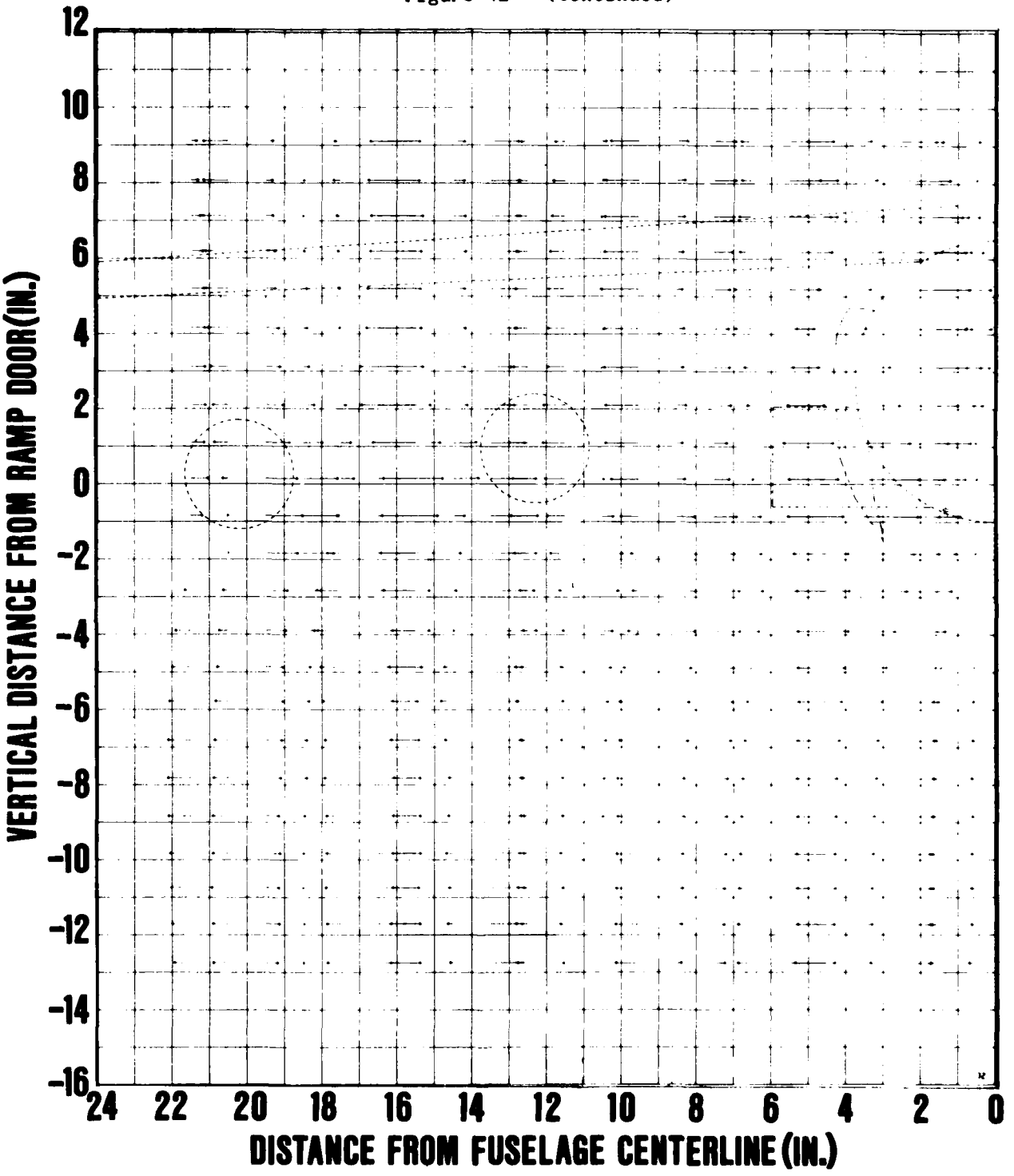

Figure 12h - X Position = 38.7 in. Downstream from Ramp Door;
Flap Setting = 20 deg

Figure 12 (Continued)

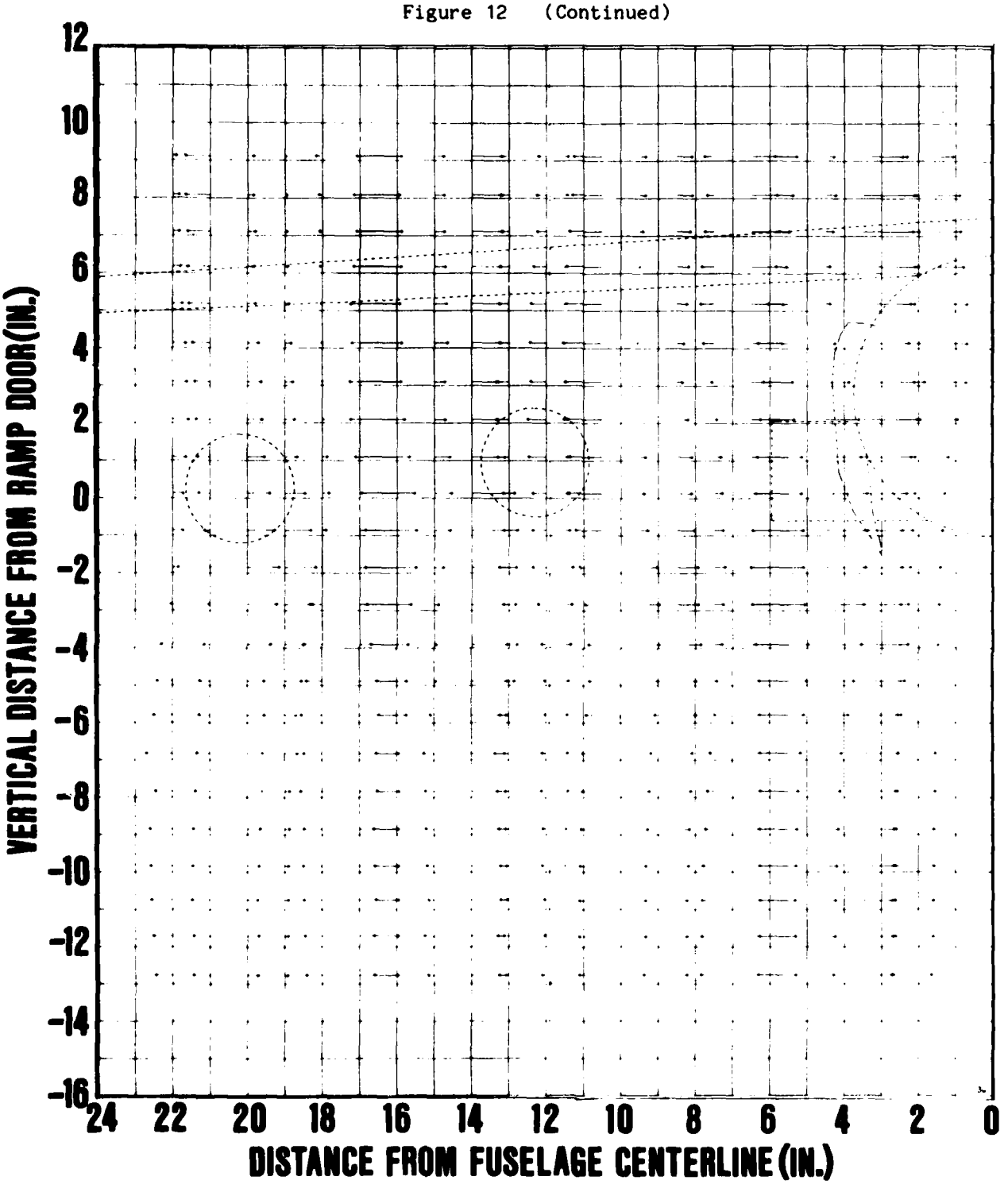

Figure 12i - X Position = 57.3 in. Downstream from Ramp Door;
Flap Setting = 20 deg

Figure 12 (Continued)

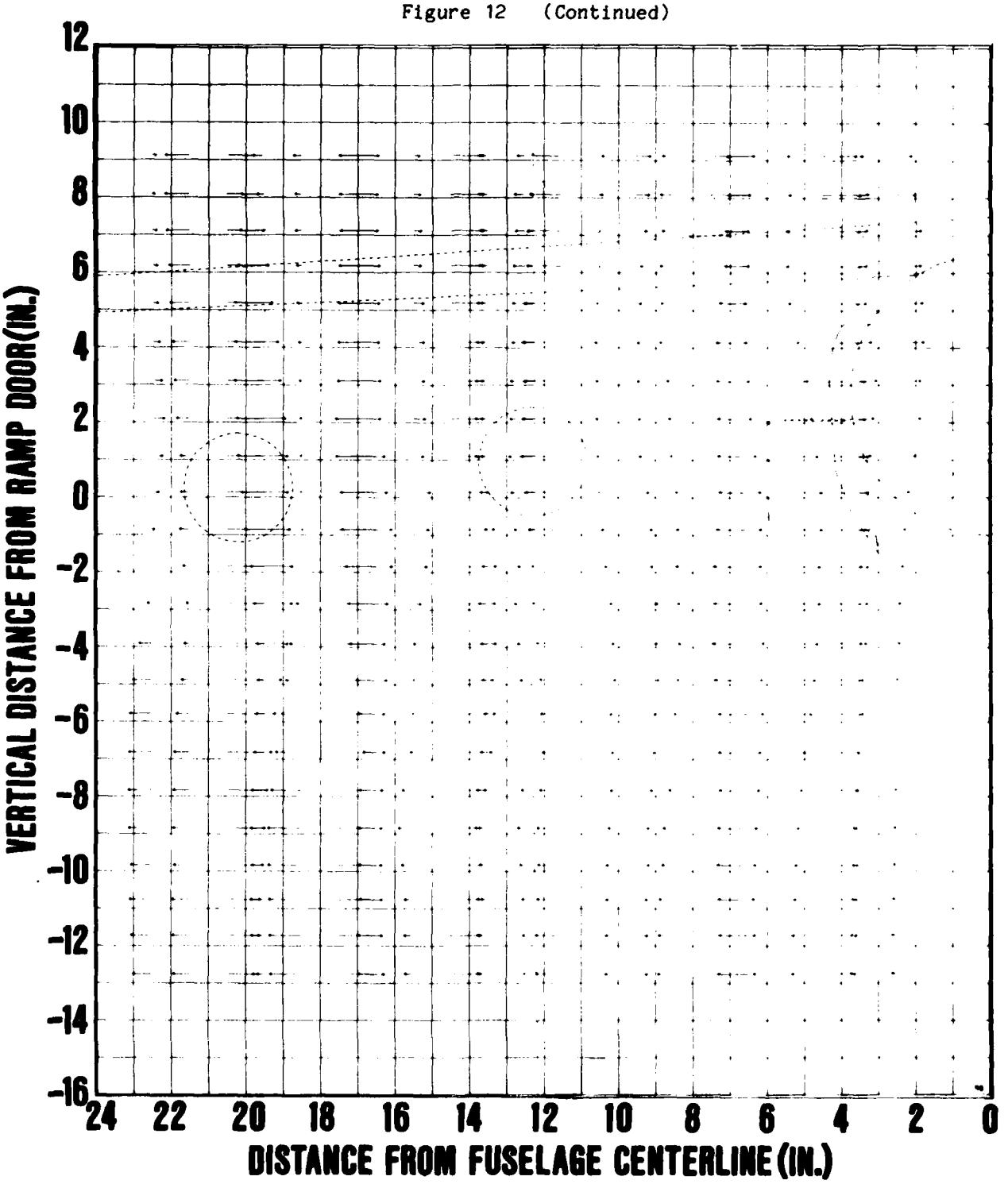

Figure 12j - X Position = 76.9 in. Downstream from Ramp Door; Flap Setting = 20 deg

Figure 12 (Continued)

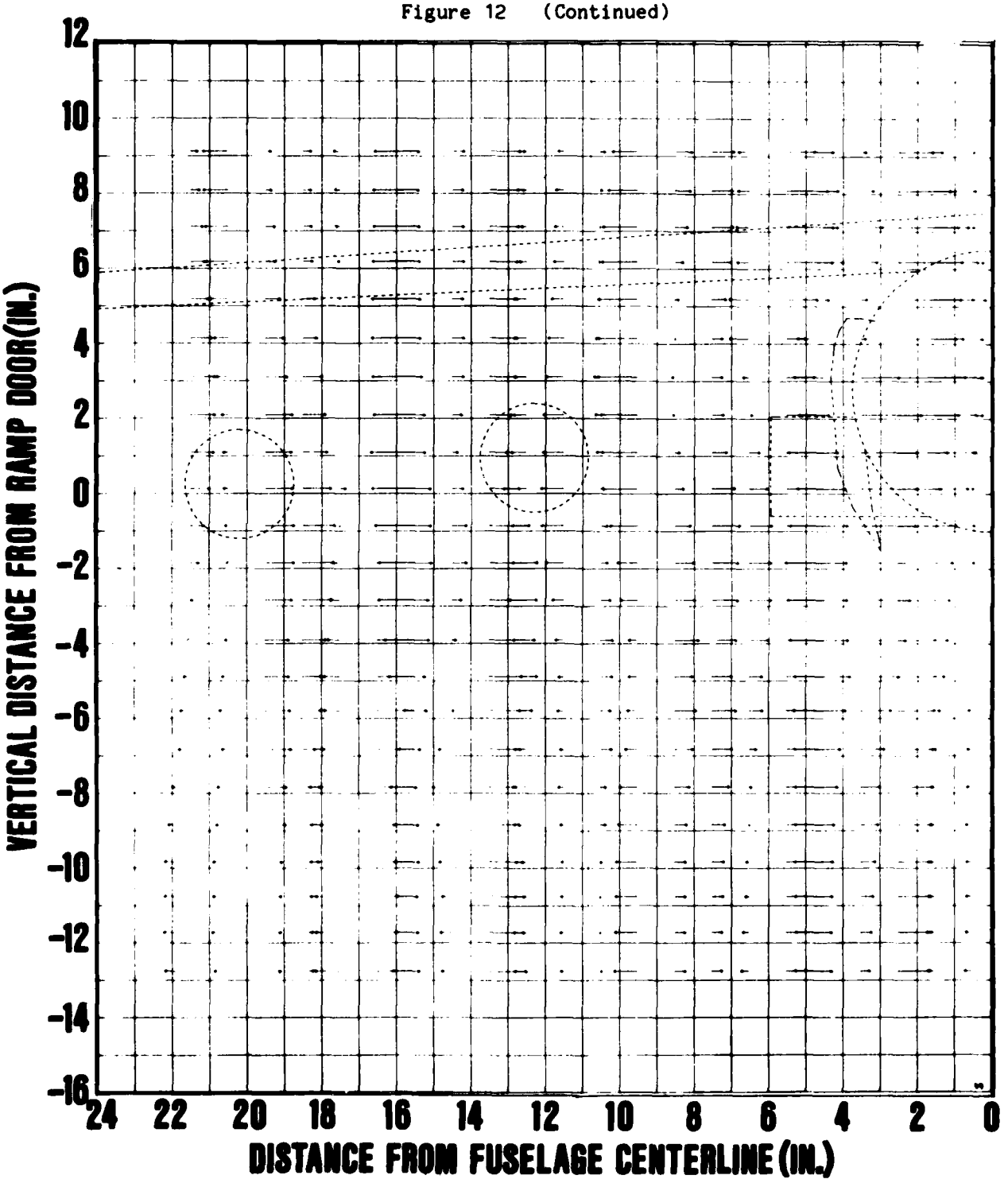

Figure 12k - X Position = 38.7 in. Downstream from Ramp Door;
Flap Setting = 30 deg

Figure 12 (Continued)

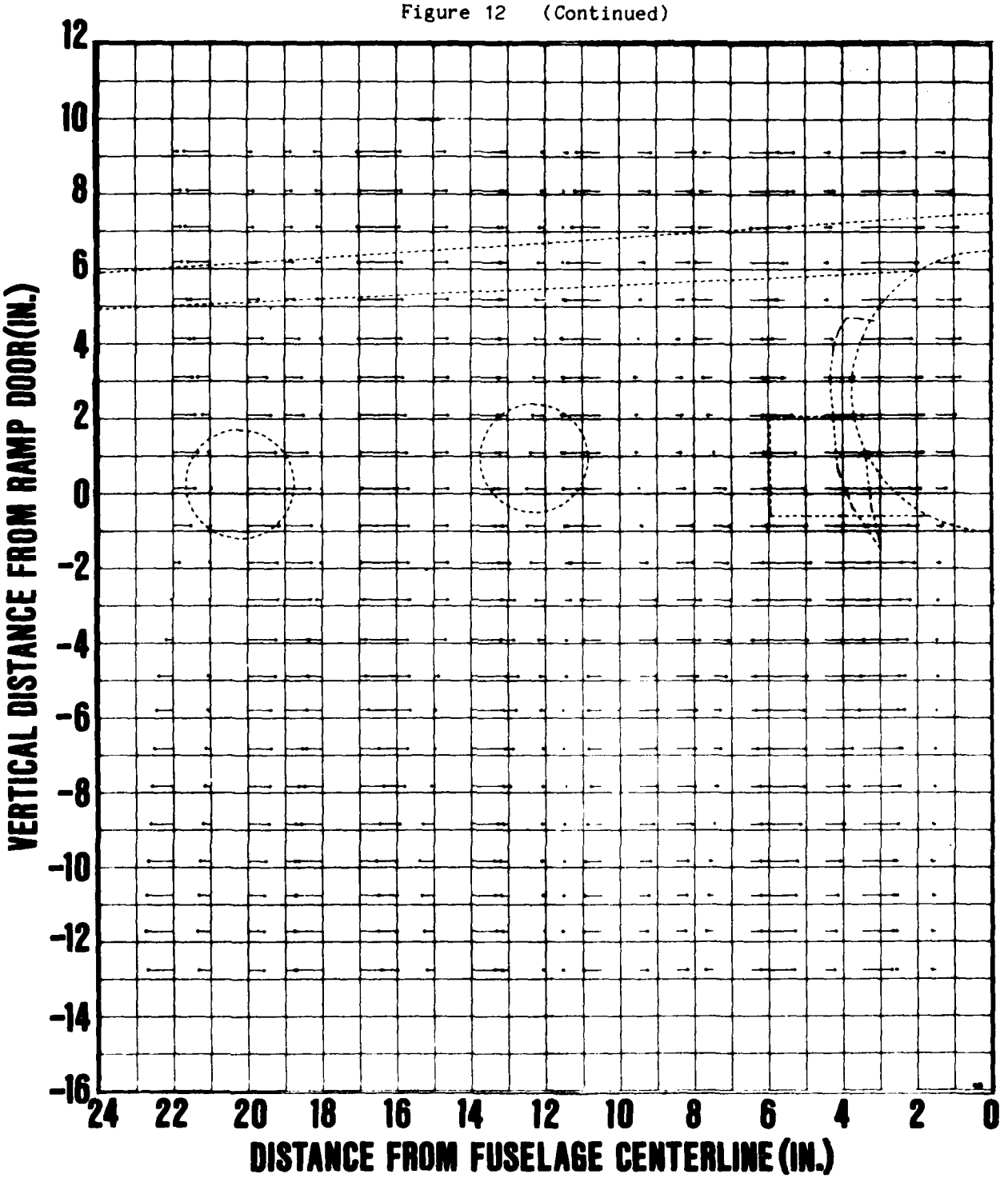

Figure 121 - X Position = 57.3 in. Downstream from Ramp Door;
Flap Setting = 30 deg

Figure 12 (Continued)

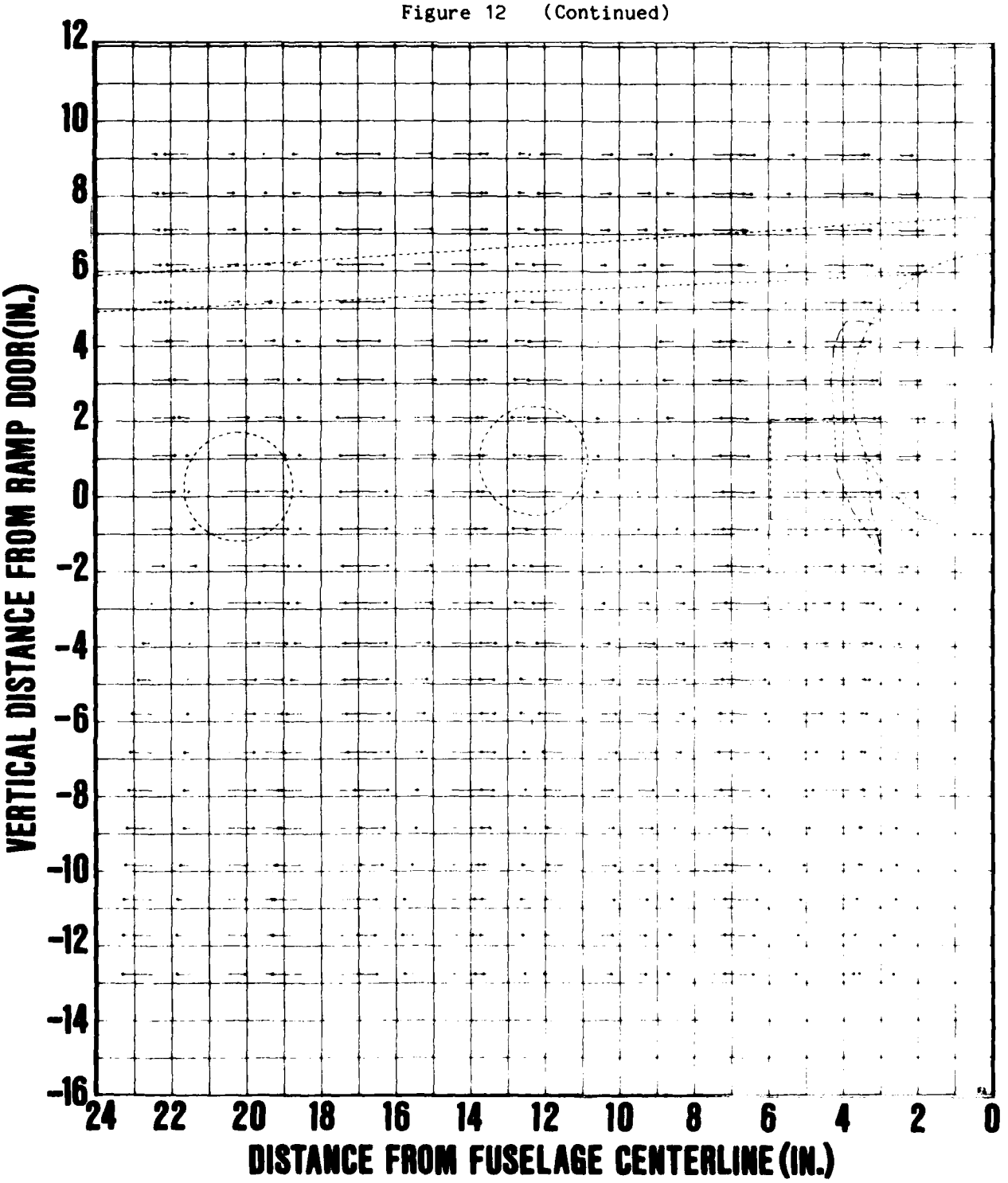

Figure 12m - X Position = 76.6 in. Downstream from Ramp Door;
Flap Setting = 30 deg

Figure 12 (Continued)

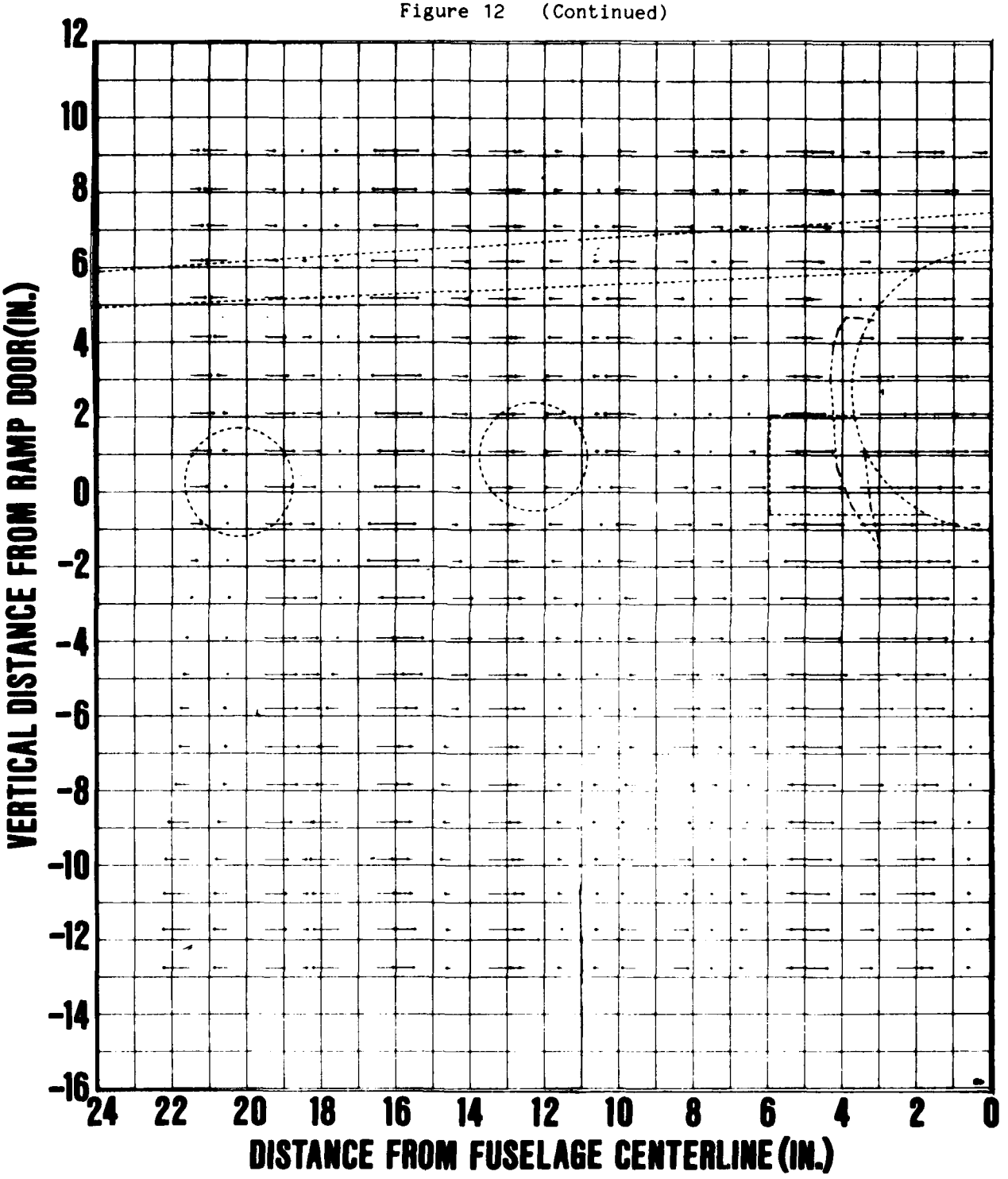

Figure 12n - X Position = 38.7 in. Downstream from Ramp Door;
Flap Setting = 30 deg; No Thrust Simulation

Figure 13 - Effect of Extraction Line Length and Parachute Size on Drag

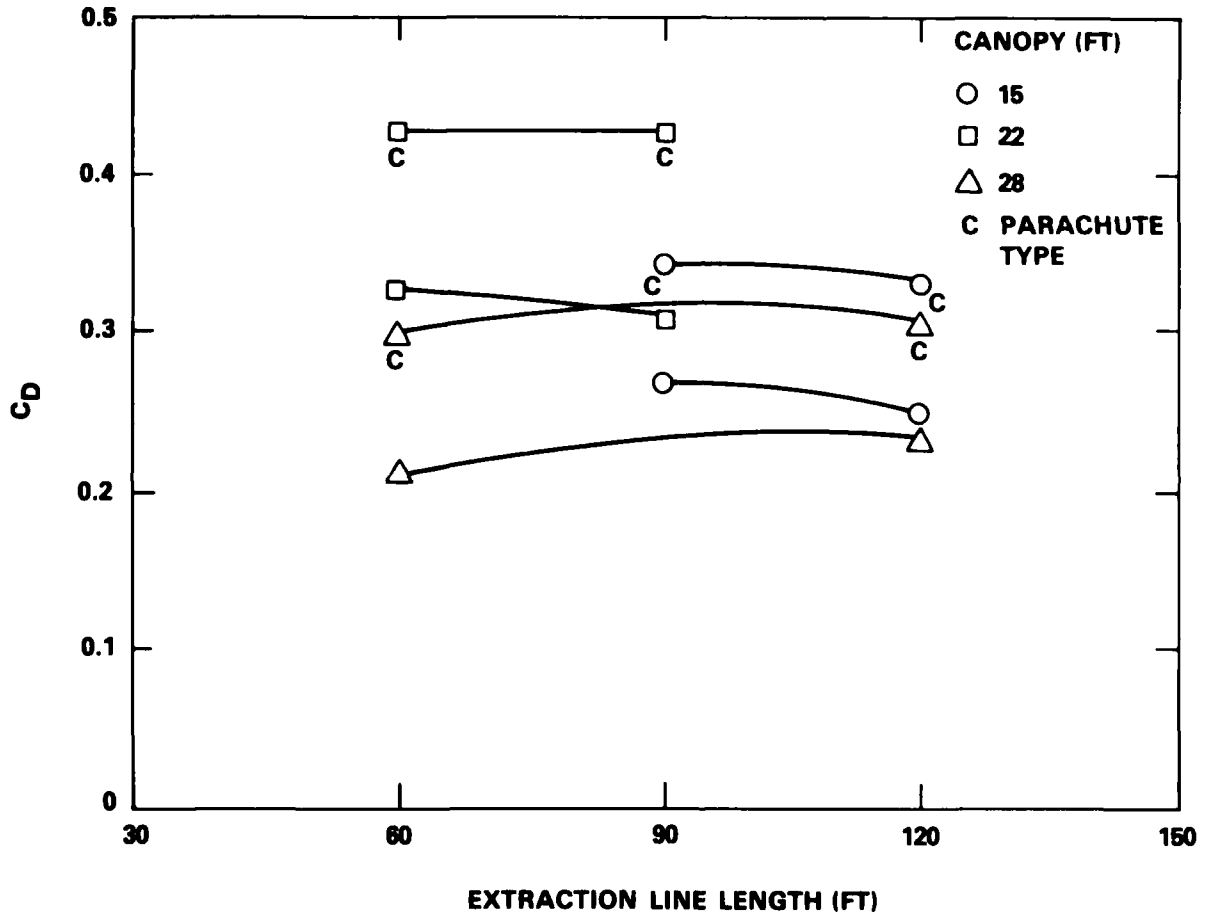

Figure 13a - Phase I, Ogive Cylinder, V_{Tunnel} = 200 ft/sec

Figure 13 (Continued)

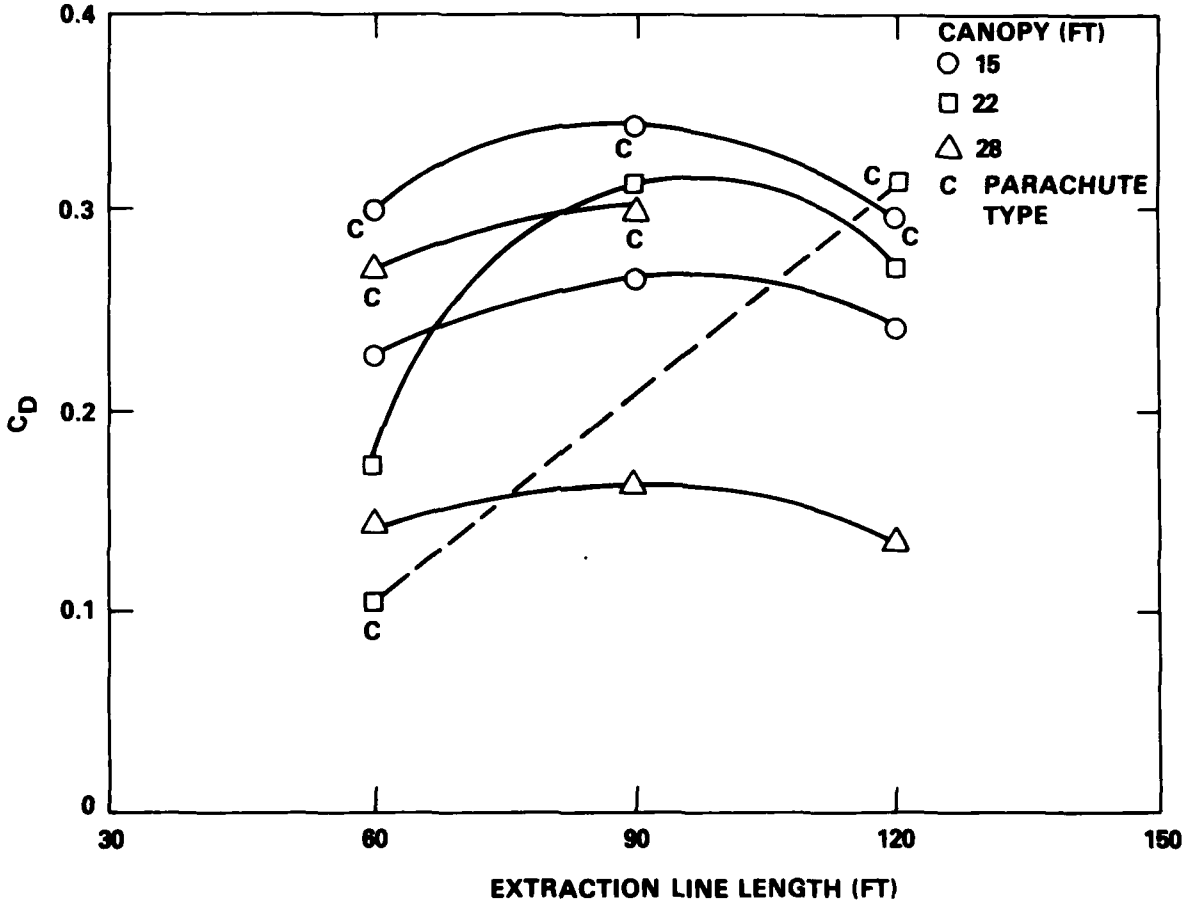

Figure 13b - Phase III, C-141B Model, V_{Tunnel} = 200 ft/sec, Flap Setting = 0 deg

Figure 13 (Continued)

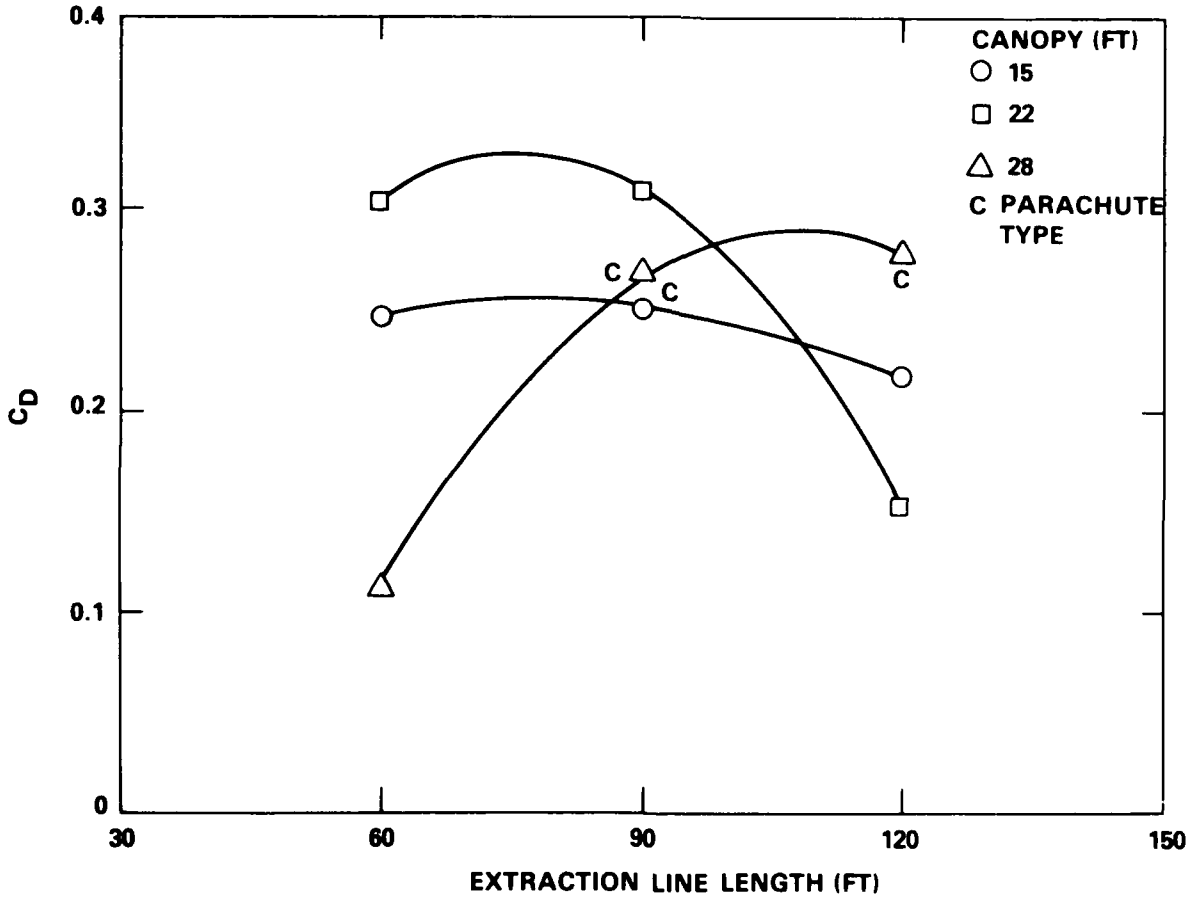

Figure 13c - Phase III, C-141B Model, V_{Tunnel} = 200 ft/sec, Flap Setting = 30 deg

NOTE: ALL DIMENSIONS ARE IN INCHES.

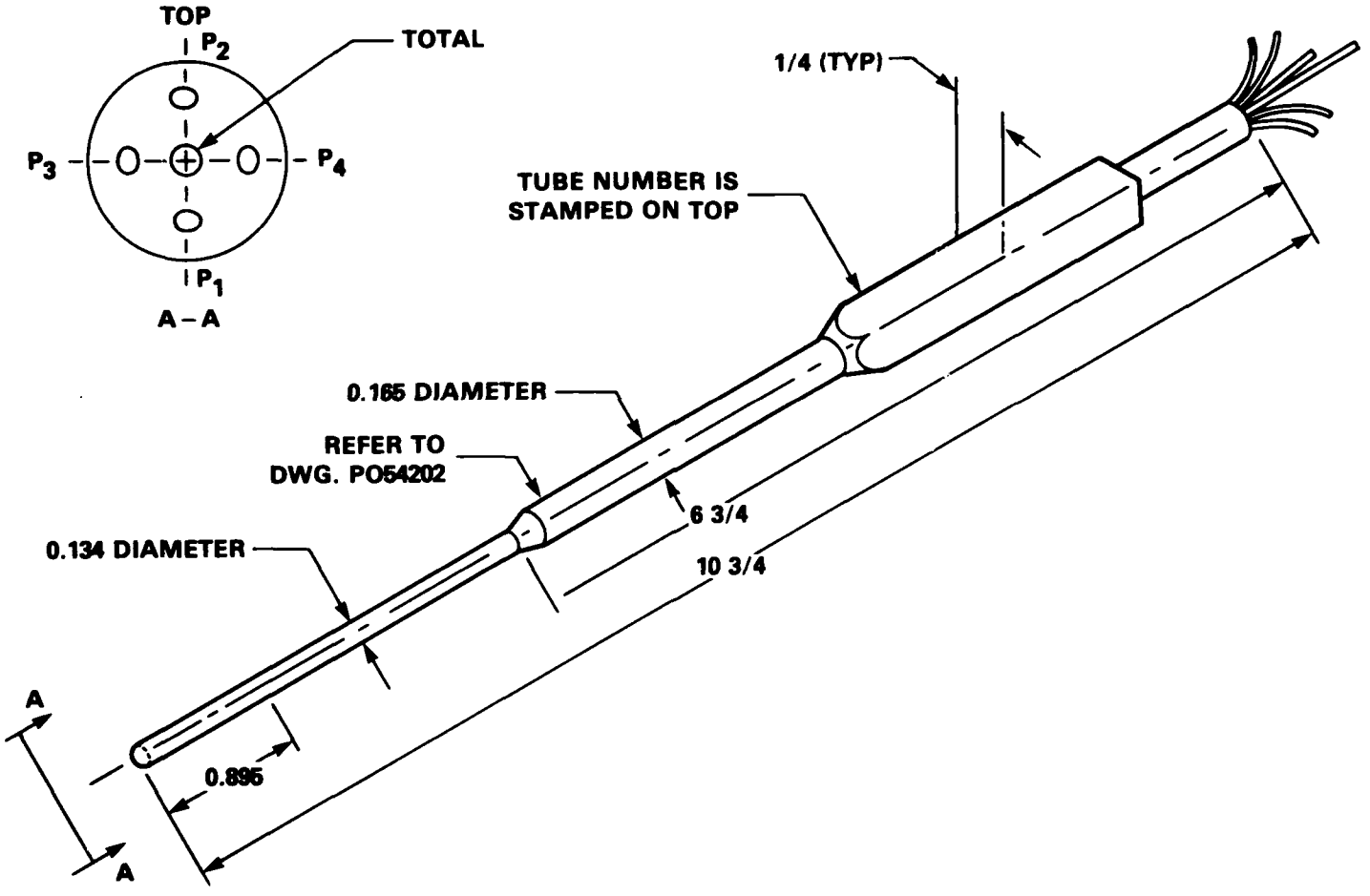

Figure B.1 - Pitot-Static Angularity Probe

NOTE: STATIC ORIFICES (ORTHOGONAL TO V_X) ARE NOT SHOWN.

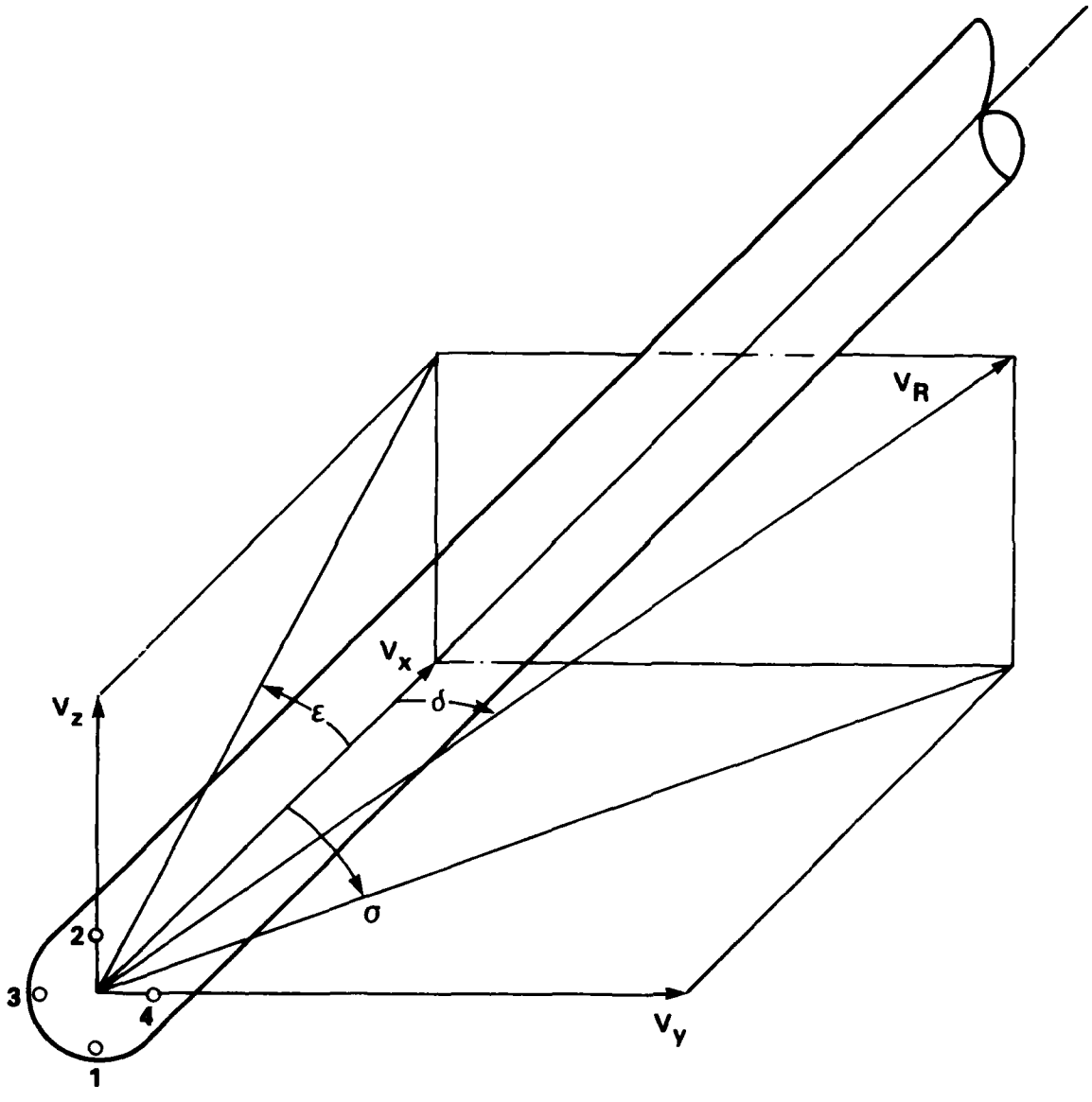

Figure B.2- Positive Directions of Upwash, Sidewash, and Velocity Components as Measured by Pitot-Static Angularity Probe

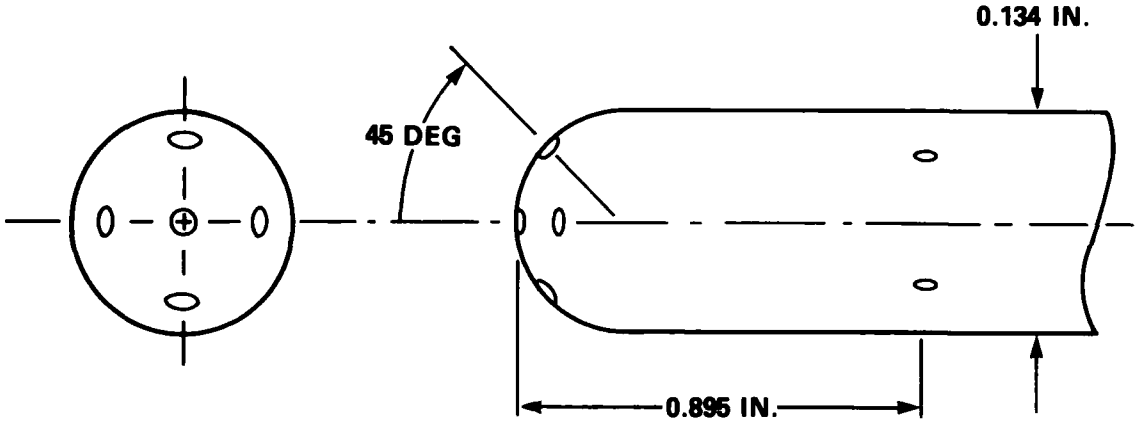

Figure B.3 - Orifice Locations on Head of Angularity Probe

DTNSRDC ISSUES THREE TYPES OF REPORTS

1. DTNSRDC REPORTS, A FORMAL SERIES, CONTAIN INFORMATION OF PERMANENT TECHNICAL VALUE. THEY CARRY A CONSECUTIVE NUMERICAL IDENTIFICATION REGARDLESS OF THEIR CLASSIFICATION OR THE ORIGINATING DEPARTMENT.

2. DEPARTMENTAL REPORTS, A SEMIFORMAL SERIES, CONTAIN INFORMATION OF A PRELIMINARY, TEMPORARY, OR PROPRIETARY NATURE OR OF LIMITED INTEREST OR SIGNIFICANCE. THEY CARRY A DEPARTMENTAL ALPHANUMERICAL IDENTIFICATION.

3. TECHNICAL MEMORANDA, AN INFORMAL SERIES, CONTAIN TECHNICAL DOCUMENTATION OF LIMITED USE AND INTEREST. THEY ARE PRIMARILY WORKING PAPERS INTENDED FOR INTERNAL USE. THEY CARRY AN IDENTIFYING NUMBER WHICH INDICATES THEIR TYPE AND THE NUMERICAL CODE OF THE ORIGINATING DEPARTMENT. ANY DISTRIBUTION OUTSIDE DTNSRDC MUST BE APPROVED BY THE HEAD OF THE ORIGINATING DEPARTMENT ON A CASE-BY-CASE BASIS.


DAT
FILM